UNIVERSITY OF SOUTHAMPTON

FACULTY OF NATURAL AND ENVIRONMENTAL SCIENCES

Ocean and Earth Science

An isotopic study of the chemical evolution of groundwater in the peridotite aquifers of the Oman-United Arab Emirates ophiolite

by

Nicolas Bompard

Thesis for the degree of Doctor of Philosophy

March 2018

UNIVERSITY OF SOUTHAMPTON

<u>ABSTRACT</u>

FACULTY OF NATURAL AND ENVIRONMENTAL SCIENCES

<u>Ocean and Earth Science</u>

An isotopic study of the chemical evolution of groundwater in the peridotite aquifers of the Oman-United Arab Emirates ophiolite
Nicolas Bompard

The low-temperature alteration of peridotite in ophiolites produces two types of fluids, $Mg-HCO_3^-$ rich, pH <10 water (Type I) in the shallow subsurface, and $Ca-OH^-$ rich, pH >10 water (Type II) deeper in the aquifer, through a combination of serpentinisation and carbonation reactions. Upon discharge, the Type II waters reacts with environmental CO_2 and precipitate massive carbonate terraces, potentially providing a powerful means to mitigate the climate change resulting from human-induced high levels of atmospheric CO_2. The impact of such carbonate precipitation on the global carbon cycle depends on the rock source of the calcium. Carbonate precipitation with Ca^{2+} derived from the dissolution of carbonate minerals has no net effect on atmospheric CO_2, whereas Ca^{2+} from the dissolution of silicate phases will contribute to a net drawdown. However, the water-rock reactions responsible for the evolution of the groundwater in peridotite aquifers and the mineral phases involved are still poorly understood. In this study, the changes in ion concentrations, $^{87}Sr/^{86}Sr$, $\delta^{44/40}Ca$ and $\delta^{88}Sr$ in water along the flow paths and the isotopic composition of a selection of rocks and secondary minerals from the Oman-United Arab Emirates ophiolite are used to investigate the water-rock reactions occurring in the ophiolite subsurface. The data reveal that multiple processes are responsible for the observed evolution of Type I and II waters: (1) Dissolution of secondary minerals, such as serpentine and brucite, which have extensively replaced peridotite primary minerals during previous alteration episodes, play an important role in the modern water-rock interactions and in the water chemistry evolution in the peridotite aquifer; (2) Dolomite precipitation affects the dissolved Ca and Mg concentrations in Type I water; and (3) Ca^{2+} remobilisation associated with Mg^{2+} exchange during dolomitisation is the main source of Ca^{2+} in Type II water, preventing any CO_2 release from the carbonates by binding the CO_3^{2-} ions with Mg^{2+}. The original source of Mg^{2+} from serpentine alteration and the subsurface exchange during dolomitisation ensures that the precipitation of carbonates in hyperalkaline springs is a sink in the global carbon cycle, and indicates that engineered peridotite alteration could be useful as a climate change mitigation strategy.

Table of Contents

Table of Tables

Table of Figures

Table of Figures

Academic Thesis: Declaration Of Authorship

I, Nicolas BOMPARD, declare that this thesis and the work presented in it are my own and has been generated by me as the result of my own original research.

An isotopic study of the chemical evolution of groundwater in the peridotite aquifers of the Oman-United Arab Emirates ophiolite

I confirm that:

1. This work was done wholly or mainly while in candidature for a research degree at this University;
2. Where any part of this thesis has previously been submitted for a degree or any other qualification at this University or any other institution, this has been clearly stated;
3. Where I have consulted the published work of others, this is always clearly attributed;
4. Where I have quoted from the work of others, the source is always given. With the exception of such quotations, this thesis is entirely my own work;
5. I have acknowledged all main sources of help;
6. Where the thesis is based on work done by myself jointly with others, I have made clear exactly what was done by others and what I have contributed myself;
7. None of this work has been published before submission

Signed: ....

Date: ....

Acknowledgements

First of all I would like to thanks my supervisors Juerg Matter and Damon Teagle, for offering me the chance to do a PhD, guide me through it, and across the final writing. Having put up with my "crazy" hypotheses and keeping me on track during these four years to become almost a geochemist… I still like bugs, sorry Damon. And of course thank you for the amazing fieldwork experiences in Oman, so many things to enjoy: landscape, geology, food, and so many things to avoid: camel spiders, scorpions, palm trees…

Next I'd like to give a big thanks to Matt Cooper for teaching me how to geochemist properly in a lab, never taking my goggles off ever again, I promise, even when looking through a Plexiglas plate. Another big thanks goes to Chris Pearce for our conversations to help me deciphering my isotopes data and understanding the ways of writing science. The Rock Lab teams: Bob & John and now Dan & Matt, for thin sections, jewellery, and "coffee" breaks when they were needed. And of course all my fellow PhD students here at NOCS (sorry, there are too many of you to quote and I don't want to make anyone jealous)

A special thought to all the people I met during the 6 months of the Oman Drilling Project-Phase 1, Peter Kelemen, Alexis Templeton and the team from Colorado, Margot Godard and les Montpellierains, the GUtech people, and all of you that I can't remember at the moment (sorry). A very special thought and thanks to the Christmas/New year Team, and to Jude Coggon for letting me play with the amazing core puzzles, that was fun.

A huge thanks to my parents that supported me even without really knowing what I was doing. Thank you to the dive club people from France and England, and all the persons I met during these years.

Finally, thank you Millie, for being in my life, and you, "~~insert name here~~" Malory, for having made these last 9 months even more… interesting, I'm looking forward to meet you my child.

"Restez curieux, c'est bien"

Mme Prévost

Chapter 1   Introduction

1.1   Peridotite alteration

The alteration of peridotite by seawater plays a role in many of the Earth's dynamic processes. It influences the style of spreading of the oceanic lithosphere (Escartin et al., 1997), mechanisms in subduction zones (Hilairet & Reynard, 2009; Hirauchi et al., 2010), and the formation of volcanic arcs (Robert J. Stern & Smoot, 1998; Ulmer & Trommsdorff, 1995). Peridotite alteration produces reduced fluids (Frost & Beard, 2007) that provide energy for deep-sea ecosystems (Brazelton et al., 2010; Santelli, 2009; Schrenk et al., 2013) and influences the geochemical cycle of carbon, water, iron and hydrogen (Hacker, 2008; Kelemen et al., 2011; Klein et al., 2009; McCollom & Bach, 2009).

Peridotites are the main rock of the Earth's mantle and are stable in the high temperature, high pressure, and reducing environment found in the Earth's interior. They are primarily composed of mafic, (Mg,Fe)-rich, minerals: olivine [$(Mg,Fe)_2SiO_4$], Ca-poor pyroxene (orthopyroxene) [$Mg_2Si_2O_6$] and Ca-rich pyroxene (clinopyroxene) [$CaMgSi_2O_6$]. They are brought near the Earth's surface via tectonic processes such as detachment faulting at slow-spreading Mid-Ocean Ridges (MOR), plate collision followed by erosion, or oceanic lithosphere obduction during the closure of an ocean. When they are exposed to the low-temperature, low-pressure, and oxidising conditions of the surface environment, peridotites become unstable (Evans, 1977; Frost, 1985; Johannes, 1969; Malvoisin, Brunet, et al., 2012; Malvoisin, Carlut, et al., 2012; Martin & Fyfe, 1970). This disequilibrium creates a strong chemical gradient between the rocks and the environment with an energy density of the order of 500 kJ/kg which drives the chemical reactions of the peridotite minerals with the surrounding fluid (Kelemen & Hirth, 2012).

The chemical alteration of ultramafic rocks consists of three main exothermic reactions: (1) serpentinisation, the hydration of olivine and pyroxene into serpentine when they are in presence of water; (2) oxidation, the oxidation of ferrous iron (Fe^{2+}) in mafic minerals by water to form iron-rich oxy(hydr)oxides (e.g. Fe_2O_3, Fe_3O_4, $FeO(OH)$, $Fe(OH)_3$) together with reduced fluids; and (3) carbonation, the binding of divalent cations (Mg^{2+}, Ca^{2+}, Fe^{2+}) that were released in the fluid by peridotite dissolution with dissolved CO_2 (HCO_3^-, CO_3^{2-}) to precipitate carbonate minerals $(Ca,Mg)CO_3$.

Chapter 1

1.1.1 Serpentinisation

Serpentinisation is the formation of serpentine from mafic minerals (Eq. 1) either by a mineral hydration process that incorporates hydroxyl groups (OH^-) in the lattice of mafic minerals or by a dissolution/precipitation process.

$$4Mg_2SiO_{4(Mg\text{-}olivine)} + (CaMg;Mg_2)Si_2O_{6(pyroxenes)} + 7H_2O = 3Mg_3Si_2O_5(OH)_{4(serpentine)} + (Ca^{2+};Mg^{2+})_{(aq)} + 2OH^-_{(aq)} \tag{1}$$
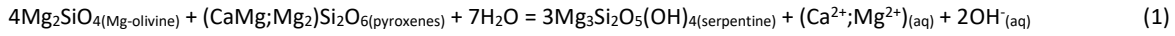
Serpentine can occur as a number of different polymorphs with different crystal structures: planar layers (lizardite), scrolled layers (chrysotile) or alternately inverted layers (antigorite) (Mével, 2003). The OH^- groups increase the mineral volume with very limited loss of matter, thereby inducing a loss of density for the rock. During serpentinisation, the peridotite density decreases from ~3.3 g/cm^3 to 2.5 g/cm^3, which is lower than the average oceanic crust (2.8 g/cm^3) (Mével, 2003). Serpentinisation also changes the strength of peridotites, thus the rheology of the oceanic lithosphere, and impacts tectonic processes such as sea floor spreading and subduction (Escartin et al., 1997; Francis, 1981; Hilairet & Reynard, 2009; Reynard, 2013).

At subduction zones, serpentine permits the oceanic plate to slide more easily under the continental plate, this can reduce earthquake strength and frequency in serpentine-rich areas (Hirauchi et al., 2010). In the subducted slab, the high pressure drives the OH^- groups out of the hydrated minerals and upward to the mantle wedge. This process hydrates the overlying mantle wedge and continental crust, lowers the melting point of rocks, and promotes the formation of magma in volcanic arc regions (Maruyama & Okamoto, 2007; R J Stern & Smoot, 1998; Ulmer & Trommsdorff, 1995). Serpentinisation also plays an important but poorly quantified role in the planetary water cycle, in particular as a recharging process for the mantle (Ohtani et al., 2004).

1.1.2 Oxidation

The reduced Fe^{2+} in mafic minerals is oxidised into Fe^{3+} when water reacts with the peridotite minerals (Eq.2). This reaction produces Fe-oxides (e.g. magnetite, hematite, goethite) and hydrogen (H_2) via hydrolysis of water molecules (Frost, 1985).

$$3Fe^{2+}_2SiO_{4(Fe\text{-}olivine)} + 2H_2O = 2Fe^{2+}Fe^{3+}_2O_{4(magnetite)} + 3SiO_{2(quartz)} + 2H_2 \tag{2}$$
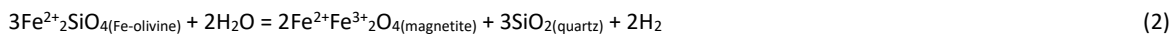
The reduction of the fluid permits the accumulation of H_2 and S^- in solution which results in the formation of a redox gradient where the alteration fluid makes contact either with seawater or freshwater. Chemolithotrophic micro-organisms use this redox gradient to power their metabolism and form the class of primary producers in deep-sea and deep aquifer ecosystems (Brazelton et al., 2010; Kelley et al., 2005; Ménez et al., 2012). These ecosystems do not use sunlight as their primary

source of energy and develop in environments with low oxygen fugacity (fO2). Furthermore, the redox and chemical gradients favour abiotic synthesis of organic matter via Fischer-Tropsch reactions (McCollom, 2016; McCollom et al., 2010). It has been speculated that the first ecosystems on Earth may have encountered similar conditions and the study of these deep-sea and deep aquifer ecosystems may help to understand the way life developed at first and started to evolve on Earth as well as on other planets (Brasier et al., 2002; J J Brocks et al., 1999; Jochen J. Brocks et al., 2003; Haqq-Misra et al., 2008; Holland, 2006; Macleod et al., 1994; Pavlov et al., 2000; Philippot et al., 2009; Poulton et al., 2004; Rosing et al., 2010).

1.1.3 Carbonation

In presence of a fluid containing dissolved CO_2 (HCO_3^-, CO_3^{2-}), the divalent cations released in solution during peridotite serpentinisation such as (Ca^{2+}, Mg^{2+}) (Eq.1) can bind with the carbonate ions (CO_3^{2-}) and precipitate carbonate minerals (Eq.4), including calcite [$CaCO_3$], dolomite [$(CaMg)CO_3$], and magnesite [$MgCO_3$]. Carbonation occurs within the aquifer, along the fractures and cracks that form the fluid pathways in rocks serpentinised zones. Away from the CO_2-rich surface, all carbonate ions present in the fluid are consumed by the precipitation of carbonate in veins, this permits the subsequent accumulation of divalent cations in solution. When these CO_2-depleted fluids surface as hyperalkaline springs, the accumulated divalent cations react with the CO_2 present in the environment and precipitate massive carbonate structures. The carbonate structures take different forms depending on their environment of precipitation: mesh network of veins within the serpentinised peridotites, chimneys on the seafloor, and travertine terraces in ophiolites (Clark et al., 1992; Kelemen et al., 2011; Ludwig et al., 2006; O'Neil & Barnes, 1971).

$$4Mg_2SiO_{4(Mg\text{-}olivine)} + (CaMg;Mg_2)Si_2O_{6(pyroxenes)} + 8H_2O + CO_{2\,(aq)} = 3Mg_3Si_2O_5(OH)_{4(serpentine)} + (Ca;Mg)CO_{3(carbonate)} \qquad (3)$$
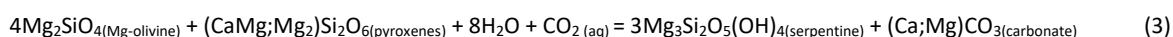
Carbonate minerals are a stable and long-term reservoir in the global carbon cycle, and the carbonation of ultramafic rocks results in a net uptake of atmospheric carbon into this reservoir (Berner et al., 1983; Urey, 1952). However, the impact on Earth's climate is difficult to estimate due to the lack of data on carbon fluxes in these systems. Kelemen & Matter (2008) and Mervine et al. (2014) calculated that around 10^7 kg of CO_2/year were sequestered via peridotite carbonation in the Oman-UAE ophiolite, but carbon fluxes have not been quantified in any other area so far. At subduction zones, the carbonates present in the oceanic lithosphere either stay in the slab and feed carbon back to the mantle or decarbonate and provide CO_2-rich fluids/gases to the overlying plate and to arc volcanism (Alt et al., 2013; Poinar, 2012).

1.2 Environments of alteration

There are three main geological settings in which peridotite alteration takes place. Although the same basic chemical reactions occur, each environment produces a distinctive end-member fluid. On the seafloor, tectonic stress results in detachment faults and fractures in the lithosphere that permit seawater to infiltrate the rocks and to enter in contact with the peridotites. The infiltrated fluid reacts with the rocks and is heated up by the subsurface environment before returning to the surface, this process is known as hydrothermal circulation. (1) Hydrothermal circulation close to Mid-Ocean Ridges (MOR), such as at the Rainbow or Logatchev fields, is powered by the heat of magma chambers. It produces acidic (pH 3), reduced, metal-rich fluids that exit at high temperature (>250ºC). Upon mixing with seawater, the hydrothermal fluid precipitates sulphide-rich chimneys called "black smokers" in reference to the dark colour of the particle-rich vent plumes (Y. Bogdanov et al., 1995; Y. A. Bogdanov et al., 1997; Douville et al., 2002). (2) Away from the MOR, hydrothermal circulation through peridotites produces clear, low-temperature (~100ºC), alkaline (pH >9), reduced, metal-poor, Mg-depleted, Ca-rich fluids. The exhausted fluids can precipitate carbonate chimneys (e.g. Lost City; (Fruh-Green et al., 2003; Kelley et al., 2001, 2005) or not (e.g. Saldanha; Barriga et al. 1998; Dias et al. 2010) upon contact with seawater. The source of heat powering the hydrothermal circulation in these systems remains debated. It could originate either from the cooling lithosphere, the exothermic reaction of peridotite serpentinisation, or a mix of both (Allen & Seyfried, 2004; Lowell & Rona, 2002; Mével, 2003). (3) On land, low-temperature serpentinisation drives the alteration of peridotites in ophiolite massifs (Barnes et al., 1978; Barnes & O'Neil, 1971). Rainwater infiltrates the peridotite-hosted aquifer and away from the atmosphere water-rock reactions produce Ca^{2+}-OH^--rich, Mg-depleted, CO_2-depleted and hyperalkaline (pH >11) fluids. Upon surfacing, these fluids react with atmospheric CO_2 or HCO_3^--rich surface waters and precipitate travertine terraces. Similar peridotite alteration is observed in the mantle section of ophiolite massifs around the world, such as in Oman (Neal & Stanger, 1985), New Zealand (Menzies, 2012), Cyprus (Neal & Shand, 2002), and the Italian Southern Alps (Bruni et al., 2002; Cipolli et al., 2004).

The difference in end-member fluid chemistry is due to the difference in reactants; different degree of alteration for the peridotites between each environments, low close to the MOR and extensive in ophiolite massifs, and different starting fluids, seawater or rainwater. The conditions of reaction, such as high or low temperature, can also influence the water-rock interactions and influence the chemistry of the end-member fluid.

1.3 Carbon mineralisation and CO$_2$ Capture and Sequestration (CCS)

In a context of climate change, due to the increase of anthropogenic CO$_2$ emissions to the atmosphere, peridotite alteration has gained new attention from the scientific community. The presence of extensive outcrops of peridotite on Earth's surface and the spontaneous precipitation of carbonates during their alteration (Eq. 3) make them an interesting candidate for CO$_2$ sequestration. This natural carbon mineralisation may provide a long-term and safe way to store industrial CO$_2$ emissions (Seifritz, 1990; Lackner et al., 1995; IPCC, 2005; Power et al., 2013). Carbon mineralisation can be accomplished *ex situ* in a reactor with crushed Mg, Ca, Fe-rich silicate minerals reacted with concentrated CO$_2$ (IPCC, 2005; Power et al., 2013; Sanna et al., 2014b; Dananjayan, Kandasamy and Andimuthu, 2016) or *in situ* by injecting CO$_2$ or CO$_2$-rich fluids into ultramafic rock aquifers (Kelemen and Matter, 2008; Matter and Kelemen, 2009; Kelemen et al., 2011; Matter et al., 2016).

1.3.1 *Ex situ* mineralisation

Ex situ mineralisation allows a better control on the reaction parameters (temperature, pressure, pH) to accelerate the reaction kinetics, and the addition of reagents, such as acids and ammonium salts, to optimised the dissolution of ultramafic minerals (Teir et al., 2007; Wang and Maroto-Valer, 2011; Sanna et al., 2014a; Madeddu et al., 2015; Sanna, Gaubert and Maroto-Valer, 2016). However, the relatively high cost of *ex-situ* carbon mineralisation ($50 to 100$/ton of CO$_2$ mineralised) may make this operation impracticable (IPCC, 2005; Gerdemann et al., 2007). Alternatives have been proposed to cut the cost, such as the use of nickel-chromium mine tailings, a serpentinite-rich, already finely crushed, unused waste that naturally experience a carbonation process while stored in heaps. Studies have shown that mine tailings have the capacity to trap and mineralise more than all the CO$_2$ emitted from the mining activities (Oskierski, Dlugogorski and Jacobsen, 2013; Harrison, Power and Dipple, 2013; Kandji et al., 2017). Turning these tailing piles into carbon mineralisation reactors could save the mineral processing (i.e. crushing) and transporting cost. Another means to reduce the cost is to use micro-organisms to optimise the dissolution of silicate phases and the precipitation of carbonates (Power, Dipple and Southam, 2010; Power et al., 2011, 2014). Known as bioleaching, this technique is already applied in low-grade ore recovery and avoids the use of expensive chemicals (Pradhan et al., 2008; Demergasso et al., 2010; Bryan et al., 2011).

1.3.2   *In situ* mineralisation

Natural mineral carbonation in the Oman-United Arab Emirates (Oman-UAE) ophiolite massif is estimated to consume 4×10^4 tons of CO_2 each year (Kelemen and Matter, 2008; Matter and Kelemen, 2009; Mervine et al., 2014). Laboratory experiments and theoretical calculations have shown that injecting heated CO_2-rich fluids into the mantle peridotites could be sufficient to enhance the peridotite carbonation rate by a factor of 106 (Kelemen and Matter, 2008; Kelemen et al., 2011). This carbon mineralisation system would be performing without the need of a reactor, significantly diminishing the cost. However, the mineral carbonation process in peridotite are still poorly constrained and further research is required. Nevertheless, field experiments in basalt aquifers have given promising results, *in situ* carbon mineralisation could be a significant part of the solution to the climate change if developed to an industrial scale (Gislason et al., 2010; Snæbjörnsdóttir et al., 2014; Matter et al., 2016).

1.3.3   Modelling of the system

The ultramafic rock-water-CO_2 (peridotite alteration) system plays a role in many processes (see 1.1 Peridotite alteration) and needs to be better understood. The characterisation of peridotite alteration would permit a prediction of the reaction of the system upon modification (e.g. increase of the CO_2 supply for the purpose of sequestration).

1.3.3.1   Bench scale: experimental water-rock reactions

Modelling this system requires information on the dissolution rates of mafic minerals, olivine and pyroxene (Oelkers, 2001; Oelkers and Schott, 2001; Daval et al., 2010; Saldi et al., 2013), the favourable conditions for carbonate precipitation (Saldi et al., 2009; Qafoku et al., 2012; Lafay et al., 2014), and the influence of secondary silicate phase formation (King, Plümper and Putnis, 2010; Daval et al., 2011; Sissmann et al., 2013). Experiments have been used to simulate the different conditions met by the system during its evolution and to observe the system reactions to parameter changes, such as pH (Pokrovsky and Schott, 2000; Daval et al., 2013) and partial pressure of CO_2 (pCO_2) (Hänchen et al., 2006; Hövelmann et al., 2011). Changes in rock permeability and porosity following primary mineral dissolution and secondary mineral precipitation are also investigated (Andreani et al., 2009; Hövelmann, Austrheim and Jamtveit, 2012; Kelemen and Hirth, 2012). These data are used to define the characteristics and the limitations of peridotite alteration in order to predict the ultramafic rock-water-CO_2 system behaviour.

1.3.3.2 Field scale: modelling a peridotite aquifer

Modelling the alteration of peridotite at field scale is limited by the access to the subsurface to study the water-rock reactions. It relies on the sampling of groundwater on the surface, in wadis and hyperalkaline springs, and at depth in wells, and comparing their chemical and isotopic composition to deduce the water-rock reactions that take place in the subsurface. The chemical evolution of groundwater in peridotite aquifers, linked to the rock alteration, was first documented in ophiolite massifs by Barnes & O'Neil (1969). Subsequent studies have suggested that the chemistry of the water evolves in two stages along the flow path in the peridotite aquifers of the Oman-UAE ophiolite massif (Neal and Stanger, 1985; Paukert et al., 2012) as well as in other peridotite-hosted systems (Barnes, O'Neil and Trescases, 1978; Bruni et al., 2002). Near the surface, groundwater is at equilibrium with the atmosphere and reacts with the peridotites in open-system conditions. This first step produces near-neutral (pH ~8), Mg^{2+}-HCO_3^--rich water (Type I). This Type I water can infiltrate deeper into the peridotite aquifer and continue to react with the rocks under closed-system conditions, isolated from the atmosphere. This second step produces hyperalkaline (pH >11), reduced, Ca^{2+}-OH^--rich, Mg^{2+}-HCO_3^--depleted waters (Type II). Bruni et al. (2002) and Paukert et al. (2012) have each proposed a reaction path model respectively based on observations in the European Southern Alps ophiolite and the Oman-UAE ophiolite. Both models are in agreement with the two-stage model proposed by Neal & Stanger (1985). However, different mechanisms are proposed to explain the chemical evolution of groundwater, in particular the pH increase between Type I and Type II waters. Paukert et al. (2012) argue that the pH increase is due to serpentinisation (Eq. 1), whereas Bruni et al. (2002) link this change to the extremely low pCO_2.

1.4   The Oman-United Arab Emirates ophiolite

An ophiolite is a piece of oceanic lithosphere that has been uplift during the closure of an ocean and emplaced on land. The oceanic lithosphere can be pinched between the two continental plates (e.g. in the Alps) or a part can be detached itself from the seafloor and be obducted on the continental shelf as the ocean close (e.g. the Oman mountains). Ophiolites provide an important, albeit imperfect, analogue of ocean lithosphere exposed on land (Dewey, 1976; Brookfield, 1977; Welland and Mitchell, 1977).
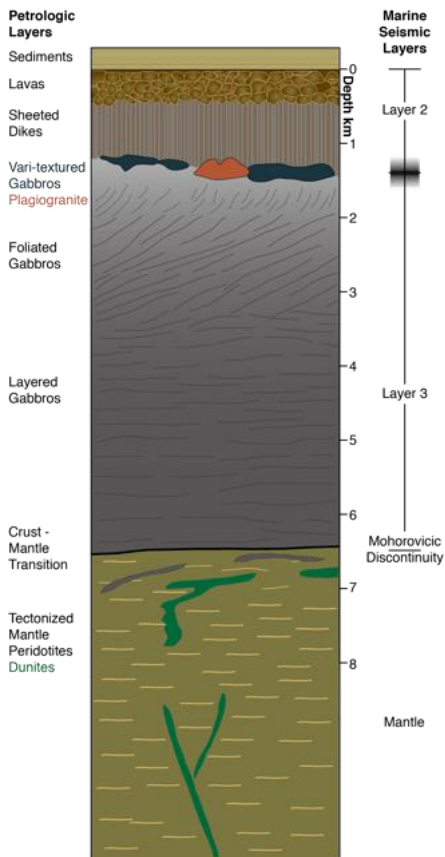
Figure 1.1: A typical ophiolite section is composed of, from top to bottom, marine sediments, pillow lavas, sheeted dikes, gabbros, layered gabbros and upper mantle peridotites.

1.4.1   History of formation

Initially called Semail ophiolite (Glennie et al., 1973, 1974), the Oman-United Arab Emirates (Oman-UAE) ophiolite crops out as a series of mountainous blocks along the north-east coast of the Sultanate of Oman and the United Arab Emirates. The name Oman-UAE ophiolite is preferred to avoid confusion with the Sumail (or Samail) massif present in the southern part of the ophiolite. The ophiolite belongs to the Tethyan ophiolite belt that spans from the Alpine-Apennine mountains in the west to the Oman mountains in the south-east that resulted from the closure of the Tethys Ocean, when the African(-Arabian) plate converged northward to meet the Eurasian plate ca. 100 Myr-ago (Coleman 1981; Fig. 1.1).
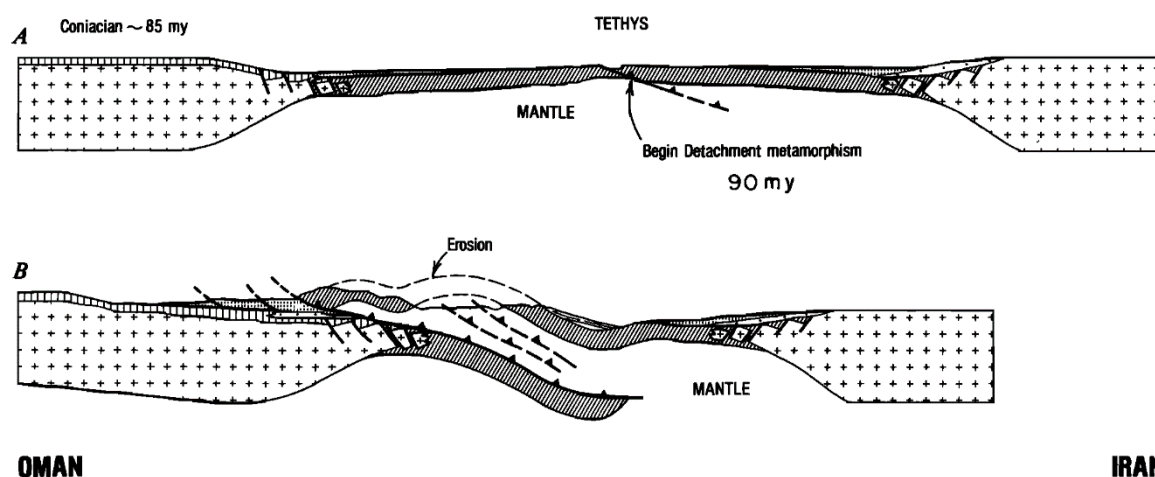
Figure 1.2: Schematic diagrams depicting detachment and initial emplacement of the Oman-UAE ophiolite. (Coleman, 1981).

The formation of the oceanic lithosphere was dated at 95 Ma ago using U-Pb ages of zircons from the Oman-UAE ophiolite crustal section (Tilton, Hopson and Wright, 1981; Rioux et al., 2012). The mechanisms of its obduction remain debated (Dewey, 1976; Gealey, 1977; Searle and Cox, 1999, 2002), but the absence of evidence of continental margin or island arc volcanism limits the number of possible processes (Coleman, 1981). Under the convergence scenario, a part of the oceanic lithosphere detached near the spreading centre; a weak point due to faulting (Fig. 1.2). The young and still hot slab was then pushed southward over the older and cooler oceanic lithosphere until it reached the Arabian continental shelf. K-Ar ages of amphibolites from the metamorphic sole, at the base of the ophiolite nappe, date this detachment at 90 Ma ago (Lanphere, 1981). After the primary uplift of the slab and the emersion of the ophiolite shortly after its detachment (Fig. 1.2), there was a series of sea transgression episodes during the Tertiary until the end of the Miocene (Bailey and Coleman, 1975). The first one is marked by the presence of pre-Maestrichtian laterite underlying Maestrichtian shallow marine limestone on top of the ophiolite nappe (Coleman, 1981). Subsequent sea transgression episodes occurred during the Tertiary, with the major ones during the lower and middle Eocene resulting in the deposition of hundreds of meters thick limestones (Stanger, 1986).

The Oman-UAE ophiolite is the most extensive slice of oceanic lithosphere thrust on land. It lies on a 475 km long NW-SE axis in a succession of massifs, extends for as much as 80 km southward, and has a relief up to 1000m (Coleman and Hopson, 1981) (Fig. 1.3). Some regions such as the Wadi Tayin massif in the south-east of the ophiolite expose a complete cross section of the oceanic lithosphere from basalts to upper mantle (Hopson et al., 1981; Boudier and Coleman, 1981). Most

of the tectonic deformations visible in the ophiolite appear to be ridge-related and metamorphic features accompanying its emplacement are almost absent (Nicolas et al., 2000a). This makes the Oman-UAE ophiolite an ideal analogue to study oceanic lithosphere settings and mechanisms (Nicolas and Boudier, 1995; Nicolas et al., 2000b).
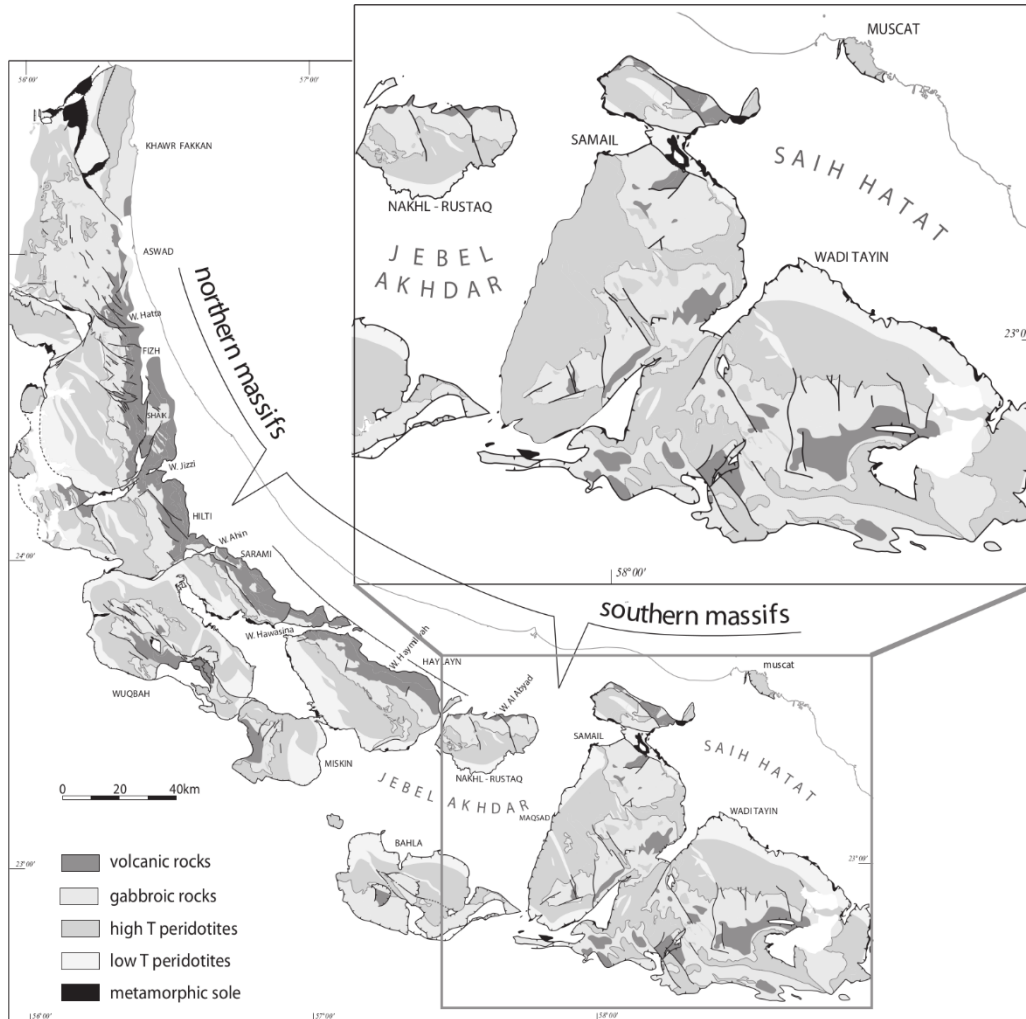
Figure 1.3: Simplified geological map of the Oman-UAE (Nicolas et al. 2000).

1.4.2   Geology of the mantle section

The mantle section of the Oman-UAE ophiolite is representative of the lithospheric (upper) mantle, in particular in the central and southern part, from Haylay to Wadi Tayin (Fig. 1.3), where the ophiolite section (Fig. 1.1) lies perpendicular to the Arabian shelf and shows limited post- or syn-obduction deformation (Nicolas et al., 2000a). The mantle section is composed of depleted peridotite (harzburgites). Its upper boundary is a dunite-rich layer called the Moho Transition Zone (MTZ) separating the crust from the mantle. Its lower boundary is the Hawasina group, which is composed of allochtonous carbonate sediments that were pushed onto the Arabian shelf during the oceanic plate obduction (Nicolas et al., 2000a). Peridotites from the Oman-UAE ophiolite are

heavily serpentinised (>50%), and are composed of olivine Fo_{90-91} (74%), orthopyroxenes En_{90-91} (24%) and clinopyroxenes (traces), and spinel (2%) as the dominant primary minerals (Boudier and Coleman, 1981; Hanghøj et al., 2010). Three types of peridotite domains with different geochemical compositions were identified in the ophiolite mantle section (Godard, Jousselin and Bodinier, 2000). (1) The residual mantle, composed of refractory and chemically homogeneous harzburgites that are extensively depleted in incompatible elements due to partial melting and melt-rock reactions (Godard, Bodinier and Vasseur, 1995; Hanghøj et al., 2010). (2) The mantle diapirs are an upwelling of partial melt from the asthenospheric (lower) mantle through the upper mantle. They are enriched in incompatible elements and favourable to the formation of chromite pods (Jousselin and Nicolas, 2000). (3) The clinopyroxene-rich harzburgites are located at the base of the mantle section. They were re-enriched by partial melts from the lower mantle (Boudier, Ceuleneer and Nicolas, 1988; Godard, Jousselin and Bodinier, 2000; Hanghøj et al., 2010).

The peridotites display lineation (elongation of minerals) and foliation (planes of aligned minerals) features in the areas associated with oceanic lithosphere magmatic and tectonic events during sea-floor spreading (Nicolas et al., 1988). The mafic and gabbroic dikes intruded into the ophiolite mantle section following these planes of weakness and are oriented parallel to the nearest tectonic deformation, such as shear zones or mantle diapir intrusions around which they are abundant (Jousselin and Mainprice, 1998; Nicolas et al., 2000c). These planes of weakness are also used by fluids, hydrothermal and groundwater to infiltrate the peridotite-hosted aquifer. Secondary minerals such as serpentine and carbonate are precipitated along these planes in veins ranging from millimetres to metres in width. They can also form a mesh network of veins <mm wide, subparallel to the foliation plane and sub-perpendicular to the lineation direction (Dewandel et al., 2003).

1.4.3   Hydrogeology

Rainfall in Oman is usually scarce but happens on a regular basis from November to April. Cold frontal troughs coming from the North Atlantic Ocean and the Mediterranean Sea are the main source of precipitation. The rainfall events are usually light (<10 mm) but can occasionally be catastrophic (>100 mm), resulting in flash floods in the wadis (Kwarteng, Dorvlo and Vijaya Kumar, 2001). From the average 250 mm/yr of rainfall, 7% (~18mm) contributes to recharge of the peridotite aquifer (Dewandel et al., 2005). The absence of soil and the long periods between each rainfall favour water infiltration before it evaporates, resulting in a high value of aquifer recharge for a semi-arid region (Dewandel et al., 2005).

During sea-floor spreading, tectonic constraints created faults in the oceanic lithosphere providing pathways for the seawater all the way down to the upper mantle (Gregory and Taylor, 1981). The infiltrated seawater was heated by the lithosphere before returning to the surface via narrow hydrothermal channels (Bickle and Teagle, 1992). Today, these faults and hydrothermal channels still play an unquantified role in the permeability of the ophiolite by channelling groundwater and allowing it to reach the deeper parts of the peridotite aquifer. The groundwater flow in the peridotite aquifer is directly linked to the rocks physical features (cracks, veins, and porosity). The upper 50 m of the peridotite rocks are fissured due to weathering, and possibly lithostatic decompression; these fractures allow rainwater to rapidly infiltrate the subsurface (Dewandel et al., 2005). In the subsurface, the rock permeability decreases quickly with increasing depth due to less fissuring and cracks filling with precipitated secondary minerals such as serpentine and carbonates. Below 50 m from the surface, in the deep aquifer, the open fissure network is not visible anymore, but the rock porosity (1%) allows further penetration of the water. The porosity comprises microcracks (0.4%) and nanopores (0.6%), and allow water flow (i.e. permeability) and water storage (i.e. storativity) in the rock (Dewandel et al., 2005). Both permeability and storativity are difficult to assess, in particular the contribution of nanopores, but are high enough to sustain a perennial water flow observed in the major wadis of the peridotite massif (Dewandel et al., 2005).
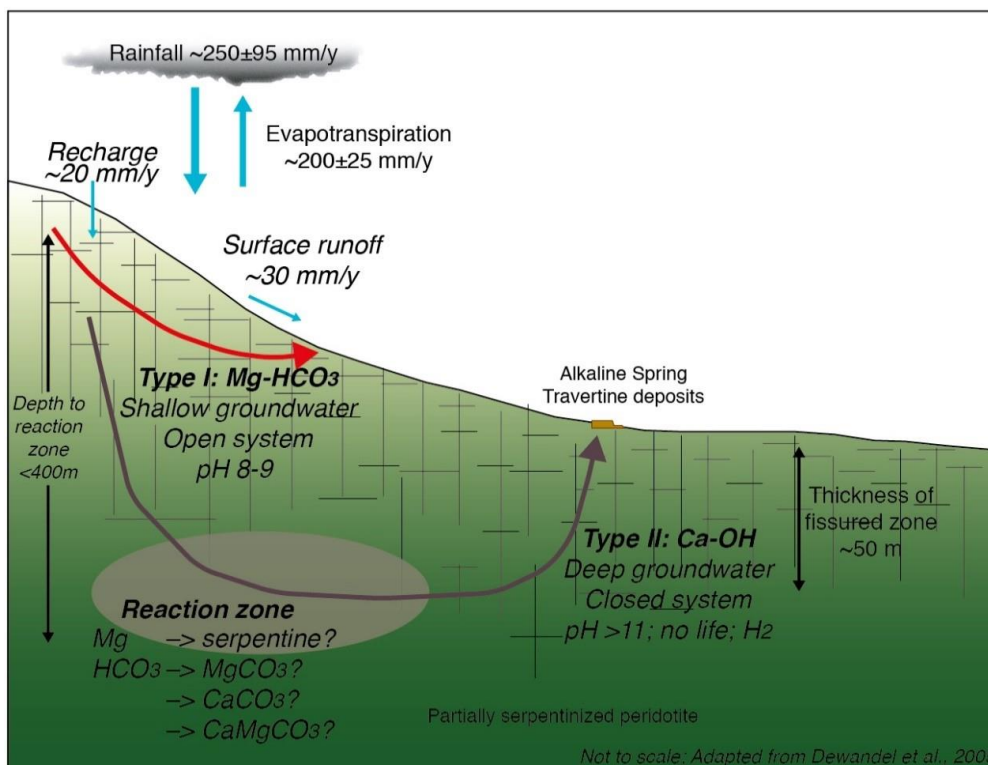
Figure 1.4: Schematic cross section of the interconnected aquifers system in the peridotite of the Oman-UAE ophiolite (Dewandel et al. 2005).

Dewandel et al. (2005) suggested a system of interconnected aquifers (Fig. 1.4), shallow and deeper, in agreement with the model proposed by Neal & Stanger (1985). (1) The water flows easily in the well fissured shallow aquifer (hydraulic conductivity = 10^{-7} m/s), reacting with the rocks and the atmosphere, and forming Type I water (see Introduction 1.3.3.2). (2) Part of the water then infiltrates the deeper aquifer and flows slowly through microcracks (hydraulic conductivity = 10^{-9} m/s) under close-system conditions, isolated from the atmosphere. The water-rock reactions in this confined aquifer produce Type II water that form hyperalkaline springs when it discharges at the surface (see Introduction 1.3.3.2). The low permeability of the deeper aquifer does not limit the extent of water-rock reaction taking place, but rather slow it down as the fluid needs to reach new surfaces, through diffusion or reaction-driven cracking of the rock, to react (Kelemen and Hirth, 2012; Plümper et al., 2016).

1.5   Other ophiolite systems

A number of ophiolite massifs exist around the world and have been studied to determine water-rock reactions taking place in their aquifers. (i) The Troodos ophiolite massif belongs to the Tethyan ophiolite belt and is located on the South-Eastern part of Cyprus, in the North-Eastern corner of the Mediterranean Sea. It comprises a full ophiolite sequence forming a dome structure and is surrounded by foothills of Cretaceous to Miocene age chalks. The annual rainfall on the ophiolite massif varies with altitude between 1000 and 500 mm (Neal and Shand, 2002). (ii) The Voltri Group ophiolite also belongs to the Tethyan ophiolite belt, it is the remains of the Liguro-Piedmont oceanic domain that was subducted and then exhumed during the Cretaceous-Tertiary Alpine convergence (Vanossi, 1984). It comprises three main units: (1) the Beigua unit is composed of metagabbros and metabasalts, (2) the Voltri-Rossiglione is composed of metasediment and metavolcanites, and (3) the Erro-Tobbio unit is composed of serpentinised lherzolites (Chavagnac et al., 2013; Cipolli et al., 2004). Antigorite is reported as the main serpentine mineral present in the lherzolites, which makes the mineralogy quite different from the Oman ophiolite (i.e. Chrysotile/lizardite in harzburgites). But extensive carbonate sediments deposits from the Cretaceous and Tertiary seems to be absent from the area (Cortesogno and Haccard, 1984; Bruni et al., 2002). The Ligurian ophiolite is much smaller than the Oman-UAE one, and their mineralogy and geological history are different. The Mediterranean climate in Liguria allows for more rainfall than in the semi-arid climate of Oman, which results in a dense vegetation coverage and more run off water readily diluting alkaline springs. All these factors seem to prevent the formation of extensive travertine terraces such as those observed in Oman. (iii) Six ultramafic bodies were studied in the western U.S.A.: Burro Mountain, Red Mountain, Table mountain, Joaquim Ridge and The Cedars massif in California and an ultramafic massif near John Day in Oregon (Barnes and O'Neil, 1971). They are discrete

ultramafic massifs sprinkled along the Western USA coastline, obducted as part of the Franciscan Subduction Complex. The Cedars is the main studied massif, it is composed of partly serpentinised (5 to 20%) harzburgite in the center of the body to completely serpentinised harzburgite in the body outter rim in contact with the surrounding rocks, marine sediments (sandstones and shales) from the Late Cretaceous (Morrill et al., 2013). The Cedars' harzburgite mineralogy (75% olivine, 25% pyroxenes) and chemistry is well characterise since it was chosen as the international peridotite standard (PCC-1) (Flanagan, 1969; Takazawa et al., 2000).

1.6   Chapter summaries

This thesis presents the results of a hydrogeochemical and isotopic study with the objective to identify and constrain the water-rock interactions responsible for the chemical evolution of groundwater along its flow path in the peridotite aquifers of the Oman-UAE ophiolite. Determining the type of rock that reacts with the groundwater enables identifying the processes, such as mineral dissolution and precipitation taking place along the flow path, and thus the potential sources and sinks for the ions in solution. The origin of calcium present in hyperalkaline springs is of prime interest and needs to be established in order to assess the potential of peridotite alteration as a sink for the carbon global cycle. A carbonate origin of Ca, from hydrothermal veins or sediments overlying the ophiolite, would not have any impact, as it would simply be a swap of a molecule of CO_2 between atmospheric and carbonate reservoirs (Eq. 4). Whereas a silicate origin, from peridotites or secondary silicate minerals, would result in a net uptake of CO_2 from the atmosphere during the precipitation of travertine terraces (Urey, 1952; Eq. 5), and make peridotite alteration a major asset in a strategy of climate change mitigation.

$$CaCO_3 + \underline{CO_{2(atm)}} = Ca\underline{CO_3} + CO_{2(atm)} \tag{4}$$

$$CaSiO_3 + \underline{CO_{2(atm)}} = Ca\underline{CO_3} + SiO_2 \tag{5}$$

Chapter 2: Isotopic system summaries

An overview of each of the three isotopic systems ([87]Sr/[86]Sr, δ^{88}Sr, and $\delta^{44/40}$Ca) used during this thesis are presented.

Chapter 3: Origin of the [87]Sr/[86]Sr signals and Strontium distribution in the altered peridotites of the Oman-UAE ophiolite

The Sr distribution and isotopic composition of five peridotite samples from the Oman-UAE ophiolite are investigated to document the alteration minerals contribution to their ^{87}Sr/^{86}Sr signal and its origin. The minerals, primary and secondary, were separated by hand picking and chemical attacks to obtain their Sr composition and determine the main ^{87}Sr/^{86}Sr signals present in the mantle section of the ophiolite.

Chapter 4: Tracing water-rock interaction in the peridotite aquifer of the Oman-UAE ophiolite using radiogenic strontium isotopes (^{87}Sr/^{86}Sr)

The ^{87}Sr/^{86}Sr ratios and major ions concentration of groundwater and rocks from the peridotite aquifer are used to investigate the water-rock interactions taking place along the flow path and determine which rocks are reacting with the water in the subsurface of the ophiolite mantle section.

Chapter 5: Tracking serpentinisation and carbonation with δ^{88}Sr and $\delta^{44/40}$Ca in the peridotite aquifer subsurface of the Oman-UAE ophiolite

The δ^{88}Sr and $\delta^{44/40}$Ca isotopic systems are used to track the geochemical processes taking place along the groundwater flow path in the peridotite aquifers. The combined use of these two isotopic systems with other chemical data (^{87}Sr/^{86}Sr, pH, [DIC], [Ca], [Mg], and [Sr]) enable distinguishing between the main water-rock reactions responsible for the development of Type I and Type II waters.

Chapter 2   Isotope system summaries

2.1 ^{87}Sr/^{86}Sr system

Radiogenic strontium ratios (^{87}Sr/^{86}Sr) are routinely used as a proxy to trace the sources and processes taking place in natural systems, such as identifying the rock sources of magma (Faure and Hurley, 1963; Gast, Tilton and Hedge, 1964) or the water-rock interactions in catchments and aquifers (Negrel et al. 2003; Frost and Toner 2004). Sr and Ca are both from the Alkaline Earth Group of chemical elements and have similar atomic radii (1.13Å & 0.99Å, respectively). Consequently, Sr^{2+} can substitute for Ca^{2+} in mineral lattice (Bailey et al., 1996; Schmitt and Stille, 2005) and Sr can be used as an, albeit imperfect, tracer for Ca.

The ^{87}Sr/^{86}Sr ratio is conventionally normalised during measurement to the natural ^{86}Sr/^{88}Sr ratio (0.1194) (Nier, 1938). This eliminates any mass-dependent isotopic fractionation effects. Whether the fractionation is natural or experimental, the ^{87}Sr/^{86}Sr measured records only the radiogenic ^{87}Sr content variations with respect to the ^{86}Sr in the sample (Faure and Hurley, 1963). The ^{87}Sr/^{86}Sr isotopic ratio increases with time as ^{87}Sr is formed via the radioactive beta decay of ^{87}Rb ($t_{1/2}$ = 4.9 x10^{10} years) (Faure and Mensing, 2005; Hurley et al., 1962). The higher the Rb/Sr ratio in the source, the higher the ^{87}Sr/^{86}Sr ratio. Thus, the ^{87}Sr/^{86}Sr of a source varies in line with two parameters: its age and its Rb content, linking the ratio to the source's nature and history of formation.

In active systems ^{87}Sr/^{86}Sr varies as a function of the mixing of Sr from different sources. The ^{87}Sr/^{86}Sr ratio of the mixture is determined by the ^{87}Sr/^{86}Sr ratio, the Sr concentration, and the fraction of Sr in the mix provided by each of the sources. Hence, the ^{87}Sr/^{86}Sr ratio and Sr concentration of a mixture can yield informations about its sources (e.g. rock, water type) and its formation such as mineral precipitation/dissolution, water mixing (Clauer, 1979; Hart, 1988; Åberg, Jacks and Joseph Hamilton, 1989; Bain and Bacon, 1994; Palmer and Edmond, 1992; Capo, Stewart and Chadwick, 1998; Faure and Hurley, 1963; Gast, Tilton and Hedge, 1964).

2.2   δ$^{44/40}$Ca system

Stable calcium isotopes have been used for a couple of decades to investigate geochemical processes such as the role of carbonate precipitation in the evolution of seawater chemistry and carbon cycle (DePaolo, 2004; Fantle and Tipper, 2014). Calcium isotope values are reported as δ$^{44/4x}$Ca=((^{44}Ca/^{4x}Ca)$_{SAMPLE}$/(^{44}Ca/^{4x}Ca)$_{STANDARD}$)−1) × 1000, typically using the isotopic ratios $^{44/40}$Ca or $^{44/42}$Ca. The $^{44/42}$Ca ratio was proposed to avoid issues due to interferences with ^{40}Ar during MC-ICP-

MS analyses (Halicz et al., 1999) or to radiogenic increase of ^{40}Ca in K-rich samples. However, ^{42}Ca has a very low abundance and increases of ^{40}Ca from ^{40}K decay have only been detected in samples with [K]>[Ca] (Hippler et al., 2003). The use of a double-spike method and measurement on a TIMS solves most of these issues and the $^{44/40}$Ca ratio is preferred because of its larger mass difference and isotope abundance (Lehn, Jacobson and Holmden, 2013). The $\delta^{44/40}$Ca ratios can be reported to three different standards: Bulk Silicate Earth (BSE) (DePaolo, 2004), seawater (Hippler et al., 2003) and NIST SRM 915 (Fantle and Tipper, 2014). The difference of $\delta^{44/40}$Ca of NIST SRM 915a to seawater was defined as -1.88 ± 0.04‰ (Hippler et al. 2003).
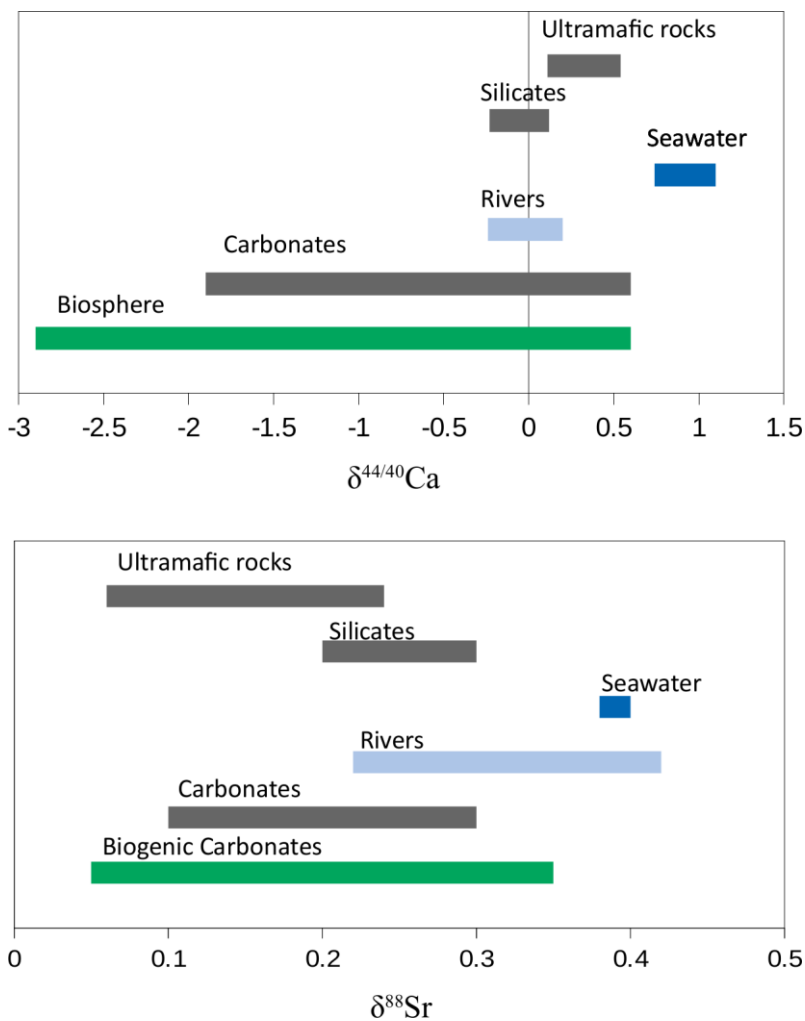
Figure 2.1: Ranges of calcium and stable strontium isotope ratios from diverse environments.

Data suggest that $\delta^{44/40}$Ca ratios vary by ~4‰ through the global Ca biogeochemical cycle, without taking into account the effect of radiogenic ^{40}Ca (Fig. 2.1; Fantle & Tipper 2014). At the Earth's surface, silicates have $\delta^{44/40}$Ca ranging from -0.23 to 0.12‰ (Skulan, DePaolo and Owens, 1997); ultramafic rocks have $\delta^{44/40}$Ca values between 0.11‰ and 0.54‰ (Amini et al., 2009); carbonates have an average $\delta^{44/40}$Ca of -0.3‰ with values varying between -1.9 and +0.6‰ (Fantle & Tipper 2014); and the biosphere display $\delta^{44/40}$Ca values between -2.9 to +0.6‰ (Fantle and Tipper, 2014).

The main terrestrial reservoir is the ocean that has an average $\delta^{44/40}Ca$ of 0.92±0.18. It is fed by rivers with an average $\delta^{44/40}Ca$ composition of -0.02‰ and values ranging from -0.24 to 0.2‰ (Schmitt, Chabaux and Stille, 2003; Fantle and Tipper, 2014), and hydrothermal fluids with $\delta^{44/40}Ca$ = -0.17 to 0.29‰ (Amini et al., 2008; Schmitt, Chabaux and Stille, 2003), both accounting for a global flux of $\delta^{44/40}Ca$ of -0.18±0.2‰ to the ocean (Schmitt, Chabaux and Stille, 2003). Schmitt et al. (2003) made an argument for a steady-state ocean during the last 19Ma based on an equivalent Ca output in carbonate sedimentation ($\delta^{44/40}Ca$ = -0.28±0.1‰). This conclusion has been challenged since and it has been argued that this carbonate sedimentation output $\delta^{44/40}Ca$ was significantly different from that of the river input (Fantle and DePaolo, 2007; Fantle and Higgins, 2014). The effect of isotopic fractionation during carbonate precipitation and diagenesis on the $\delta^{44/40}Ca$ of carbonates and associated pore-fluids has been investigated to account for this imbalance (Fantle and Higgins, 2014).

Carbonate precipitation preferentially incorporates lighter Ca isotopes, with the extent of isotopic fractionation varying from 0.0‰ to -1.5‰. This is due to the Ca^{2+} ions forming stronger bonds with aqua-complexes than with carbonate ions (Marriott et al., 2004; Lemarchand, Wasserburg and Papanastassiou, 2004; DePaolo, 2004; Ohno et al., 2008; Böhm et al., 2012; Fantle and DePaolo, 2007). The fractionation factor between carbonate and solution is determined by two main processes. (1) The availability of Ca^{2+} to precipitate with carbonate ions, which depends on the saturation state, pH, and temperature of the solution that control the ions diffusion from the bulk solution to the precipitating crystal surface; if Ca^{2+} is readily available, the lighter isotopes will preferentially precipitate as they require less energy to move, hence increasing the fractionation factor (Gussone et al., 2005; Tang et al., 2008; DePaolo, 2011; Lemarchand, Wasserburg and Papanastassiou, 2004); and (2) The capacity of the crystal surface to re-equilibrate with the solution before being buried in the mineral lattice, which depends on the rate of precipitation and the temperature; the faster the rate of precipitation the lesser time for re-equilibration, and the higher the temperature the faster calcium isotopes can re-equililibrate (Fantle and DePaolo, 2007; Tang et al., 2008; DePaolo, 2011). It has been shown that given enough time equilibrium is always reached between the carbonate and the fluid ($\Delta_{calcite-fluid}$ = 0‰), such as in deep sediment during diagenesis (Fantle and DePaolo, 2007), but also in carbonate-hosted aquifers (Jacobson and Holmden, 2008). The fractionation factor of Ca between carbonate and fluid also depends on the type of carbonate, probably due to the differing layout of calcium atoms in the crystal lattice of each minerals. Aragonite has been shown to have a constant offset of -0.6‰, compared to calcite at the same precipitation conditions (Amini et al., 2008; Gussone et al., 2005); whereas dolomite displays a maximum $\Delta_{dolomite-fluid} \leq 0.4$‰ and $\delta^{44/40}Ca$ between -0.74‰ and 0.76‰, with an average of $\delta^{44/40}Ca_{dol}$ = 0.44‰, clearly distinctive from the average carbonate values (Blattler, Miller and

Higgins, 2015; Fantle and Tipper, 2014). However, in a more recent study, Fantle & Higgins (2014) found that dolomite formed during diagenesis had an average $\delta^{44/40}$Ca within error of the one from surrounding limestones.

In terrestrial systems, the $\delta^{44/40}$Ca of river water is mainly influenced by the precipitation of secondary carbonates and clays, and by the uptake of Ca by plants, both processes driving the riverine $\delta^{44/40}$Ca toward higher values ($\Delta_{biosphere-Ca\ source} \leq$ -1‰) (Cenki-Tok et al., 2009; Ockert et al., 2013; Jacobson et al., 2015; Liu et al., 2017; Schmitt, Chabaux and Stille, 2003; Fantle and Tipper, 2014). Riverine $\delta^{44/40}$Ca variations can also result from conservative mixing of different sources and recycling of Ca from plants (Jacobson and Holmden, 2008; Moore et al., 2013; Fantle and Tipper, 2014).

In hydrothermal systems, the $\delta^{44/40}$Ca of the exiting fluid is close to that of silicate rocks (av. $\delta^{44/40}$Ca = -0.04 ± 0.19‰; Schmitt et al., 2003), suggesting that no fractionation takes place (Zhu and Macdougall, 1998; Schmitt, Chabaux and Stille, 2003). However, anhydrites found at the Logatchev hydrothermal field have a $\delta^{44/40}$Ca ~ -0.18‰, that would require the fluid from which they precipitated to have a $\delta^{44/40}$Ca between -0.25 and -0.53‰ (Amini et al., 2008). This challenges the assumption that no fractionation occurs in hydrothermal systems, and would require that the contribution of hydrothermal systems to the Ca budget of the ocean be reconsidered.

2.3 δ^{88}Sr system

Stable strontium isotopes have become a new geochemical tool to track and characterise rock alteration processes. Unlike ^{87}Sr/^{86}Sr, which is normalised to a fixed ^{86}Sr/^{88}Sr ratio of 0.1192 and hence is insensitive to mass-dependant fractionation, the ^{88}Sr/^{86}Sr is reported as δ^{88}Sr=((^{88}Sr/^{86}Sr)$_{SAMPLE}$/(^{88}Sr/^{86}Sr)$_{NBS987}$)−1) × 1000, which is sensitive to mass-dependant fractionation occurring during geological processes. δ^{88}Sr values measured so far in natural and reference materials cover a total range of ~2.4‰ (Fig. 2.1; Neymark et al. 2014). The δ^{88}Sr values reported in the literature for terrestrial rocks vary by ~0.60‰ with values between +0.1‰ and +0.3‰ for terrestrial carbonate rocks (Halicz et al., 2008; Ohno et al., 2008); +0.05‰ and +0.35‰ for biogenic marine carbonates (Fietzke and Eisenhauer, 2006; Halicz et al., 2008; Rüggeberg et al., 2008; Stevenson et al., 2014), and an overall average carbonate value of 0.28±0.13‰ (Halicz et al., 2008). Terrestrial silicate rocks have δ^{88}Sr values between +0.2 and +0.3‰ (Charlier et al., 2012;Ma et al., 2013; Moynier et al., 2010), with an average silicate earth δ^{88}Sr value of 0.27±0.05‰ (Moynier et al. 2010).

River water generally have δ^{88}Sr values between 0.22‰ and 0.42‰, with an average value of 0.32±0.005‰ exported to the oceans (Pearce et al., 2015; Andrews et al., 2016; Liu et al., 2017).

But seasonal variations and high carbonate-alkalinity in streams can result in a wider range from 0.15‰ to 0.66‰ (Wei et al., 2013; Shalev et al., 2017). Hydrothermal end-member fluids have $\delta^{88}Sr$ ~0.24‰, similar to the value of the oceanic crust. A few outliners display higher $\delta^{88}Sr$ values linked to the precipitation of alteration phases (e.g. anhydrite) (Pearce et al., 2015). Seawater has a $\delta^{88}Sr$ of 0.39±0.01‰ (Fietzke and Eisenhauer, 2006; Ohno and Hirata, 2007; Pearce et al., 2015; Halicz et al., 2008). Compared to riverine and hydrothermal systems, the seawater value is higher, which can be explained by the preferential incorporation of lighter isotopes within carbonate during precipitation (Fietzke and Eisenhauer, 2006; Ohno et al., 2008; Böhm et al., 2012).

Similar to the Ca-isotope system, heavier Sr isotopes preferentially stay in solution. Diverse processes can uptake Sr from water and isotopically fractionate it, such as carbonate precipitation (Fietzke and Eisenhauer, 2006; Bohm et al., 2012; Stevenson et al., 2014), clay formation (Halicz et al., 2008; Wei et al., 2013; Pearce et al., 2015), and plant uptake (Souza et al., 2010; Andrews et al., 2016). Incongruent mineral dissolution is thought to preferentially release heavier Sr isotopes (Wei et al., 2013; Chao et al., 2015, Pearce et al., 2015). Some of these mechanisms are more prevalent than others depending on the environmental conditions. For example, fractionation within calcite increases with its precipitation rate but is negligible at equilibrium: $\Delta^{88}Sr_{cal\text{-}aq}$ = 0.00 to −0.37‰ (Fietzke and Eisenhauer, 2006; Ohno et al., 2008; Böhm et al., 2012; Raddatz et al., 2013; Vollstaedt et al., 2014; Stevenson et al., 2016; Liu et al., 2017; Shalev et al., 2017), whereas aragonite appears to have a constant/independant $\Delta^{88}Sr_{arag-aq}$ = -0.2‰ (Fruchter et al., 2016). During soil formation, plant uptake can fractionate the Sr pool by 0.2 to 0.5‰, but it will be significant only in the soil water of areas with dense vegetation (Souza et al., 2010; Andrews et al., 2016). Pedogenic carbonate precipitation consumes Sr in the groundwater, resulting in substantial ^{88}Sr enrichment of the residual Sr in soil water (up to $\delta^{88}Sr$ = 0.66‰) (Shalev et al., 2017) Incongruent mineral dissolution preferentially release heavier isotopes but has limited fractionation power and would mainly be observable in waters with low Sr concentration (Pearce et al., 2015; Liu et al., 2017). Finally, the preferential adsorption of lighter isotopes onto particles would drive the soil water $\delta^{88}Sr$ toward higher values ($\Delta^{88}Sr_{part\text{-}aq}$ = ~0.07) but with negligible effects (Chao et al., 2015; Liu et al., 2017; Shalev et al., 2017).

2.4   Methodologies

Sr-isotopes ratios (both $\delta^{88}Sr$ and $^{87}Sr/^{86}Sr$) were measured on a Thermal Ionisation Mass Spectrometer (TIMS) Triton at the University of Southampton. Sub-samples containing 1 µg of Sr were separated in two aliquots containing 500 ng of Sr each. An appropriate amount of ^{84}Sr-^{87}Sr double spike was added to one of them before separating the Sr by following a standard column

procedure using an Eichrom strontium specification ion exchange resin (Pearce et al. 2015). Radiogenic (^{87}Sr/^{86}Sr) ratios were directly measured in the unspiked aliquots and normalised to a fixed ^{86}Sr/^{88}Sr ratio of 0.1194 (Nier, 1938). The stable Sr (δ^{88}Sr) ratios were determined by combining unspiked and ^{84}Sr-^{87}Sr spiked aliquot data and by deconvolving them using the exponential fractionation law and Newton-Raphson iteration technique in ^{87}Sr denominator space (Pearce et al. 2015). This methodology allows to measure both Sr-isotope system in one sample and is in place as a routine protocol at the university of Southampton. The NIST987 standard has a δ^{88}Sr long-term value of 0.00‰ ($2\sigma = 0.01$‰) and an ^{87}Sr/^{86}Sr long-term value of 0.710256 ($2\sigma = 0.000013$) on our instrument, and the ^{87}Sr/^{86}Sr ratios were normalised to a NIST987 value of 0.710248 to allow the comparison between different studies (McArthur et al. 2012).

Samples were sent to the department of Earth Sciences at the University of Cambridge where they were combined with a ^{42}Ca-^{48}Ca double spike and calcium was separated using a Dionex ICS-5000$^+$ IC system. The $\delta^{44/40}$Ca isotopic ratios were then measured on a TIMS (Bradbury and Turchyn, 2018). During a preliminary study some of our samples were measured, following a similar protocol, in the department of Earth and Planetary Science at the University of California, Berkeley.

The main obstacle to measure these isotopic systems is the effective separation of the element of interest. In the case of the Sr, separating 1 µg of Sr from a sample with very low Sr concentration can require to process inadequate quantity of material. Developing a methodology requiring less Sr to run these analyses could help improve the overall procedure (Andrews et al., 2016). In the case of Ca, a high concentration of Mg can mask the Ca pic during the Dionex ICS-5000$^+$ analyse and make the separation of Ca based on its pic location impossible. An attempt at separating the Mg first in order to reduce its signal using Mg column was unfortunately unsuccessful. A procedure allowing the effective separation of Ca even from samples with a high Mg concentration should be addressed in future studies.

Chapter 3   Origin of the ^{87}Sr/^{86}Sr signals and strontium distribution in the altered peridotites of the Oman-UAE ophiolite

Abstract:

Low-temperature peridotite alteration produces two types of fluid in the Oman-United Arab Emirates ophiolite, (I) Mg-HCO3 rich, pH <10 fluids and (II) Ca-OH rich, pH >10 fluids. The sources of Ca^{2+} in the hyperalkaline fluids and the chemical evolution of the water composition in the peridotite aquifers were previously investigated using radiogenic strontium isotope ratios (^{87}Sr/^{86}Sr) and changes in the chemical composition of groundwater. The data indicated a combination of water-rock reaction pathways with both primary and secondary minerals found within the aquifer rocks. Groundwater evolution is dominated by low-temperature serpentinisation and carbonate dissolution/precipitation reactions, but the ^{87}Sr/^{86}Sr ratios of pre-existing secondary minerals such as serpentine and carbonates, and the Sr distribution between the different minerals in the peridotites remain unconstrained. In this study, the main secondary minerals, serpentine, carbonates, and brucite were separated by hand picking and a set of chemical reaction with reagents targetting specific minerals in order to measure their ^{87}Sr/^{86}Sr ratio and Sr concentration. The data obtained reveal that the primary mantle ^{87}Sr/^{86}Sr ratio is not the dominant signal in the altered peridotites of the Oman-UAE ophiolite. The ^{87}Sr/^{86}Sr ratios of the peridotites result from the mixing of four signals: primary mantle (^{87}Sr/^{86}Sr = 0.7023-0.7045), Cretaceous seawater (^{87}Sr/^{86}Sr = 0.7072-0.7079), Tertiary seawater (^{87}Sr/^{86}Sr = 0.7080 to 0.7085), and modern seawater (^{87}Sr/^{86}Sr = ~0.7092). The Sr concentration of secondary alteration minerals exceeds that of the remaining primary minerals, suggesting that their ^{87}Sr/^{86}Sr signal will be dominant during water-rock reactions. Furthermore, the determination of the ^{87}Sr/^{86}Sr signals within the peridotites and the secondary minerals enable us to match them with past seawater and gather information on the ophiolite alteration history.

Chapter 3

3.1   Introduction

In ophiolite massifs, the low-temperature alteration of peridotite produces high pH, Ca-OH-rich fluids that precipitate massive carbonates deposits (travertine terraces) upon surfacing in springs and reacting with atmospheric CO_2 or HCO_3^--rich surface waters (Barnes and O'Neil 1971; Kelemen and Matter 2008). Serpentinisation, oxidation, and carbonation of peridotites (Eq. 1, 2, & 3) are the three main reactions taking place and controlling the chemical evolution of groundwater along its flow path in peridotite aquifers (Johannes 1969; Martin and Fyfe 1970; Evans 1977; Frost 1985; Malvoisin et al. 2012).
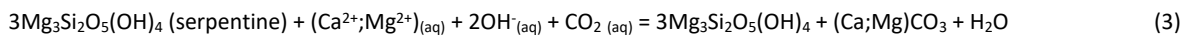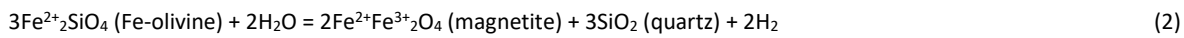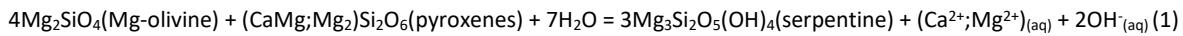
$4Mg_2SiO_4(Mg\text{-}olivine) + (CaMg;Mg_2)Si_2O_6(pyroxenes) + 7H_2O = 3Mg_3Si_2O_5(OH)_4(serpentine) + (Ca^{2+};Mg^{2+})_{(aq)} + 2OH^-_{(aq)}$ (1)

$3Fe^{2+}_2SiO_4 (Fe\text{-}olivine) + 2H_2O = 2Fe^{2+}Fe^{3+}_2O_4 (magnetite) + 3SiO_2 (quartz) + 2H_2$ (2)

$3Mg_3Si_2O_5(OH)_4 (serpentine) + (Ca^{2+};Mg^{2+})_{(aq)} + 2OH^-_{(aq)} + CO_{2\ (aq)} = 3Mg_3Si_2O_5(OH)_4 + (Ca;Mg)CO_3 + H_2O$ (3)

These water-rock reactions can induce rock fracturing (Jamtveit, Putnis, and Malthe-Sørenssen 2009; Kelemen and Hirth 2012), provide a carbon sink (Kelemen and Matter 2008; Matter and Kelemen 2009; Kelemen et al. 2011; Paukert et al. 2012), and support extremophile microbial communities (Macleod et al. 1994; Miller et al. 2016; Shibuya, Russell, and Takai 2016; Rempfert et al. 2017).

Analysis of $^{87}Sr/^{86}Sr$ ratios is a geochemical tool commonly used to determine the sources of water and the rocks with which it has reacted in aquifers through a simple mixing equation between two Sr sources (Eq. 4) (Faure & Mensing, 2005).

$[Sr]_M \times {}^{87}Sr/{}^{86}Sr_M = f \times [Sr]_A \times {}^{87}Sr/{}^{86}Sr_A + (1\text{-}f) \times [Sr]_B \times {}^{87}Sr/{}^{86}Sr_B$ (4)

With A and B being the two sources of Sr that combine to produce the mixing end-member M, and f the fraction of source A in M.

In another study (Chapter 4), $^{87}Sr/^{86}Sr$ ratios were used to follow the groundwater evolution and determine the extent of the water-rock reactions in the peridotite aquifer of the Oman-United Arab Emirates (Oman-UAE) ophiolite. Based on the model proposed by Dewandel et al. (2005), rainwater and peridotites were chosen as the two main Sr sources reacting together to produce the hyperalkaline spring end-member. There are no $^{87}Sr/^{86}Sr$ ratios published for rainwater in the Oman-UAE ophiolite and it was assumed to be the same as that of modern seawater (0.7092) (McArthur et al., 2012). But there are 27 published $^{87}Sr/^{86}Sr$ ratios for peridotites from the Oman-UAE ophiolite (McCulloch et al. 1980; Boudier and Coleman 1981; Lanphere, Coleman, and Hopson 1981; Kawahata et al. 2001; Gerbert-Gaillard 2002; Stephen 2014). They cover a wide range, from 0.7031 to 0.7088 (av.$^{87}Sr/^{86}Sr$ =0.7066 ±0.0016; Table 3.1; Fig. 3.1), and are reported as whole rock
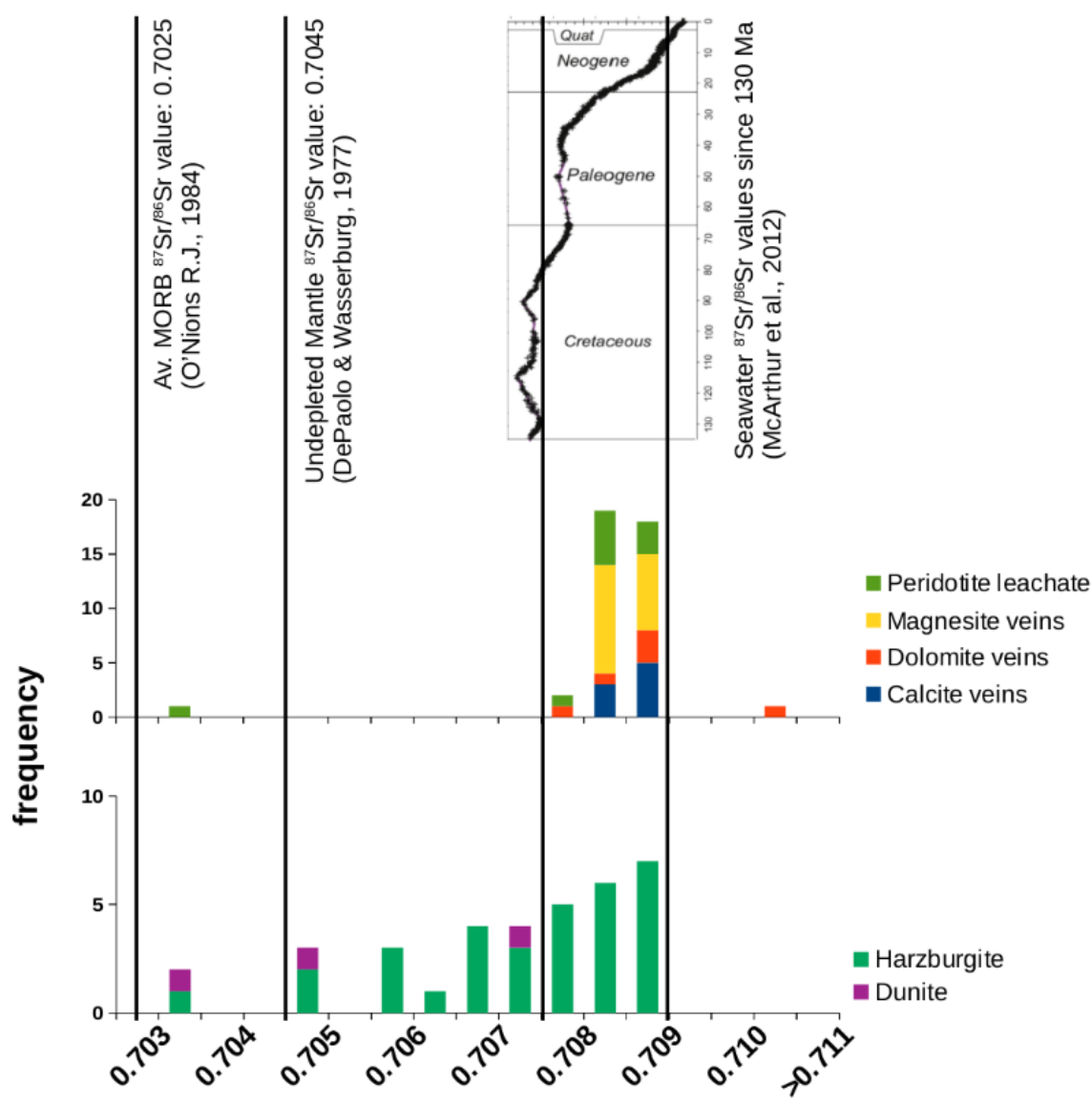
Figure 3.1: Compilation of Sr-isotope values ($^{87}Sr/^{86}Sr$) of rock samples from the literature and this study. The frequency represents the number of samples within each interval of $^{87}Sr/^{86}Sr$ value. Rock samples are from the mantle section of the southern part of the ophiolite (Samail and Wadi Tayin massifs).

values with little or no indication about the rock preparation prior to analyses (e.g. handpicked minerals, acid cleaning). However, the lower part of the range is in agreement with the primary $^{87}Sr/^{86}Sr$ ratio inferred for mantle peridotites at spreading ridges based on the $^{87}Sr/^{86}Sr$ of mid-oceanic ridge basalts (0.7023 – 0.7033) (O'Nions and Pankhurst 1974; Hart, Erlank, and Kable 1974; Snow, Hart, and Dick 1994). The study of Lanphere et al. (1981) indicates that igneous rocks in the Oman-UAE ophiolite come from a depleted mantle region consistent with a spreading-ridge context. The higher $^{87}Sr/^{86}Sr$ values of peridotites are most likely the result of hydrothermal alteration of the peridotites by seawater (Lanphere et al., 1981). The published $^{87}Sr/^{86}Sr$ data (Table 3.1) originate from peridotite samples that are lightly to extensively altered, but no $^{87}Sr/^{86}Sr$ ratios have been published for the alteration minerals (e.g. serpentine, talc, saponite, brucite). Nevertheless, 18 leachates of peridotite were analysed by Gerbert-Gaillard (2002) with $^{87}Sr/^{86}Sr$

ratios between 0.7076 and 0.7089 (one outliner has an $^{87}Sr/^{86}Sr$ = 0.7031; Table 3.2; Fig. 3.1), and 31 carbonate veins, present within the mantle rocks of the Oman-UAE ophiolite, were reported with a similar range ($^{87}Sr/^{86}Sr$ = 0.7077 to 0.7088; Table 3.2; Fig. 3.1) (Weyhenmeyer, 2000; Kelemen et al., 2011, Stephen, 2014). This suggests that alteration minerals have an $^{87}Sr/^{86}Sr$ signal different from the mantle value, and more similar to a seawater $^{87}Sr/^{86}Sr$ ratio, potentially corresponding to the time of their formation.

Table 3.1: Compilation of published $^{87}Sr/^{86}Sr$ ratios of peridotites from the Oman-UAE ophiolite.

Sample ID	Published in	Rock type	$^{87}Sr/^{86}Sr$ Norm	2σ (10⁻⁶)	Sr μmol/kg	%RSD
JGU31.3		Harzburgite	0.70858	18	16.0	D.Lim = 1.1µmol/kg
ASO6	Stephen (2014)	Harzburgite	0.70478	18	3.4	D.Lim = 1.1µmol/kg
RTU11		Harzburgite	0.70878	18	8.0	D.Lim = 1.1µmol/kg
RTU11		Harzburgite	0.70812	18	8.0	D.Lim = 1.1µmol/kg
94OE11		Cpx harzburgite	0.70852	12	53.4	0.6
94OE13		Cpx harzburgite	0.70663	8	3.4	3.1
94OE17		Cpx harzburgite	0.70597	15	0.9	12.5
94OE8		Cpx harzburgite	0.70626	15	8.1	1.3
99OL18		Cpx harzburgite	0.70757	15	10.6	2.2
99OL3		Cpx harzburgite	0.70850	17	6.9	2.8
OMB14		Cpx harzburgite	0.70734	10	1.2	5.4
OMB27		Cpx harzburgite	0.70697	12	10.7	4.8
93OA11A	Gerbert-Gaillard (2002)	Dunite impr.	0.70709	15	62.1	1.7
95OD74A		Dunite impr.	0.70307	10	857.1	0.8
93OF22		Harzburgite	0.70561	10	9.0	6.4
95OD107		Harzburgite	0.70821	10	na	na
96OF59		Harzburgite	0.70730	12	72.6	2
99OL26		Harzburgite	0.70796	8	26.5	1.1
99OL46		Harzburgite	0.70699	18	68.3	1.6
99OL48a		Harzburgite	0.70746	8	280.6	1.1
91OA29		Harzburgite	0.70751	5	na	na
94OE27		Harzburgite	0.70460	9	3.9	3.5
FZ-1A	Kawahata et al. (2001)	Harzburgite tectonite serpentinized	0.70688	na	6.8	<2
FZ-1B		Harzburgite tectonite serpentinized	0.70778	na	26.2	<2
K-22-p1	Lanphere et al. (1981)	Harzburgite tectonic	0.70592	24	12.6	1
K20-p2		Cpx dunite	0.70459	22	46.2	1
K22 (non-normalised)	McCulloch et al. (1980)	Harzburgite	0.70313	9	4.9	Blk = 0.1ng

Based on the simple mixing model, a low mantle $^{87}Sr/^{86}Sr$ value (~0.7030) was expected for the fluid end-members, but the $^{87}Sr/^{86}Sr$ ratios of the water samples range from 0.70670 to 0.70916 (Chapter 4) closer to the range of alteration minerals rather than that of peridotites. Two hypothesis are considered: (1) that the peridotites of the Oman-UAE ophiolite have a mantle $^{87}Sr/^{86}Sr$ value but groundwater does not interact sufficiently with the rocks to reach the mantle isotopic composition; thus, groundwater $^{87}Sr/^{86}Sr$ ratios are a mix between rainwater and peridotites $^{87}Sr/^{86}Sr$ ratios. (2) Groundwater interacts significantly with the peridotites to take up their $^{87}Sr/^{86}Sr$ ratio but the peridotites no longer have a mantle primary $^{87}Sr/^{86}Sr$ value; seawater and rainwater $^{87}Sr/^{86}Sr$ signals have replaced, or mixed with, the mantle signal of peridotites during the successive alteration episodes throughout the geological history of the ophiolite, from its formation in the Cretaceous sea floor, through obduction, to the modern environment.

Table 3.2: Compilation of published ^{87}Sr/^{86}Sr ratios of peridotite leachates and carbonate veins from the Oman-UAE ophiolite.

Sample ID	Published in	Rock type	^{87}Sr/^{86}Sr Norm	2σ (10^{-6})	Sr mmol/kg
94OE11		Cpx harzburgite leachate	0.70860	9	na
94OE13		Cpx harzburgite leachate	0.70890	10	na
94OE17		Cpx harzburgite leachate	0.70825	8	na
94OE8		Cpx harzburgite leachate	0.70856	16	na
99OL18		Cpx harzburgite leachate	0.70792	8	na
99OL3		Cpx harzburgite leachate	0.70859	14	na
OMB14		Cpx harzburgite leachate	0.70843	11	na
OMB27		Cpx harzburgite leachate	0.70827	21	na
93OA11A		Dunite impr. leachate	0.70840	13	na
95OD74A	Gerbert-Gaillard (2002)	Dunite impr. leachate	0.70310	9	na
91OA29		Harzburgite leachate	0.70851	9	na
93OF22		Harzburgite leachate	0.70857	8	na
94OE27		Harzburgite leachate	0.70762	17	na
95OD107		Harzburgite leachate	0.70843	18	na
96OF59		Harzburgite leachate	0.70846	12	na
99OL26		Harzburgite leachate	0.70823	12	na
99OL46		Harzburgite leachate	0.70842	8	na
99OL48a		Harzburgite leachate	0.70851	10	na
ASO20-C1		Calcite vein	0.70831	18	2.26
ASO20-C4		Calcite vein	0.70839	18	1.52
ASU52-C1		Calcite vein	0.70875	18	63.14
ASU52-C2		Calcite vein	0.70874	18	36.46
ASU54-C15		Calcite vein	0.70882	18	3.08
ASU54-C19		Calcite vein	0.70869	18	10.55
ASO1-C		Magnesite vein	0.70846	18	2.37
ASO2-C	Stephen (2014)	Magnesite vein	0.70848	18	1.59
ASU11-C		Magnesite vein	0.70848	18	7.34
ASU3-C		Magnesite vein	0.70865	18	4.49
ASU70-C		Magnesite vein	0.70866	18	163.56
ASU72-C		Magnesite vein	0.70844	18	8.22
ASU8-C		Magnesite vein	0.70825	18	0.49
JGU23.12-C		Magnesite vein	0.70868	18	30.48
JGU3.1-C		Magnesite vein	0.70837	18	0.16
JGU3.2-C		Magnesite vein	0.70838	18	0.33
OM07-30B		Calcite vein	0.70855	na	4.49
OM07-17		Calcite/Dolomite vein	0.70848	na	3.04
OM07-05	Kelemen (2011)	Dolomite vein	0.70869	na	16.47
OM07-27		Dolomite vein	0.70850	na	3.52
OM07-54		Dolomite vein	0.70858	na	11.22
OM07-61C		Dolomite/Magnesite vein	0.70857	na	6.37
CW-61		Dolomite vein (triassic)	0.71027	na	1.04
CW-20		Dolomite vein (Late permian)	0.70770	na	13.83
CW-13A		Magnesite vein	0.70844	na	4.62
CW-13B		Magnesite vein	0.70843	na	4.79
CW-14	Weyhenmeyer (2000)	Magnesite vein	0.70830	na	na
CW-50B		Magnesite vein	0.70866	na	5.43
CW-53		Magnesite vein	0.70864	na	5.49
CW-54		Magnesite vein	0.70862	na	5.77
F-1		Magnesite vein	0.70855	na	na

In this study, the Sr-isotopic compositions of five peridotite rock samples from the Oman-UAE ophiolite are investigated to document the alteration mineral component of the $^{87}Sr/^{86}Sr$ signal and its origin. The peridotite samples show different types and extents of alteration, reflecting a diversity of abundance of the remaining primary minerals (e.g. olivine and pyroxenes), and a diverse range of secondary minerals such as calcite, dolomite, magnesite, serpentine, brucite, and talc. Minerals were separated by hand picking and chemical reactions with reagents targetting specific minerals to measure their respective $^{87}Sr/^{86}Sr$ ratios and obtain the Sr-isotope signal of the rocks of peridotite aquifers in the Oman-UAE ophiolite.

3.2   Materials and Methods

Rock samples description and mineral identification were carried out using optical microscopy, X-Ray Diffraction (XRD), and Scanning Electron Microscopy (SEM) analyses. Thin sections were observed with an Olympus BH-2 microscope fitted with a Nikon D70s in transmitted light.

XRD analyses were made on finely ground powders randomly orientated on a silicon disc. Analysis of the samples was achieved using a PANalytical X'Pert pro diffractometer machine, fitted with a Cu X-ray tube and utilising the following setup conditions; 35kV, 40mA, automatic slits and a step size of 0.02º 2θ at 1 second/step. Semi-quantitative mineral identification was undertaken using the PANalytical X'pertHighScore software and the ICDD PDF-4/Minerals 2016 database (Hardy 1988; Moore and Reynolds 1989).

SEM analyses was undertaken using a Carl Zeiss LEO1450VP Scanning Electron Microscope (SEM) using a backscattered electron detector for compositional (atomic number-based) imaging of thin section(s). For this operation, SEM operating conditions were 20kV at a working distance (WD) of 19mm (i.e. focal length). The Energy Dispersive X-ray Spectroscopy (EDS) instrumentation for elemental microanalysis and elemental mapping was an Oxford Instruments X-Act 10mm2 area Silicon Drift Detector, coupled with the AZtec Energy software system (v.3.1). The calculated data have been acquired using standardless analysis, and all results are normalized to 100%. Minimum detection limits are 0.195% for Na Kα and decreasing to 0.085% for Ca Kα (Goldstein et al. 2003).

3.2.1   Rock samples

The five rock samples used in this study were collected across the wadi Tayin massif in the Oman-UAE ophiolite (Fig. 3.2), and represent a range of the ultramafic rocks that can be found in the mantle section. They display a range of degree and type of alteration that are commonly observed on the surface. Peridotite (OM15_R5) is only lightly serpentinised with a matrix composed of primary minerals (olivine and pyroxene) and alteration confined to fine serpentine veins. In

contrast, OM15_R1 is highly altered with very few remaining primary minerals and a dense network of serpentine and carbonate veins. Two types of alteration progression are observed, (1) through the widening of veins, associated with a change in mineralogy from ultramafic in the matrix to Ca-carbonate in the vein (OM15_R2). (2) Through the progression of a halo of alteration from the veins across the matrix without major chemistry changes (OM15_R4).
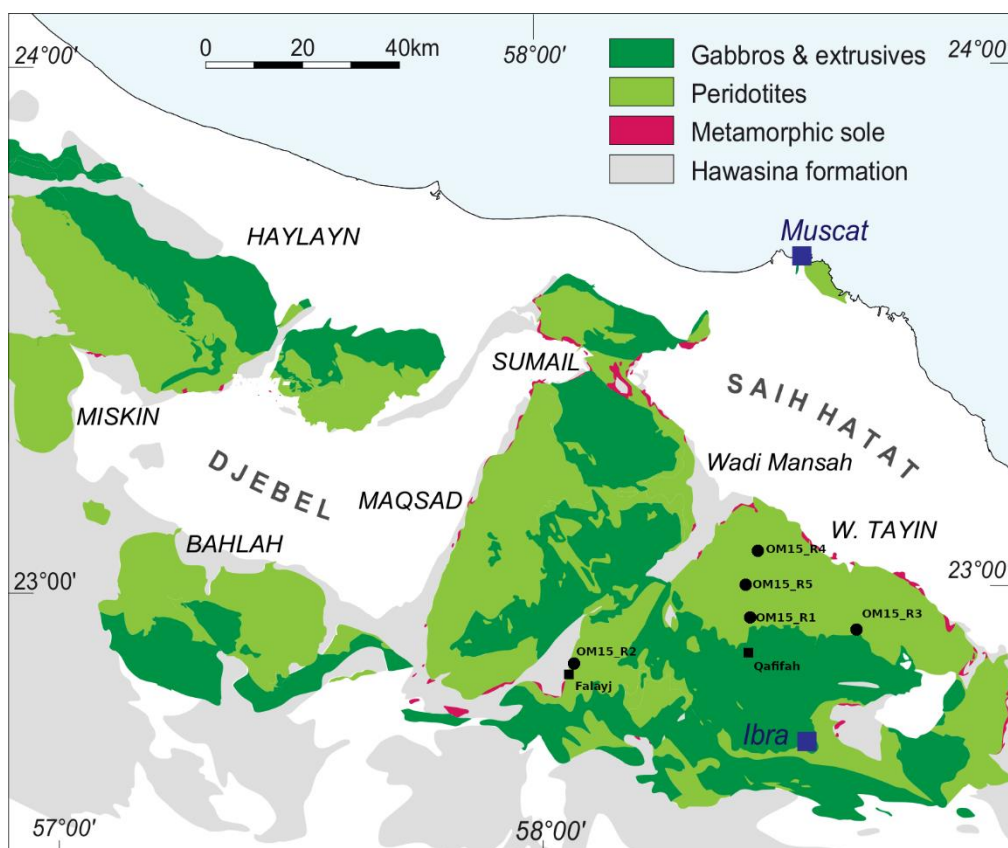
Figure 3.2: Rock sample locations in the southern massifs of the Oman-UAE ophiolite. Simplified geological map modified from Nicolas et al. (2000) by J. Coggon.

3.2.1.1   Samples description

OM15_R1 is a highly serpentinised peridotite collected from wadi Qafifah. The matrix is brown colour with numerous fine (< 1 mm wide) white carbonate veins and green serpentine veins (< 1 mm to 2 mm wide). The matrix (35-46 wt% of the rock sample) is mainly composed of highly serpentinised olivine, displaying the well-known mesh network of serpentine veins, and mildly altered orthopyroxenes that are partially replaced by carbonate minerals. Traces of tremolite and clinochlore were detected by XRD. The vein network (42 to 53 wt% of the rock sample) is composed of fine-grained dolomite (Fig. 3.3).

OM15_R2 is a serpentinised peridotite sample collected near Falaij. The matrix is mainly composed of dark green serpentine (67-71 wt% of the rock sample) and is cut by a network of light green serpentine (10-14 wt% of the rock sample) and Ca-carbonate veins (white) (11-15 wt% of the rock

sample). The Ca-carbonates are fine-grained on the edges of the veins and form phenocrysts in the middle, and some display layers of magnetite (black microcrystalline minerals) trapped within the crystal growth layers (Fig. 3.4). Their Mg content varies from 6 wt% to 1 wt%, suggesting that vein composition is not homogeneous across the rock. Traces of brucite and saponite were detected in the vein network by XRD. A mineral layering, with changes in chemical composition, is observed by SEM between veins and matrix, suggesting a replacement of serpentine by carbonates (see below, Fig. 3.8).
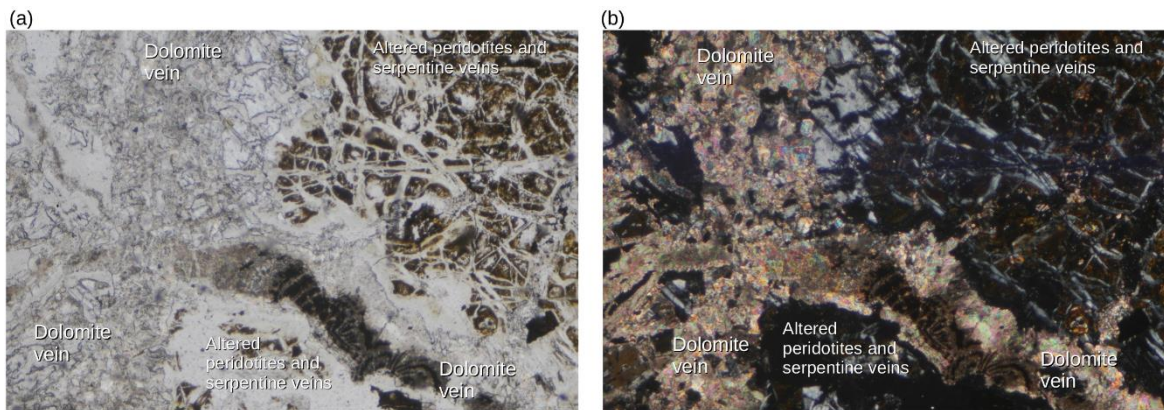
Figure 3.3: Thin section image (in transmitted light; x40) in PPL (a) and XPL (b) of OM15_R1 sample. The olivine and pyroxene minerals are heavily altered and cut by numerous serpentine veins (grey in XPL). Dolomite veins are composed of a mix of fine cristals and phenocrystals.
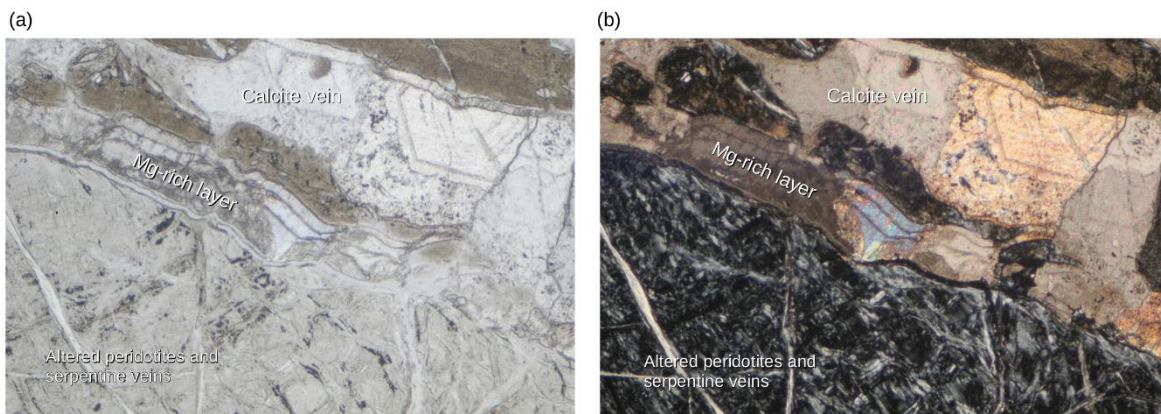
Figure 3.4: Thin section image (in transmitted light; x40) in PPL (a) and XPL (b) of OM15_R2 sample. The olivine and pyroxene minerals are completely serpentinised, cut by serpentine veins (black in XPL) and carbonate veins (light colour in XPL). Major calcite veins are bordered by Mg-rich carbonate layers, better visible in SEM. Phenocrystals of calcite are present in the middle of the major veins, some displaying hexagonal shape highlighted by black lines

OM15_R3 is a pyroxenite dyke collected in the dunite body along the Batin-Tayin road. The matrix is made of fresh, slightly altered clinopyroxene phenocrysts (93 wt% of the rock sample) and altered fractured olivine (7 wt% of the rock sample). Accessory minerals, such as Fe-oxides and amorphous

silica, and traces of saponite are associated with olivine. A few very fine veins and cracks occur between grains (Fig. 3.5).
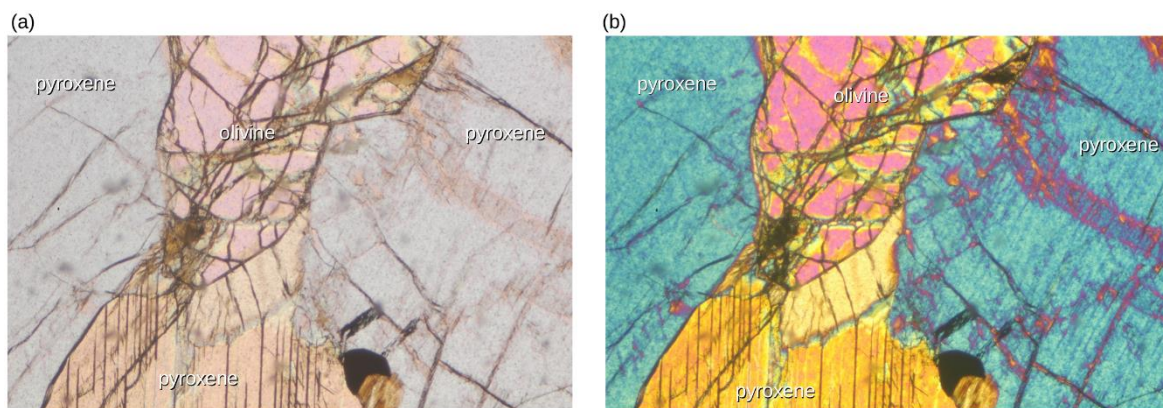
Figure 3.5: Thin section image (in transmitted light; x40) in PPL (a) and XPL (b) of OM15_R3 sample. The olivine is fairly altered and cracked, whereas pyroxene minerals are mostly fresh. There is visible alteration paths in pyroxenes mainly along cracks and between minerals.

OM15_R4 is a serpentinised peridotite collected from wadi Tayin. The matrix of serpentinised olivine (~70 wt% of the rock sample) is cut by mm-wide chrysotile-serpentine veins (~30 wt% of rock sample). An oxidative front of alteration progresses from these veins, resulting in a red rim bordering the dark brown core of the section (Fig. 3.6). Brucite and traces of saponite, detected by XRD, are present in association with serpentine veins.
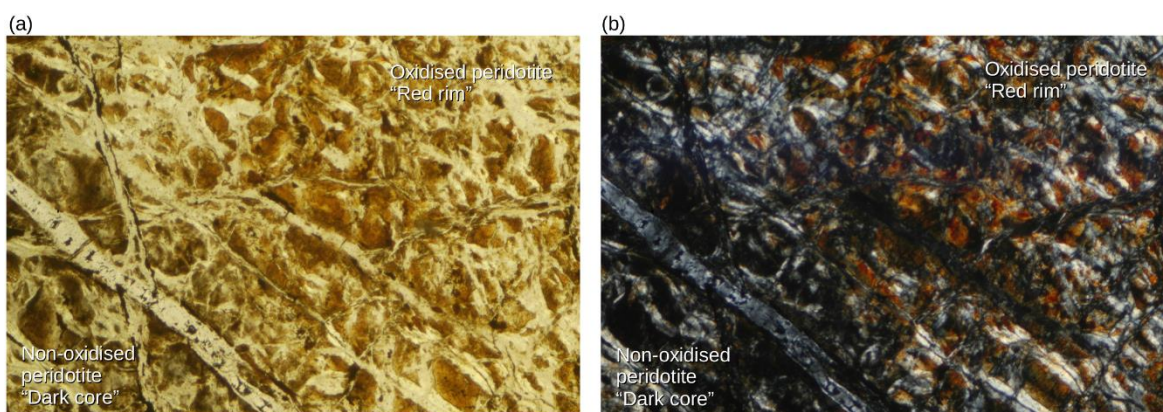
Figure 3.6: Thin section image (in transmitted light; x40) in PPL (a) and XPL (b) of OM15_R4 sample. The olivine and pyroxene minerals are heavily altered and cut by numerous serpentine veins (light in PPL, black in XPL). The alteration front is well visible in XPL with minerals turning red, probably due to Fe oxidation, on the right side.

OM15_R5 is a lightly serpentinised peridotite collected in wadi Dima. The matrix of olivine and orthopyroxene are cut by fine black veins of serpentine. Olivine minerals appear fresh and fractured by serpentine veinlets, orthopyroxenes are fresh and lightly altered. Serpentine is present in veins in association with carbonates, and traces of saponite detected by XRD. Major veins contain

magnetite (opaque, microcrystalline) in the middle, serpentine that fills most of the vein, and a layer of light brown minerals (e.g. Fe-rich secondary minerals) at the edges (Fig. 3.7).
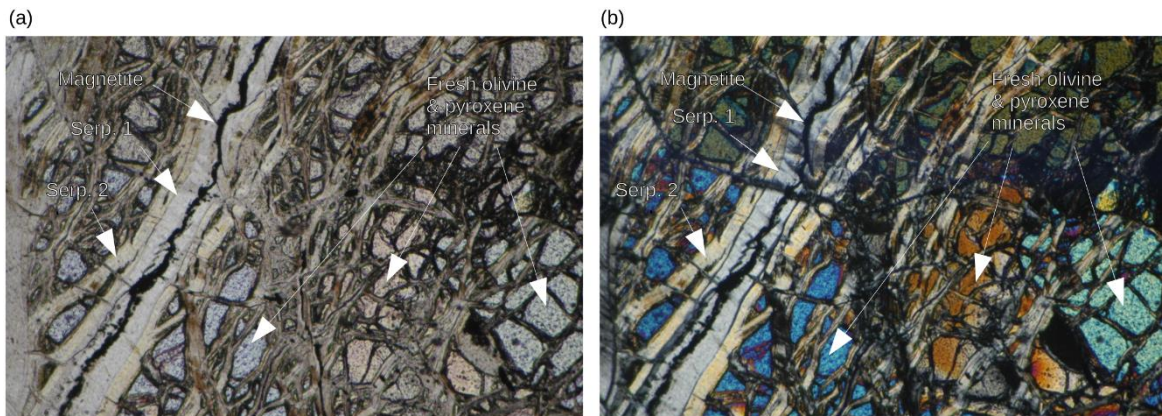
Figure 3.7: Thin section image (in transmitted light; x40) in PPL (a) and XPL (b) of OM15_R5 sample. The olivine and pyroxene minerals are lightly altered and cut by numerous serpentine veins in a mesh pattern (light brown in PPL, greyish in XPL). Opaque minerals (magnetite) are observable as a line in the middle of serpentine veins, and an outlayer (lighter grey in PPL, light brown in XPL) is present around the major vein, suggesting two serpentinisation events.

3.2.1.2   Types of alteration

Two clear examples of alteration are observed in our samples with different types of progression, OM15_R2 exhibits a developed vein network with an evolution of mineral compositions between the matrix and the vein centre. OM15_R4 shows a clear alteration front within an otherwise homogeneous rock. But beside the reddish colour progressing from major veins, no changes in mineralogy nor chemistry were found to support an oxidative alteration.

OM15_R2 has a homogeneous serpentinised matrix ($Mg_{2.9},Fe_{0.1})SiO_5(OH)_4$) even across alteration features such as veinlets. A shift from Mg-rich to Ca-rich mineral phases is taking place at the vein borders from the silicate matrix to the carbonate vein (Fig. 3.8, Transect 1). The mineral composition changes from $Mg_{1.6}(Ca,Fe)_{0.4}SiO_4$ to a mixture of $Mg_{1.9}Fe_{0.1}SiO_4 + 2CaO$, and finally turns into magnesium-rich calcite (($Ca_{0.8},Mg_{0.2})CO_3$) in the veins.

OM15_R4 matrix is mainly composed of two minerals, serpentine and brucite, in different proportions; brucite is mostly present away from the veins ($Mg_{2.8}Fe_{0.2})Si_2O_5(OH)_4 + 15\ Mg(OH)_2$, and tends to be absent near to the veins ($Mg_{2.7},Fe_{0.3})Si_2O_5(OH)_4 + Mg(OH)_2$ (Fig. 3.9). However, despite the clear alteration front visible on the hand-specimen, no difference in abundance or composition of the mineral phases were detected by SEM analyses between the "dark core" and "red rim". Surprisingly magnetite is present in veins in the "dark core" region but is absent from the "red rim",

suggesting that the dark core as already experienced some level of oxidation, and that Fe is completely oxidised in the "red rim", potentially present as amorphous iron-oxide.
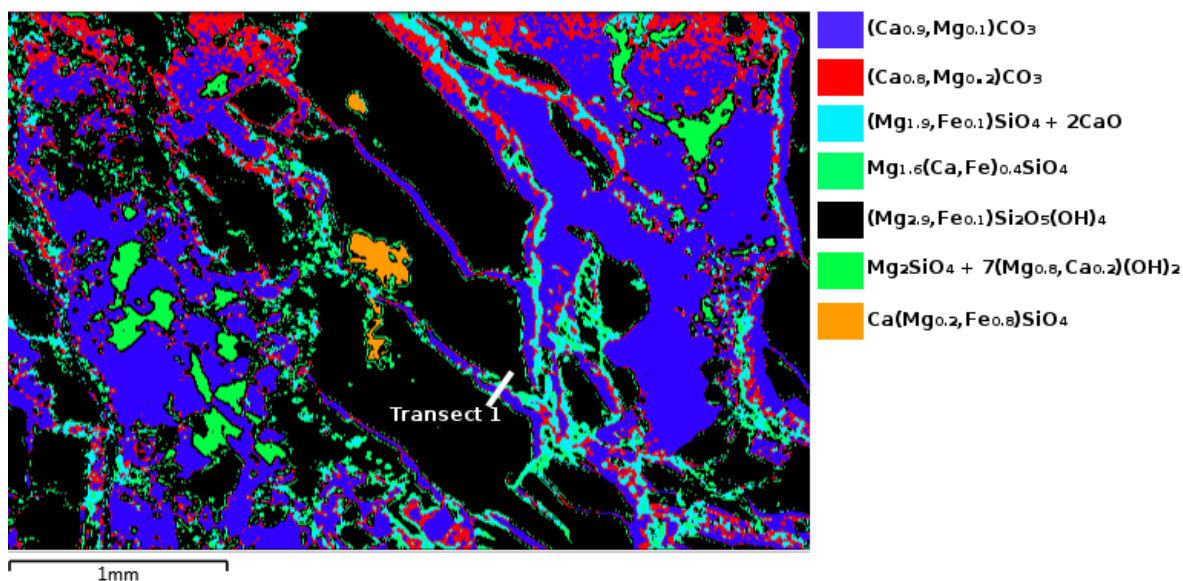
Figure 3.8: SEM image of OM15_R2 vein network with coloured mineral and mixed phases.
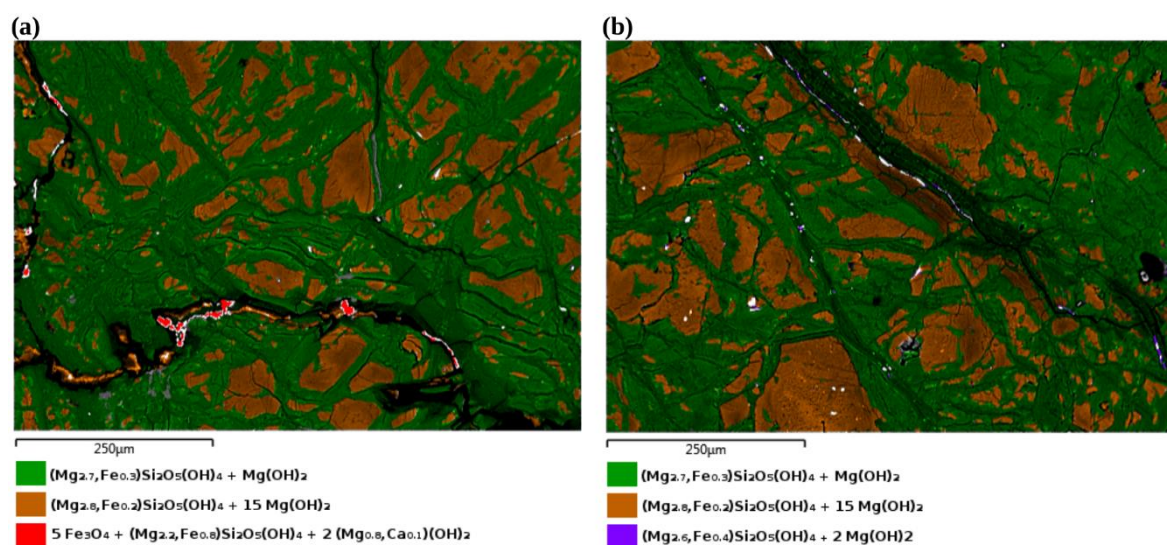
Figure 3.9: SEM image og OM15_R4 with coloured mineral and mixed phases in the dark core (a) and in the red rim area (b)

3.2.2 Samples digestion and leaching

3.2.2.1 Samples preparations

The rocks were crushed and sieved to separate the different grain sizes. The fraction of grains with a size between 1mm and 0.5mm of each rock samples were separated under a stereomicroscope into mineral fractions based on their mineralogy and degree of alteration. Each fraction was stored in a glass bottle and cleaned three times for 5 min in an ultrasonic bath with MilliQ water. One gram

of each of the mineral fractions was then ground to fine powder with an agate pestle and mortar and sub-sampled for XRD analyses. The rest was used for digestion and sequence leaching experiments.

3.2.2.2 Full digestion

A portion of finely ground powder (50mg) was sub-sampled for elemental and isotopic analyses. The powder is activated with 10 drops of sub-boiled concentrated (~15M) HNO_3 and digested with 2mL of HF for 24h at 130°C in a closed 15mL teflon vial. At the end of the digestion the vial is opened and the sample is let to dry on a hotplate. The dry residue is re-dissolved in 7 mL of sub-boiled 6M HCl and digested for 24h at 130°C in a closed vial, then let to dry on a hotplate. The final dry residue is re-dissolved in sub-boiled 6M HCl and transferred in a 30mL HDPE bottle topped up with MilliQ water to make a "mother" solution that will be used for analyses. Samples with a high carbonate content were soaked in an acetic acid-acetate buffer (pH 4.5) for 24h previous to the full digestion. Once the decarbonation was complete, the bulk of the buffer solution is removed by carefully tipping the vial to avoid losing any powder, and the powder is dried on the hotplate. The mineral fraction composed of carbonate were dissolved the same way to avoid contamination from minor phases. Blank solution concentrations were used to define the limit of detection of elements.

3.2.2.3 Sample leaching

The 3 principal minerals present in altered peridotite targeted were brucite, carbonate, and serpentine. No other secondary minerals were detected in sufficient abundance or with sufficiently high concentration of Sr to play a significant role in the Sr isotopic signal of the rocks. The choice for reagents and experimental conditions to leach each mineral was based on previous published experiments (Poulton & Canfield 2005; Teir et al. 2007; Wittig et al. 2009; Wang & Maroto-Valer 2011; Huang et al. 2012). The accuracy of each mineral dissolution is determined by the set of parameters used for the reaction (i.e. reagent, reagent strength, reagent/powder ratio, temperature, and time of reaction).

3.2.2.3.1 Selection of reagents

NH_4Cl is routinely use to leach the exchangeable cation pool in clays and has been reported to dissolve brucite without dissolving serpentine (Benson 1982; Teir et al. 2007; Wang and Maroto-Valer 2011). Furthermore, NH_4Cl has a pKa of 9.24 which limits its capacity to dissolve carbonates (Wang & Maroto-Valer 2011).

Sodium acetate buffered with acetic acid is used to dissolve the carbonate fraction of rocks in numerous studies (Tessier, Campbell, and Bisson 1979; Robinson 1980; Koschinsky and Halbach

1995; VonderHaar, Mahoney, and McMurtry 1995; Lerouge et al. 2010). Poulton & Canfield (2005) recommend a buffer adjusted at pH = 4.5 that is more efficient at dissolving poorly crystalline Fe-carboantes (e.g. ankerite and siderite) than the more commonly used pH 5 buffer. Acetic acid has a poor capacity to extract Mg, Fe and Si from serpentine, with less than 5% extracted of each element regardless of the acid strength (Teir et al. 2007), hence it should not significantly attack this mineral.

HCl is routinely used to leach altered parts of minerals and dissolve grain boundary contamination to obtain fresh minerals for analyses. It allows a thorough "cleaning" of refractory mineral surfaces (e.g. pyroxenes) without important elemental loss from the mineral itself nor isotopic fractionation of the elements (Clauer et al. 1993; Wittig et al. 2009). HCl is very effective at extracting Mg and Fe from serpentine into solution with 60% of Fe extracted for a 100% of Mg in 1h at 70°C. This rate of extraction increases with the acid strength (Teir et al. 2007). However, Si is not significantly dissolved by HCl, for any acid strength, and stays as amorphous silica (Teir et al. 2007).

3.2.2.3.2   Leaching procedure

A single-leaching experiment was run on each rock samples two times, on different subsamples, (1) to determine if the reagent used is effective to dissolve the targeted phase, (2) to adjust the parameters of the reactions to optimise the specificity and the completion of the targeted phase dissolution. The setups of leaching experiments are summarised in table 3.3. One mineral was targeted in each mineral fraction, and a protocol was selected to dissolve it (Table 3.3). The powders were reacted in 50 mL acid-cleaned falcon tubes placed in a water bath (Medline BS-11) to maintain a constant reaction temperature and agitate the mix. All the single-leachings were run simultaneously. A water temperature of 70°C was chosen as the best compromise between the temperatures used with the reagents as reported in the literature (Poulton and Canfield 2005; Teir et al. 2007; Wang and Maroto-Valer 2011; Huang et al. 2012). The leachates were collected by centrifuging the falcon tubes for 5 min at 3000 rpm to separate the powder from the solution, and transferring the supernatant in another acid-cleaned falcon tube. The residual powders were analysed by XRD to determine if the targeted mineral has been dissolved in totality and if other minerals have been significantly attacked. The leachates were analysed to determine cation concentrations and Sr-isotopes ratios ($^{87}Sr/^{86}Sr$ and $\delta^{88}Sr$).

Table 3.3: Summary of leaching experiment protocols and setups.

		2M NH4Cl (3h; 70ºC)	1M Na acetate/acid acetic buffer (pH 4.5; 24h; 70ºC)	6M HCl (14h; 70ºC)	HF/HNO3
	Reagent				
	Targeted mineral	brucite	Carbonates	Serpentine	full digestion
Sample ID	**Major minerals (XRD) | Reference**	Teir et al. (2007 & Wang et al. (2011)	Poulton & Canfield (2005)	Huang (2012)	na
OM15_R1c	Dolomite + Serpentine (traces)		x		
OM15_R1w	Serpentine/Clinochlore + Tremolite (traces)			x	x
OM15_R2c	Calcite +Serpentine/Brucite (traces)		x		
OM15_R2s	Serpentine/Calcite +Saponite (traces)		x		x
OM15_R2w	Serpentine + Calcite/Saponite (traces)		x		x
OM15_R3	Cpx+Forsterite + Saponite (traces)				x
OM15_R3b	Forsterite/cpx + Saponite (traces)			x	x
OM15_R3f	Clinopyroxene			x	x
OM15_R4	Serpentine + Brucite +Saponite (traces)	x	x	x	x
OM15_R4d	Serpentine + Brucite + Saponite (traces)	x			x
OM15_R4r	Serpentine + Brucite + Saponite (traces)	x			x
OM15_R4s	Serpentine			x	x
OM15_R4out	Serpentine + Saponite (traces)			x	x
OM15_R5	Forsterite/Serpentine + Pigeonite/Saponite (traces)			x	x

3.2.3 Chemical and Sr-isotopes analyses

Cation concentrations were measured on an Inductively Coupled Plasma-Mass Spectrometer (ICP-MS) quadrupole Thermo X-Series 2 at the University of Southampton. A volume of 1 mL was sub-sampled from the "mother" solution and dried on a hotplate in a Savillex pot. The dry residue was then re-dissolved in a solution of sub-boiled 3% HNO_3 spiked with 20 ppb Be and 5 ppb In and Re, and subsequently diluted x4000 and x40000. The two solutions obtained were used to analyse minors and majors. The samples were run with standard reference materials BHVO2, BIR-1, JA-2, JB-3, JB1a, and JGb-1 that went through the same protocol. JA-2 was run as an unknown and used to assess the accuracy of the measurements. The others standards were used to calibrate the measurements in counts per second to concentration in the PlasmaLab software used to process the results. Other processing of the results include (1) the monitoring of internal drift using the detection of the Be, In, and Re added as spike. (2) The determination of the limit of detection (LoD) of each element using blank measurements and the formula: Blank average + 3σ = LoD, measurements falling below the LoD were rejected. (3) The monitoring of internal precision by measuring each sample 4 times and calculating the percentage relative standard deviation (%RSD), which is the expression of the standard deviation as a percentage of the mean, data with %RSD of >10 % were rejected.

Sr-isotope ratios (both $\delta^{88}Sr$ and $^{87}Sr/^{86}Sr$) were measured on a Triton Thermal Ionisation Mass Spectrometer (TIMS) at the University of Southampton. A volume containing 1 μg of strontium was subsampled from the "mother" solution and dried on a hotplate in a Savillex PFA vial. The dry residue was re-dissolved in 2 mL of 2M HNO_3 and separated in two aliquots containing 500 ng of Sr each. An appropriate amount of ^{84}Sr-^{87}Sr double spike was added to one of the aliquots before separating the Sr by following a standard column procedure using an Eichrom strontium specification ion exchange resin (Pearce et al. 2015). The solution with the purified strontium was collected in Savillex PFA vials and dried on a hotplate. The dry residue was re-dissolved in 1.5 μL of laboratory prepared sub-boiled 1M HCl and loaded onto an oxidised tantalum filament with a Ta activator solution before analysis. Radiogenic ($^{87}Sr/^{86}Sr$) ratios were directly measured in the unspiked aliquots and normalised to a fixed $^{86}Sr/^{88}Sr$ ratio of 0.1194 (Nier 1938). The stable Sr ($\delta^{88}Sr$) ratios were determined by combining unspiked and ^{84}Sr-^{87}Sr spiked aliquot data and by deconvolving them using the exponential fractionation law and Newton-Raphson iteration technique in ^{87}Sr denominator space (Pearce et al. 2015). The NIST987 standard has a $\delta^{88}Sr$ long-term value of 0.00‰ (2σ = 0.01‰) and an $^{87}Sr/^{86}Sr$ long-term value of 0.710256 (2σ = 0.000013) on our instrument, and the $^{87}Sr/^{86}Sr$ ratios were normalised to a NIST987 value of 0.710248 to allow the comparison between different studies (McArthur et al. 2012).

Samples were sent to the department of Earth Sciences at the University of Cambridge where they were combined with a ^{42}Ca-^{48}Ca double spike and calcium was separated using a Dionex ICS-5000$^+$ IC system. The $\delta^{44/40}Ca$ isotopic ratios were then measured on a TIMS (Bradbury and Turchyn 2018). During a preliminary study some of our samples were measured, following a similar protocol, in the department of Earth and Planetary Science at the University of California, Berkeley.

3.3   Results

3.3.1   Rock and Leachates Chemistry

The cation concentrations and the isotopic ratios of the rock samples and their leachates are reported in Table 3.4 and 3.5. The R1c carbonate phase has a Ca/(Mg+Ca) molar ratio (Ca#) of 53%, which is in agreement with a dolomite composition. The R1w fraction has a Mg# of 85.63%, it is the most Fe-rich mineral fraction of our samples, and has a minor Ca component with a Ca# of 3%. The mineral phase leached from R1w has similar cation concentrations with the exception of Ca, Al, and Cr that have lower concentrations, suggesting that pyroxenes weren't attacked. The two fractions R1c and R1w have similar $^{87}Sr/^{86}Sr$ ratios: 0.70859 and 0.70848 respectively, but different $\delta^{88}Sr$ ratios: 0.31‰ and 0.06‰. The dolomite composing the carbonate fraction R1c has a $\delta^{44/40}Ca$ ratio of -0.23‰.

Table 3.4: Cation concentrations and $^{87}Sr/^{86}Sr$ ratios of fully digested whole rocks and of mineral fraction samples.

Sample ID	Major minerals (XRD)	Mg mmol/kg	Al mmol/kg	Ca mmol/kg	Cr mmol/kg	Fe mmol/kg	Ni mmol/kg	Cu µmol/kg	Sr µmol/kg	$^{87}Sr/^{86}Sr$ norm.	2 s.e 10^{-6}
OM15_R1c$_{WF}$	Dolomite + Serpentine (traces)	3723	1	4154	0	11	1.4	7.9	5105	0.70859	3.84
OM15_R1w$_{WF}$	Serpentine/Clinochlore + Tremolite (traces)	7448	422	267	39	1250	40	233	302	0.70848	4.16
OM15_R2c$_{WF}$	Calcite +Serpentine/Brucite (traces)	1090	0	6654	0	bdl	0.1	1.0	7580	0.70838	4.11
OM15_R2s$_{WF}$	Serpentine +Saponite (traces)	7660	291	164	8	647	14	60	103	0.70831	4.07
OM15_R2w$_{WF}$	Serpentine + saponite (traces)	8279	328	15	22	811	30	108	57	0.70788	7.13
OM15_R3$_{WF}$	pyroxenite dyke	10500	301	164	35	1044	38	396	34	na	na
OM15_R3b$_{WF}$	Forsterite+px +saponite (traces)	9910	317	966	18	1046	20	11954	83	0.70609	3.78
OM15_R3f$_{WF}$	(Clino)pyroxene	4694	554	3763	61	330	3.4	1159	122	0.70402	3.86
OM15_R4$_{WF}$	Serpentine + Brucite +saponite (traces)	11373	235	26	8	969	42	23	34	0.70905	11.49
OM15_R4d$_{WF}$	Serpentine + Brucite +saponite (traces)	10693	224	22	9	1021	43	19	33	0.70918	542.22
OM15_R4r$_{WF}$	Serpentine + Brucite +saponite (traces)	11452	227	20	14	1093	48	24	33	na	na
OM15_R4s$_{WF}$	Serpentine	12839	227	17	9	864	41	28	36	na	na
OM15_R4out$_{WF}$	Serpentine + Saponite (traces)	11027	227	8	3	593	7.9	67	41	0.70928	248.50
OM15_R5$_{WF}$	Forsterite/Serpentine +Pigeonite/Saponite (traces)	10456	302	147	29	1041	37	329	34	0.70554	729.14

Table 3.5: $\delta^{44/40}Ca$, $\delta^{88}Sr$, and $^{87}Sr/^{86}Sr$ isotopic ratios of mineral fractions and rock leachates.

Sample ID	Type	Treatment	$\delta^{44/40}Ca$ BSE	2s.e. ‰	$\delta^{88}Sr$	2s.e. ‰	$^{87}Sr/^{86}Sr$ norm.	2s.e. 10^{-6}
OM15_R1c$_{WF}$	Carbonate vein (Dolomite)	Full digestion	-0.23	0.06	0.31	0.01	0.708587	3.8
OM15_R1w$_{WF}$	Heavily serpentinised peridotite	Full digestion	na	na	0.06	0.01	0.708460	4.2
OM15_R2c$_{WF}$	Carbonate vein (Calcite)	Full digestion	-0.04	0.06	0.30	0.01	0.708376	4.1
OM15_R2s$_{L}$	Serpentine vein (carbonate fraction)	Leaching	-0.08	0.06	0.30	0.01	0.708355	9.1
OM15_R2s$_{WF}$	Serpentine vein (decarbonated)	Full digestion	na	na	0.23	0.01	0.708291	4.1
OM15_R2w$_{WF}$	Serpentinised peridotite	Full digestion	na	na	0.23	0.01	0.707856	7.1
OM15_R3b$_{L}$	Pyroxenite dyke (olivine-rich fraction)	Leaching	na	na	0.07	0.01	0.707633	3.8
OM15_R3f$_{L}$	Pyroxenite dyke (pyroxene-rich fraction)	Leaching	-0.09	0.06	0.15	0.01	0.706935	3.8
OM15_R5$_{L}$	Lightly serpentinised peridotite	Leaching	na	na	0.24	0.01	0.706190	4.0

The carbonate phase of R2c has a Ca# of 79%, in agreement with magnesian calcite. R2s and R2w, decarbonated prior to dissolution, have similar Mg# (92% and 91% respectively) but Ca concentration is ~10 times higher in R2s than in R2w. The leaching of R2s and R2w, that targeted their carbonate component, have Ca# (38% and 8%) too low to be associated with calcite and suggest that a Mg-rich phase (e.g. serpentine) was also attacked. However, the leachate of R2s have an $^{87}Sr/^{86}Sr$ ratio very close to that of R2c (R2c =0.70838; R2s$_{Leach}$=0.70836), whereas R2s $^{87}Sr/^{86}Sr$ is slightly lower (R2s =0.70831), and R2w is significantly lower (R2w=0.70788). The $\delta^{88}Sr$ ratios of R2c and R2s$_{Leach}$ are also very close, both at 0.30‰, as well as close $\delta^{44/40}Ca$ ratios, -0.04‰ and -0.08‰, respectively. R2s and R2w have the $\delta^{88}Sr$ ratio of 0.23‰. The Sr leached from R2w had a lower concentration than the blank and its $^{87}Sr/^{86}Sr$ and $\delta^{88}Sr$ ratios couldn't be measured.

The R3 whole rock sample has a Mg# of 91% and a Ca# of 2%, R3b and R3f have similar Mg# (90% and 93%) but higher Ca# (9% and 44%). The high Ca# of R3f is in agreement with a clinopyroxene composition. Its leaching yields a lower Ca# (17%), potentially provided by the altered mineral surfaces. The leaching of R3b has a Ca# of only 0.3%, suggesting that the Ca is mostly contained in the pyroxenes present. As the R3f fraction is dominant in R3 (93 wt%), a lower Ca# for R3 was expected, however, many of the element concentrations in R3 are lower than in R3b and R3f. This suggests that R3 digestion may have not been complete. The $^{87}Sr/^{86}Sr$ of R3f (0.70402) is the closest to the primary mantle value, whereas R3b appears more altered and its $^{87}Sr/^{86}Sr$ (0.70609) would correspond to a mix between primary mantle and alteration fluid values. Both of their leaching $^{87}Sr/^{86}Sr$ ratios are higher (R3b$_{Leach}$ = 0.70763; R3f$_{Lesach}$ = 0.70694), suggesting that the rock has reacted with a fluid having a higher $^{87}Sr/^{86}Sr$ ratio. R3f$_{Leach}$ has a $\delta^{88}Sr$ ratio of 0.15‰ and a $\delta^{44/40}Ca$ ratio of -0.09‰, while R3b$_{Leach}$ has a $\delta^{88}Sr$ ratio of 0.07‰. The $\delta^{88}Sr$ ratios of the full fractions (R3b and R3f) could not be measured, same for the $\delta^{44/40}Ca$ ratio of R3b$_{Leach}$.

The R4 whole rock sample has a Mg# of 92% and a Ca# of 0.2%, in the range of the R4 mineral fractions, R4d (Mg# = 91%; Ca# of 0.2%), R4out (Mg# = 95%; Ca# = 0.1%), R4r (Mg# = 91%; Ca# = 0.2%), and R4s (Mg# = 94%; Ca# = 0.1%). The mineral fractions R4out and R4s are both serpentine, but their chemical compositions differ, R4s has significantly higher concentrations (>50%) of Ca, Cr, and Ni, whereas R4out has a higher concentration of Cu. The R4 whole rock sample and its fractions R4d and R4out have the highest $^{87}Sr/^{86}Sr$ ratios of the rock samples (R4=0.70905, R4d=0.70918, and R4out=0.70928). These values are surprisingly homogeneous as R4d and R4out are on each side of the alteration front. Furthermore, the leaching of R4out has an $^{87}Sr/^{86}Sr$ = 0.70851, lower than the mineral fraction which is unexpected.

R5 has an Mg# of 91% and Ca# of 1%, its leaching has similar values (Mg# = 90% and Ca# = 1%) and an $^{87}Sr/^{86}Sr$ of 0.70619, similar to the R3b mineral fraction that also comprises altered olivine but a different $\delta^{88}Sr$ ratio of 0.24‰.

3.3.2 Sample leaching experiment

The reagents used for single-leaching were (1) acetic acid buffered with sodium acetate (1M; pH 4.5; 24h; 70°C) to target carbonate in mineral fractions R1c, R2c, R2s, and R2w, (2) NH_4Cl (2M; 3h; 70°C) to dissolve brucite in mineral fractions R4d and R4r, and (3) HCl (6M; 14h; 70°C) for serpentine in mineral fractions R1w, R3b, R3f, R4out, R4s, and R5. The leaching was successful for the mineral fractions R1w, R2s, R2w, R3f, R4d, and R4r. The minerals targeted in R1c, R2c, and R4out were not completely dissolved. A stronger attack was used during the second leaching by increasing the reagent/powder ratio that completely dissolve all the carbonates. The leaching of R3b and R5

dissolved forsterite as well as the serpentine that was targeted, hence the second leaching used a lighter attack on these two mineral fractions by limiting the reaction time to 3h and successfully preserved forsterite in the residue. This reduction of reaction time was also applied to R1w, R3f, and R4out leachings and showed no negative impact.

The OM15_R4 mineral fractions, R4d, R4r, and R4s, were not used for the second leaching. The unsorted rock powder was used instead because of the very little quantity of Sr retrieved from the brucite fraction. The reagent quantity was increased (x4) as well as the powder quantity (x40), in order to increase the quantity of Sr that could be retrieved from the brucite. However, this approach was also unsuccessful in Sr-extraction. The main reason identified is the cleaning of the powders that is probably responsible for washing away most of the brucite, thus future experiments should avoid this step. The quantity of reagent and powder used were also increased for the leaching of R3b, R3f, R4out, and R5, with success; more than 1 µg of Sr was released in every leachates, whereas R4 only yielded 450 ng.

3.4   Discussion

3.4.1   Leaching

The Sr concentrations in leachates did not excessively vary between the two single-leaching experiments, except for OM15_R4 and OM15_R5 (Table 3.6). This suggests that the targeted mineral were dissolved consistently, but improvements are necessary regarding the quantities of rock and reagent that can be efficiently used. Low Sr concentration in rocks and leached minerals is also problematic for Sr-isotope analysis, and may require more material to be processed than it is practical. This leads to great amounts of dry residues to be re-dissolved and passed through the Sr-spec column, though no problems were found with the Sr-isotopes results. Some did not succeed because of too little Sr within an important quantity of residue. Some reagents and other element present in excess in regards to Sr could be remove from the solution prior to drying, such as NH_4Cl through degassing NH_4^+ as NH_3 by increasing the solution pH above 9.25; the NH_3/NH_4^+ pKa value, and removing Mg via a cation column.

3.4.2 $^{87}Sr/^{86}Sr$ signals

The chemical composition of the peridotite samples is mostly homogeneous away from carbonate veins and is similar between rock matrix and serpentine veinlets, but the $^{87}Sr/^{86}Sr$ ratios measured in the different samples and their leachates clearly vary. This is due to the interaction between rocks and seawater throughout the ophiolite history. Seawater has a Sr concentration of ~90

µmol/kg (Palmer and Edmond 1989), one order of magnitude higher than that of most peridotite sample (Table 3.1), and will progressively overtake the Sr-isotopic signal of the rocks. Four $^{87}Sr/^{86}Sr$ signals were identified: (1) a primary mantle signal ($^{87}Sr/^{86}Sr$ = 0.7023-0.7045; DePaolo and Wasserburg 1977; Lanphere, Coleman, and Hopson 1981) which was measured in the pyroxenes whole fraction (R3f$_{WF}$ = 0.70402), and in some other minerals, whole fraction and leaching, mixed with the signal of the alteration fluid (R3b$_{WF}$ = 0.70609; R3f$_{Leach}$ = 0.70694; R5$_{WF}$ = 0.70545; R5$_{Leach}$ = 0.70619). (2) A Cretaceous seawater-like signal ($^{87}Sr/^{86}Sr$ = 0.7072-0.7079; McArthur et al., 2012), measured in R2w (R2w$_{WF}$ = 0.70788) and in the leachate of R3b (R3b$_{Leach}$ = 0.70763), suggesting that OM15_R2 and OM15_R3 were altered during the Upper Cretaceous (< 90 Ma). (3) A Tertiary seawater-like signal ($^{87}Sr/^{86}Sr$ = 0.7080 to 0.7085; McArthur et al., 2012), corresponding to the transgression episode during the Paleogene and the early Miocene, imprinted in OM15_R2 vein network, in serpentine (R2s$_{WF}$ = 0.70831) and calcite (R2c$_{WF}$ = 0.70838; R2s$_{Leach}$ = 0.70836). This Tertiary signal is also present in OM15_R1 vein network as well as in the rock matrix (R1c$_{WF}$ = 0.70859; R1w$_{WF}$ = 0.70848), suggesting that seawater has penetrated through the whole rock during the Tertiary episodes of alteration and overprinted the Cretaceous $^{87}Sr/^{86}Sr$ signal. (4) A modern seawater-like signal ($^{87}Sr/^{86}Sr$ ~ 0.7092) was measured in OM15_R4, suggesting that rocks are still being altered by modern rainfall water. However, the error on these values is high (2S.E. (x10^{-6}) = 11.49 to 542.22) and thus this signal is most likely a late Tertiary (Neogene) to Quaternary signal rather than modern.

Table 3.6: Results of leaching experiments. [Sr] is the Sr concentration of the whole samples (Table 3.4). [Sr] 2nd leach is a duplicate with the adjusted reaction parameters. Leached Sr (%) is the percentage of Sr from the whole sample that was retrieved by leaching. The quantity (Qty) of Sr is in µmol of Sr per kg of whole rock. The $^{87}Sr/^{86}Sr$ remaining is the calculated $^{87}Sr/^{86}Sr$ of the sample residue after leaching.

Sample ID	weight %	[Sr] µmol/kg	[Sr] 1st leach µmol/kg	[Sr] 2nd leach µmol/kg	Leached Sr %	Qty of Sr µmolSr/kg	$^{87}Sr/^{86}Sr$ norm.	2 s.e 10^{-6}	$^{87}Sr/^{86}Sr$ remaining
OM15_R1c	49	5158	5158	5105	100	2501	0.70859	3.8	na
OM15_R1w	41	302	296	240	98	124	na	na	na
OM15_R2c	11	7580	7580	6292	100	849	0.70838	4.1	na
OM15_R2s	11	103	932	na	909	11	0.70836	3.7	na
OM15_R2w	67	57	na	na	na	38	na	na	na
OM15_R3b	7	83	34	28	41	6	0.70763	3.8	0.70518
OM15_R3f	93	122	12	11	10	113	0.70694	3.8	0.70370
OM15_R4d	39	33	1	0	2	13	na	na	na
OM15_R4r	29	33	1	0	2	10	na	na	na
OM15_R4s	32	36	3	0	7	11	na	na	na
OM15_R4out	na	41	3	4	8	na	0.70851	6.2	na
OM15_R5	100	34	2	6	6	34	0.70619	4.0	0.70545

3.4.3   Sr sources

The fraction of the Sr extracted during leaching varies between each mineral fraction, mostly due to the Sr content of the targeted phase. It varies from 100% in the carbonate fractions (R1c and R2c) to 0.1% in the brucite-leached fractions (R4d and R4r) (Table 3.6). Strontium concentration is the highest in dolomite (R1c = 5158 μmol/kg) and calcite (R2c = 7580 μmol/kg) and accounts for more than 90% of the Sr present in the mineral fractions of R1c, R2c, and R2s. Serpentine and other alteration phases contain 3 to 296 μmol/kg of Sr that represent 7% to 89% of the Sr present in the mineral fractions of R1w, R2w, R3b, R3f, R4s, and R4out (Table 3.6). The combination of Sr concentration and $^{87}Sr/^{86}Sr$ ratios in leachates and whole rocks allows us to calculate the $^{87}Sr/^{86}Sr$ of the remaining minerals after leaching, i.e. fresh minerals before alteration (Table 3.6). OM15_R3b and OM15_R5 would have similar $^{87}Sr/^{86}Sr$ ratios (0.70518 and 0.70545) close to a mantle signal, but both samples contain olivine which could provide a higher $^{87}Sr/^{86}Sr$ ratio than pyroxenes (Menzies and Murthy 1978). OM15_R3f fresh pyroxenes would have an $^{87}Sr/^{86}Sr$ of 0.70370 comparable to a primary mantle value at mid-oceanic spreading-ridges (O'Nions and Pankhurst 1974). OM15_R4 and OM15_R4d $^{87}Sr/^{86}Sr$ values of 0.70905 and 0.70918 could be evidence that modern alteration is ongoing and overprints the $^{87}Sr/^{86}Sr$ signal of previous alteration episodes (R4out$_{Leach}$ = 0.70851) with a modern seawater-like signal.

In these peridotite samples, the Sr is mainly present in dolomite (OM15_R1) and calcite (OM15_R2) which contain ~95% on average of the Sr of the whole rock sample with respectively 2500 and 850 μmol of Sr per kg of rock (μmolSr/kg) (Table 3.6). The serpentinised matrices of OM15_R1 and OM15_R2 contain 124 and 38 μmolSr/kg; pyroxenes have 113 μmolSr/kg in OM15_R3. The serpentine in OM15_R4 and OM15_R5 contain >34%, and 12% of the rock Sr corresponding to 11 and 4 μmolSr/kg. Carbonates and serpentinised matrices have the highest concentration of Sr and are more readily to react with water, whereas the serpentine present in veins contains less Sr and is in equilibrium with the groundwater, and pyroxenes, which are refractory minerals, are less prone to be dissolved by water. Therefore, carbonates and serpentinised matrices are most likely to influence the $^{87}Sr/^{86}Sr$ ratio of groundwater.

3.5   Conclusions

During this study, it was determined that the mantle primary $^{87}Sr/^{86}Sr$ ratio is not the dominant signal in the altered peridotites of the Oman-UAE ophiolite. The $^{87}Sr/^{86}Sr$ ratios of peridotite samples result from a mix of four signals: primary mantle ($^{87}Sr/^{86}Sr$ = 0.7023-0.7045), Cretaceous seawater ($^{87}Sr/^{86}Sr$ = 0.7072-0.7079), Tertiary seawater ($^{87}Sr/^{86}Sr$ = 0.7080 to 0.7085), and modern seawater ($^{87}Sr/^{86}Sr$ = ~0.7092). The most prominent $^{87}Sr/^{86}Sr$ signal in our samples is the Tertiary

seawater value, present in calcite and dolomite and in the serpentinised rock matrix. This confirms the hypothesis (2) that the water-rock reactions are extensive enough for groundwater to reach the $^{87}Sr/^{86}Sr$ value of the peridotites it interacts with, and that primary mantle $^{87}Sr/^{86}Sr$ signal has been overprinted by the seawater signal as part of the peridotite alteration during the geological history of the ophiolite.

Mineral phases within altered peridotite were separated by hand picking and targeted chemical reactions in order to measure their $^{87}Sr/^{86}Sr$ ratios. This method has allowed us to access the $^{87}Sr/^{86}Sr$ signal of alteration minerals within the rock and to match them with the sea transgressions that occurred throughout the ophiolite history. However, the method needs further improvement, in particular regarding the quantity of material left as dry residue prior to purifying Sr; an important quantity of sample is required to amount to 1 µg of Sr when they have low Sr concentration, some reagents such as NH_4Cl and the acetate buffer also represent an important quantity of material once dry. This excess of material in the dry residue makes it impractical to process it through the Sr purifying protocol, a major improvement to the method would be to remove this surplus of material. Some exploratory ideas comprise degassing the ammonium (NH_4^+) by forming ammonia (NH_3), and removing major elements such as Mg through a cation column. Another point of interest for improvement is the cleaning step of the powders. The removal of dust-like particles from the grains surface makes their identification much easier when separating the mineral phases by hand picking, but it seems that it potentially also removes critical mineral phases such as brucite. This needs to be investigated and the method's steps adapted accordingly to the finding.

The $\delta^{88}Sr$ and $\delta^{44/40}Ca$ ratios were not discussed in this chapter as they are the object of a more extensive study (see chapter 5).

Chapter 4 Tracing water-rock interaction in the peridotite aquifer of the Oman-UAE ophiolite using strontium isotopes (^{87}Sr/^{86}Sr)

Abstract

Low-temperature alteration of peridotite creates steep chemical gradients that allow ecosystems to thrive in the absence of sunlight and produces hyperalkaline fluids rich in calcium (Ca^{2+}) that can sequester large amount of CO_2 from their environment via the precipitation of carbonate. The extent to which such carbonate precipitation impacts the global carbon cycle is uncertain as it depends on the source of the Ca^{2+} ions in solution. The release of Ca^{2+} from the dissolution of carbonate minerals has no net effect on atmospheric CO_2, whereas the dissolution of silicate phases will contribute to a net drawdown. In this study, the sources of Ca^{2+} in the hyperalkaline fluids, and the chemical evolution of the water composition in the peridotite aquifers of the Oman-United Arab Emirate (Oman-UAE) ophiolite were investigated using the radiogenic strontium isotope ratios (^{87}Sr/^{86}Sr) and the changes in the chemical composition of groundwater. The ^{87}Sr/^{86}Sr composition and major ion concentration data indicate a combination of water/rock reaction pathways with both primary and secondary minerals found within the aquifer rocks. Groundwater evolution is dominated by low-temperature serpentinisation and carbonate dissolution/precipitation reactions. Serpentinisation drives the pH toward hyperalkaline conditions, shifts ^{87}Sr/^{86}Sr in groundwater toward peridotite values and releases Mg^{2+} into solution. Carbonate dissolution/precipitation buffer the pH rise, shifts ^{87}Sr/^{86}Sr toward carbonate values, and results in the decrease of either Ca^{2+} or Mg^{2+} concentrations in the solution depending on the type of carbonate precipitated. Two clear stages can be identified in the groundwater evolution of the Oman-UAE ophiolite complex: Type I water that are Mg-rich with a pH < 10, and Type II water that are Ca-rich with a pH >10. We hypothesise that the change from Mg-rich to Ca-rich fluids in the aquifers is driven by the dolomitisation of the precipitated carbonates and that part of the Ca^{2+} in the Type II fluids originates from this replacement process. This clear shift in groundwater chemistry suggests that peridotite alteration is not a continuous process but rather a succession of discrete stages that are associated with different dominant reactions and a significant role of the secondary minerals.

Chapter 4

4.1   Introduction

Peridotite is the principle rock type found in the Earth's mantle, and is stable under the high temperature, high pressure, reducing environments found in the Earth's interior. When exposed to the low temperature, low pressure, oxidising conditions of the surface environment, peridotites become unstable, creating a chemical gradient that drives the alteration of the primary peridotite minerals (Johannes, 1969; Martin and Fyfe, 1970; Evans, 1977; Frost, 1985; Malvoisin *et al.*, 2012). This alteration occurs via two main exothermic reactions: serpentinisation and oxidation (Eq. 1 & 2).

$4Mg_2SiO_4(\text{Mg-olivine}) + (CaMg;Mg_2)Si_2O_6(\text{pyroxenes}) + 7H_2O = 3Mg_3Si_2O_5(OH)_4(\text{serpentine}) + (Ca^{2+};Mg^{2+})_{(aq)} + 2OH^{-}_{(aq)}$ (1)

$3Fe^{2+}_2SiO_4 (\text{Fe-olivine}) + 2H_2O = 2Fe^{2+}Fe^{3+}_2O_4 (\text{magnetite}) + 3SiO_2 (\text{quartz}) + 2H_2$ (2)
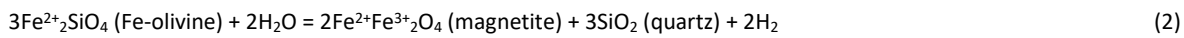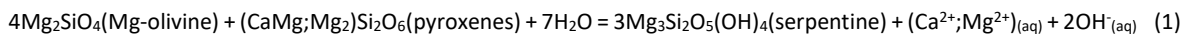
Peridotite alteration in this manner typically occurs in three environments: (i) high temperature alteration near mid-oceanic ridges (MOR); (ii) low temperature alteration in off-axis MOR environments; (iii) low-temperature alteration by fresh water in continental ophiolites. Although the same basic chemical reactions occur in each setting (Eq. 1 & 2), the different environments produce distinctive end-member fluids. Peridotite alteration close to MOR, such as that occurring in the Rainbow (Fouquet *et al.*, 1998; Charlou *et al.*, 2002; Douville *et al.*, 2002) and Logatchev (Kuhn *et al.*, 2004; Schmidt *et al.*, 2007) hydrothermal fields, produce acidic (pH ~3), reduced, metal-rich fluids containing high concentrations of hydrogen and methane produced via Fischer-Tropsch reaction (McCollom *et al.*, 2016), and exiting at high temperatures (>250ºC). Off-axis alteration, such as those observed at the Lost City (Kelley *et al.*, 2001) and Saldanha (Barriga *et al.*, 1998; Dias *et al.*, 2011) hydrothermal fields, produce clear, low-temperature (<100ºC), alkaline (pH >9), reduced, Ca-rich fluids that also contain a high concentration of hydrogen and methane. In ophiolite sequences, the low-temperature serpentinisation of peridotites produces Ca-rich, Mg-depleted, dissolved inorganic carbon (DIC)-poor, and both hydrogen- and methane-rich fluids, with a temperature <40°C and pH>11 upon surfacing (Barnes and O'Neil, 1971; Neal and Stanger, 1983, 1985; Bruni *et al.*, 2002; Neal and Shand, 2002; Cipolli *et al.*, 2004; Frost and Beard, 2007; Kelemen and Matter, 2008; Menzies *et al.*, 2016). The alkalinity and high Ca^{2+} content of the fluids produced by low-temperature MOR systems and in ophiolites, drive the precipitation of massive carbonate deposits upon contact with atmospheric or dissolved CO_2 (Eq. 3) (O'Neil and Barnes, 1971; Clark, Fontes and Fritz, 1992; Kelley *et al.*, 2001; Ludwig *et al.*, 2006)

$3Mg_3Si_2O_5(OH)_4 (\text{serpentine}) + (Ca^{2+};Mg^{2+})_{(aq)} + 2OH^{-}_{(aq)} + CO_{2\ (aq)} = 3Mg_3Si_2O_5(OH)_4 + (Ca;Mg)CO_3 + H_2O$ (3)
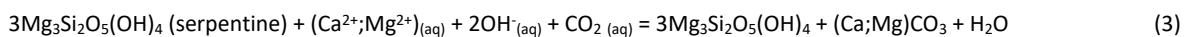
Together, these peridotite alteration reactions (Eq. 1, 2 & 3) can support extremophile microbial communities (Macleod *et al.*, 1994; Miller *et al.*, 2016; Shibuya, Russell and Takai, 2016), induce

rock fracturing (Jamtveit, Putnis and Malthe-Sørenssen, 2009; Kelemen and Hirth, 2012), and provide a carbon sink (Kelemen and Matter, 2008; Matter and Kelemen, 2009; Kelemen, J. Matter, *et al.*, 2011; Paukert *et al.*, 2012; Alt *et al.*, 2013; Schwarzenbach *et al.*, 2013). The origin of the Ca^{2+} in the hyperalkaline fluids is of particular interest for CO_2 sequestration as Ca^{2+} originating from silicate minerals would represent a net uptake of CO_2 when precipitating as carbonates (Berner, Lasaga and Garrels, 1983; Seifritz, 1990), whereas Ca^{2+} derived from the dissolution of carbonates precipitated at an earlier stage would not affect the CO_2 balance (Urey, 1952). Radiogenic strontium ratios ($^{87}Sr/^{86}Sr$) are routinely used as a proxy to trace water/rock interactions in natural systems (Negrel *et al.*, 2003; Frost and Toner, 2004). In this study, we measured changes in the concentration of major and minor dissolved elements (e.g. Mg^{2+}, Ca^{2+}, Sr^{2+}, DIC) and $^{87}Sr/^{86}Sr$ ratios in groundwater to characterise the water/rock interactions that occur in the peridotite aquifers of the Oman-UAE ophiolite, and to determine the rock source of the Ca^{2+} in the hyperalkaline fluids.

4.2 Materials and methods

4.2.1 Geological and hydrological setting

The Oman – United Arab Emirates ophiolite lies along the northern coast of Oman in a succession of massifs, covering ~38000km^2 and with a relief of up to 1000m (Fig. 1.3). It is the most extensive slice of oceanic lithosphere thrust on land (Coleman and Hopson, 1981; Hopson *et al.*, 1981). The upper crustal unit of the ophiolite is formed of plagiogranites, basalt and troctolites produced by the fractional crystallisation of melts, whereas the lower crustal unit is formed of gabbroic rocks. Both units are cut by gabbroic and diabase dikes produced from evolved mantle melts, and epidosite veins derived from hydrothermal alteration (McCulloch *et al.*, 1980; Lanphere, Coleman and Hopson, 1981; Benoit, Polvé and Ceuleneer, 1996; Kawahata *et al.*, 2001; Davis, 2003). The ophiolite mantle unit is mainly composed of harzburgites made of olivine Fo90-91 (85% - 74%), orthopyroxene En90-91 (24% - 10%), trace clinopyroxene (<<1%), and spinel (5% - 2%) (Boudier and Coleman, 1981; Hanghøj *et al.*, 2010). The peridotites were extensively altered by seawater during the Cretaceous and Tertiary periods, and have been heavily serpentinised (30% in average to >90%) (Chavagnac *et al.*, 2013). Mafic dikes and dunite resulting from magmatic processes within the mantle section are also found in the mantle unit along with hydrothermal veins and carbonate veins that cut through the peridotites with variable abundance depending on the local geology (Nicolas *et al.*, 2000; Kelemen and Matter, 2008).

The peridotite unit hosts a system of interconnected aquifers of different permeabilities (Barnes and O'Neil, 1971; Neal and Stanger, 1985; Dewandel *et al.*, 2005). During rain events, water infiltrates the peridotites via physical features, such as faults and cracks, recharging the shallow, unconfined aquifer (upper 50m) and forming Mg-, HCO_3-rich "Type I" waters with a pH between 7 and 10 (Dewandel *et al.*, 2005). Groundwater can also infiltrate the less permeable confined aquifer in which porosity comprises microcracks, nanopores and mineral interspaces, and reacts with the rocks to form Ca-, OH-rich "Type II" water that have a pH >11 (Dewandel *et al.*, 2005; Paukert *et al.*, 2012). However, the mechanisms that govern the formation and evolution of each type of water in the peridotite aquifer are not yet established, such as the timing of formation, the sources and sinks of major elements (e.g. Mg, Ca), and the relationship between the two types of water are still unconstrained.

4.2.2   Sample collection
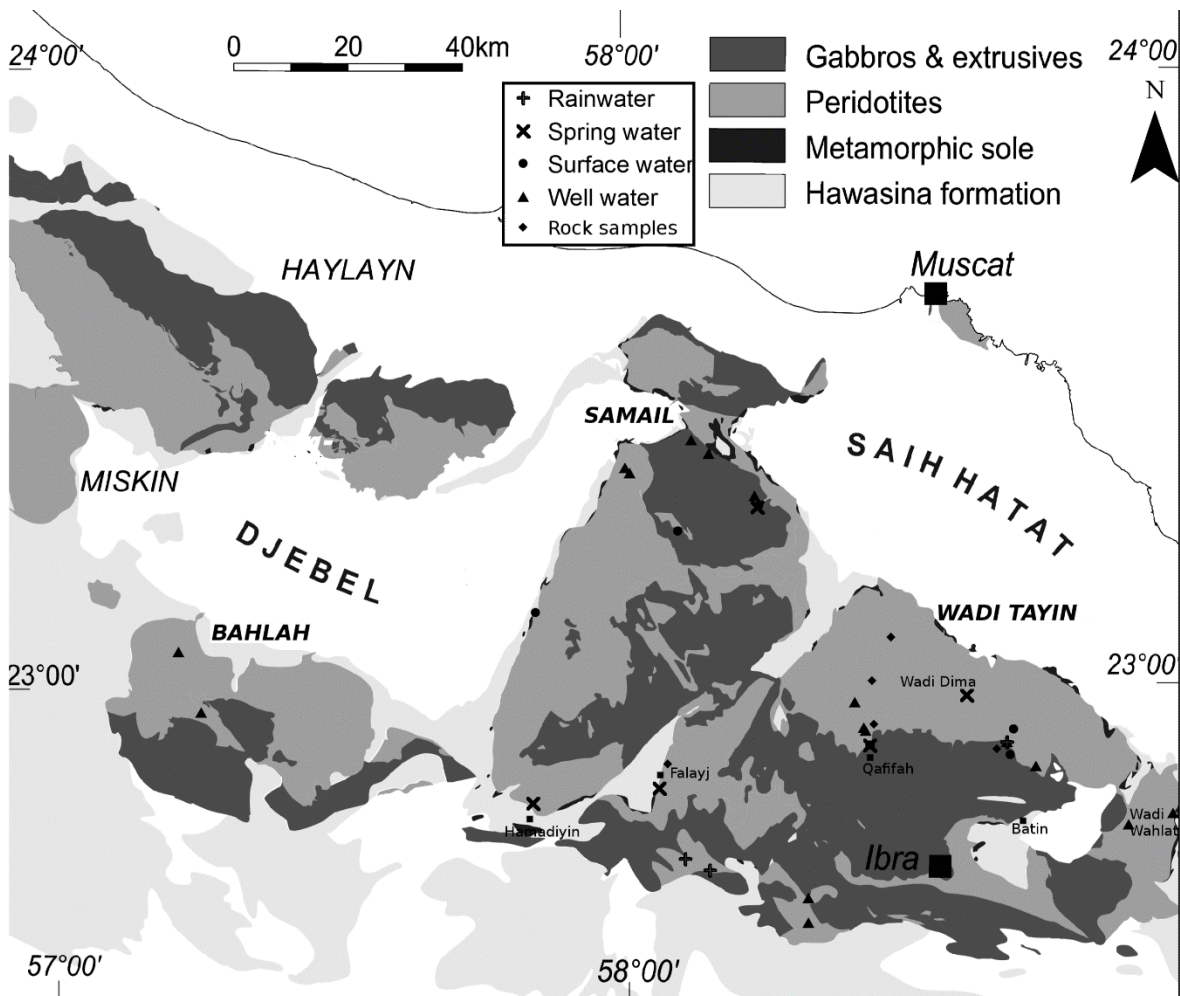
Figure 4.1: Sample locations in the southern massifs of the Oman-UAE ophiolite (left to right): Bahla, Samail, Wadi Tayin. Simplified geological map modified from Nicolas et al. (2000) by J.Coggon

Water samples were collected from wells, previously drilled to explore the water content of aquifers. They all have open holes or were equipped with discrete opening in the casing (screen), and were selected from areas surrounded by peridotites by using the geological maps and borehole log reports made available by the Ministry of Regional Municipalities and Water Resources. 34 water samples were collected from 15 wells in the northern part of the Samail massif, the Wadi Tayin massif and the Bahla massif, over the course of 6 field seasons between 2009 and 2016 (Fig. 4.1). In addition, 8 water samples were collected from wadi/falaj and 11 from hyperalkaline springs flowing in peridotite areas. The well water samples were collected using a submersible pump when the water table was less than 20m below top casing (mbtc). A discrete water sampler on a wireline (bailer) was used to sample deeper water. In addition, a Grundfos SQ 2-85N submersible pump was used during the 2016 campaign, which enable 3 times the borehole volume to be pumped before sampling in order to have access to fresh groundwater from the aquifer. In all cases, water was pumped for at least 20 min to remove the upper layer of stagnant water before sampling. Samples for chemical and isotopic analysis were taken using new syringes, filtered using 0.8 or 0.2μm sterile Acrodisc filters and transfered into new 125 and 30 mL polyethylene bottles for cation and Sr-isotopes, and anion analysis respectively, and 40mL $HgCl_2$-treated glass flasks for DIC analyses (Paukert *et al.*, 2012). Electrical conductivity (EC), pH, temperature and redox potential (Eh) were measured in the field using a WTW multi 3400i meter. Five samples representative of the rock-types and range of alteration present in the peridotite body were also collected from the study region, with the Sr concentration and $^{87}Sr/^{86}Sr$ isotopic ratio being measured on the bulk rock, handpicked mineral phases and leachate solutions derived from these samples.

4.2.3 Rock sample leaching

A leaching protocol adapted from Poulton & Canfield (2005) was used to separately dissolve the different mineral phases present in altered peridotite in order to measure their $^{87}Sr/^{86}Sr$ ratios (see chapter 3). The principal minerals targeted by this process were the carbonate and serpentine phases. No other secondary minerals were present in sufficient quantity to play a meaningful role in the water/rock interactions. The choice for reagents and experimental conditions to leach each mineral phases was based on previous published experiments (Poulton and Canfield, 2005; Teir *et al.*, 2007; Wittig *et al.*, 2009; Wang and Maroto-Valer, 2011; Huang *et al.*, 2012).

4.2.4 Chemical and isotopic analysis

Cation concentrations were measured on an Inductively Coupled Plasma-Mass Spectrometer (ICP-MS) quadrupole Thermo X-Series 2 at the University of Southampton. A volume of 1 mL was sub-sampled from the sample solution and dried on a hotplate in a Savillex pot. The dry residue was

then re-dissolved in a solution of sub-boiled 3% HNO_3 spiked with 20 ppb Be and 5 ppb In and Re, and an additional solution diluted x100 was made. The two solutions obtained were used to analyse minors and majors. A set of solutions with a range of concentration of the elements of interest was made from standard solutions. This set was then used to calibrate the measurements in counts per second to concentration in the PlasmaLab software used to process the results. The samples were run with standard reference material NIST1640a that went through the same protocol and was run as an unknown assess the accuracy of the measurements. The data only being used if the NIST1640a concentrations measured during the run were within an accepted range (%RSD < 15 for 12 runs, except for ^{44}Ca and ^{39}K, where a %RSD of 18 and 30 was respectively used due to argon plasma interferences). Other processing of the results include (1) the monitoring of internal drift using the detection of the Be, In, and Re added as spike. (2) The determination of the limit of detection (LoD) of each element using blank measurements and the formula: Blank average + 3σ = LoD, measurements falling below the LoD were rejected. (3) The monitoring of internal precision by measuring each sample 4 times and calculating the percentage relative standard deviation (%RSD), which is the expression of the standard deviation as a percentage of the mean, data with %RSD of >10 % were rejected (Menzies, 2012).

Anions concentrations were measured by ion chromatography on a Dionex Ion Chromatograph 25 with IonPac AS9-HC IC columns at the University of Southampton. Repeat analysis of IAPSO seawater as well as single anion standards indicates that the reproducibility of the Cl and SO_4 analyses is better than ±2% (Marieni, 2016).

$^{87}Sr/^{86}Sr$ ratios were measured on a Thermal Ionisation Mass Spectrometer (TIMS) Triton at the University of Southampton. A volume containing 1µg of Sr was subsampled from the water sample and dried on a hotplate in a Savillex PFA vial. The dry residue was re-dissolved in 200µL of laboratory prepared 3M HNO_3 and a standard procedure for cation exchange column with Eichrom Sr-specific resin was used to separate the Sr (Pearce *et al.*, 2015). The solution with the purified Sr was collected in Savillex PFA vials and dried on a hotplate. The dry residue was re-dissolved in 1.5µL of laboratory prepared 1M HCl and loaded onto an oxidised tantalum filament with a solution of Ta activator before analysis. The data were normalised to a value of 0.710248 for the standard reference material NIST-987 used during the analyses to allow the comparison between the different studies (McArthur, Howarth and Shields, 2012).

4.3   Results

4.3.1 $^{87}Sr/^{86}Sr$

Rock $^{87}Sr/^{86}Sr$ ratios from the Oman-UAE ophiolite have previously been published (McCulloch *et al.*, 1980; Boudier and Coleman, 1981; Lanphere, Coleman and Hopson, 1981; Benoit, Polvé and Ceuleneer, 1996; Weyhenmeyer, 2000; Kawahata *et al.*, 2001; Gerbert-Gaillard, 2002; Davis, 2003; Bosch *et al.*, 2004; Kelemen, J. M. Matter, *et al.*, 2011; Stephen, 2014) and are compiled together with the $^{87}Sr/^{86}Sr$ ratios from the rock samples analysed in this study in Figure 4.2. Our ultramafic rocks $^{87}Sr/^{86}Sr$ ratios range from 0.70400 to 0.70926 (Table 4.1; see chapter 3), which is within the range of the ultramafic rocks $^{87}Sr/^{86}Sr$ ratios published (0.70307 to 0.70878). However, three of our samples have higher ratios (OM15_R4: 0.70903, OM15_R4d: 0.70916, and OM15_R4out: 0.70926) (Fig. 4.2). The ultramafic rock $^{87}Sr/^{86}Sr$ ratios have the largest range of values, published crustal rocks are in the lower part of the range (0.70261 to 0.70735), whereas carbonates are in the upper part of it (0.70759 to 0.70886). Silica-based sediments have the highest range of $^{87}Sr/^{86}Sr$ ratios in the ophiolite (0.711940 to 0.771970).

Table 4.1: Element concentrations and $^{87}Sr/^{86}Sr$ of altered peridotite mineral whole fractions (WF); see chapter 3 for more details.

Sample ID	Major minerals (XRD)	Mg mmol/kg	Al mmol/kg	Ca mmol/kg	Cr mmol/kg	Fe mmol/kg	Ni mmol/kg	Cu µmol/kg	Sr µmol/kg	$^{87}Sr/^{86}Sr$ norm.	2 s.e 10^{-6}
OM15_R1c$_{WF}$	Dolomite + Serpentine (traces)	3723	1	4154	0	11	1.4	7.9	5105	0.70859	3.84
OM15_R1w$_{WF}$	Serpentine/Clinochlore + Tremolite (traces)	7448	422	267	39	1250	40	233	302	0.70848	4.16
OM15_R2c$_{WF}$	Calcite +Serpentine/Brucite (traces)	1090	0	6654	0	bdl	0.1	1.0	7580	0.70838	4.11
OM15_R2s$_{WF}$	Serpentine +Saponite (traces)	7660	291	164	8	647	14	60	103	0.70831	4.07
OM15_R2w$_{WF}$	Serpentine + saponite (traces)	8279	328	15	22	811	30	108	57	0.70788	7.13
OM15_R3$_{WF}$	pyroxenite dyke	10500	301	164	35	1044	38	396	34	na	na
OM15_R3b$_{WF}$	Forsterite+px +saponite (traces)	9910	317	966	18	1046	20	11954	83	0.70609	3.78
OM15_R3f$_{WF}$	(Clino)pyroxene	4694	554	3763	61	330	3.4	1159	122	0.70402	3.86
OM15_R4$_{WF}$	Serpentine + Brucite +saponite (traces)	11373	235	26	8	969	42	23	34	0.70905	11.49
OM15_R4d$_{WF}$	Serpentine + Brucite +saponite (traces)	10693	224	22	9	1021	43	19	33	0.70918	542.22
OM15_R4r$_{WF}$	Serpentine + Brucite +saponite (traces)	11452	227	20	14	1093	48	24	33	na	na
OM15_R4s$_{WF}$	Serpentine	12839	227	17	9	864	41	28	36	na	na
OM15_R4out$_{WF}$	Serpentine + Saponite (traces)	11027	227	8	3	593	7.9	67	41	0.70928	248.50
OM15_R5$_{WF}$	Forsterite/Serpentine +Pigeonite/Saponite (traces)	10456	302	147	29	1041	37	329	34	0.70554	729.14

Water $^{87}Sr/^{86}Sr$ ratios from the Oman-UAE ophiolite have previously been reported by Weyhenmeyer 2000 & Semhi et al. 2017 and are compiled together with data from this study in Figure 4.3. Our groundwater $^{87}Sr/^{86}Sr$ ratios range from 0.70672 to 0.70873 (Table 4.2), within the range of published $^{87}Sr/^{86}Sr$ ratios for water samples from peridotite aquifer (0.70670 to 0.70916). Water samples from other rock-type aquifers have a similar range of $^{87}Sr/^{86}Sr$ ratios, such as gabbro aquifer (0.70701 to 0.70867, one outliner at 0.70565), and carbonate aquifer (0.70773 to 0.70861; one outliner at 0.71141). But water samples from some other aquifers have a range of $^{87}Sr/^{86}Sr$ ratios with higher values, such as water samples from alluvium aquifer (0.70750 to 0.71061) and from the Hajar Super Group (HSG) aquifer (0.70772 to 0.71312).

The $^{87}Sr/^{86}Sr$ ratios of water from the peridotite and carbonate aquifers overlap the range of ultramafic and carbonate rock values (Fig. 4.2 & 4.3). The ranges of $^{87}Sr/^{86}Sr$ ratios of water samples from the gabbro aquifers and of gabbro rock samples do not overlap, instead, the $^{87}Sr/^{86}Sr$ ratios of water from gabbro aquifers overlap with ultramafic rock and carbonate values. In the peridotite aquifers, the $^{87}Sr/^{86}Sr$ of water is correlated to the pH with a general negative trend (Fig. 4.4). The samples can be separated by pH in two major groups, one with pH<10 and $^{87}Sr/^{86}Sr$ ratios between 0.70900 and 0.70800 (with one exception at 0.70768), and one with pH>10 and $^{87}Sr/^{86}Sr$ ratios from 0.70850 to 0.70650 (Fig. 4.4, Table 4.2). These groups correspond to Type I and Type II waters, respectively.
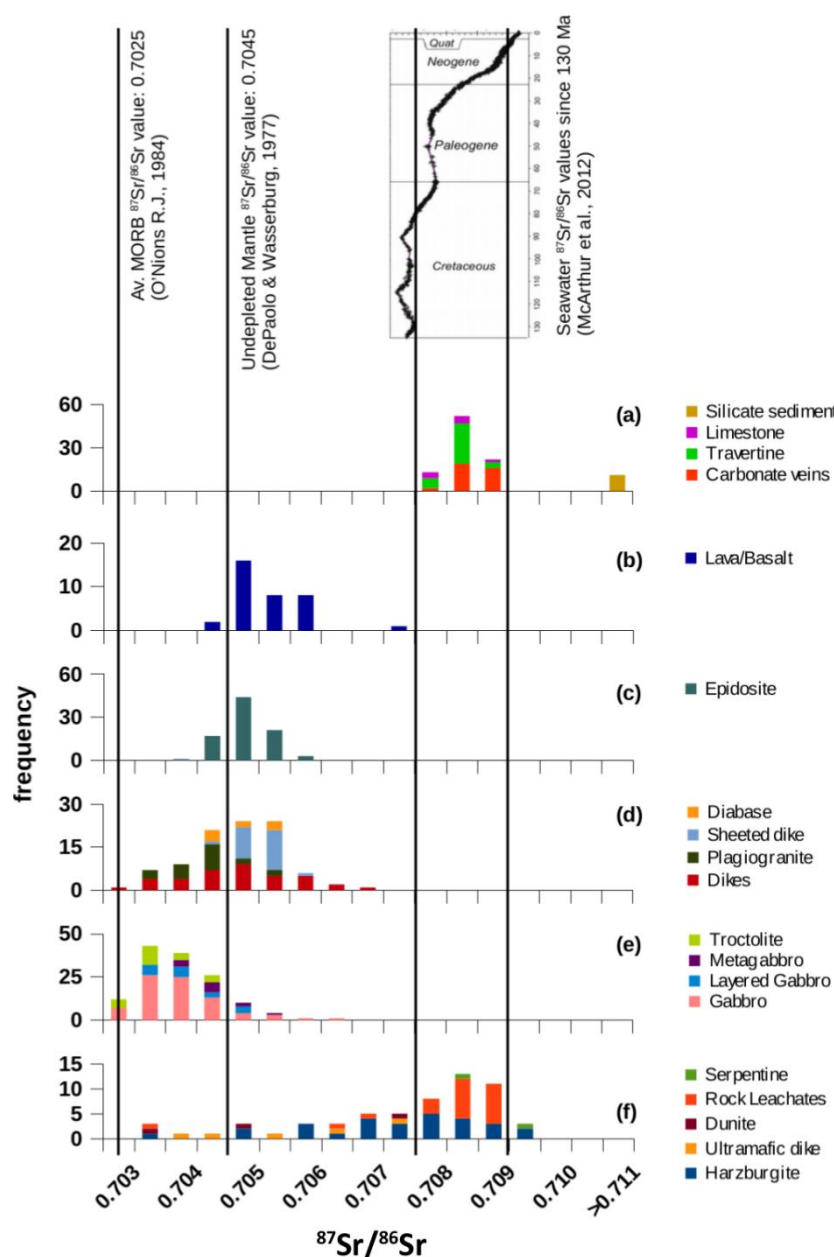
Figure 4.2 Compilation of Sr-isotope values (^{87}Sr/^{86}Sr) of rock samples from the Oman-UAE ophiolite from the literature and this study. The frequency represents the number of samples within each interval of ^{87}Sr/^{86}Sr value. Rock samples are from the southern part of the ophiolite (Samail and wadi Tayin massifs). They are separated by sample type: (a) Carbonate rocks comprising limestones, travertine terraces & veins of calcite, dolomite and magnesite found within the peridotites. The silicate sediment comprises sandstones and siltstones (ref 5; 10; 11; 12). (b) Epidosite, rock leachates and serpentine are produced via rocks alteration (ref 6; 8; 9; 12). (c) Harzburgites, dunites and ultramafic dikes are found in the mantle section of the ophiolite (ref 1; 2; 3; 6; 7; 11; 12). (d) Plagiogranites, lava/basalt and troctolites form the upper part of the crust (ref 1; 3; 4; 6; 8). (e) Dikes, diabase and sheeted dikes are produced from evolved mantle melts (ref 1; 3; 6; 8; 9). (f) Gabbroic rocks form the lower part of the crustal section of the ophiolite (ref 1; 2; 3; 4; 6; 8; 9; 11).

(1)McCulloch et al., 1980; (2)Boudier & Coleman, 1981; (3)Lanphere et al., 1981; (4) Benoit et al., 1996; (5)Weyhenmeyer, 2000; (6)Kawahata et al., 2001; (7)Gerbert-Gaillard, 2002; (8)Davis, 2003; (9)Bosch et al., 2004; (10)Kelemen et al., 2011; (11)Stephen, 2014; (12)this study.
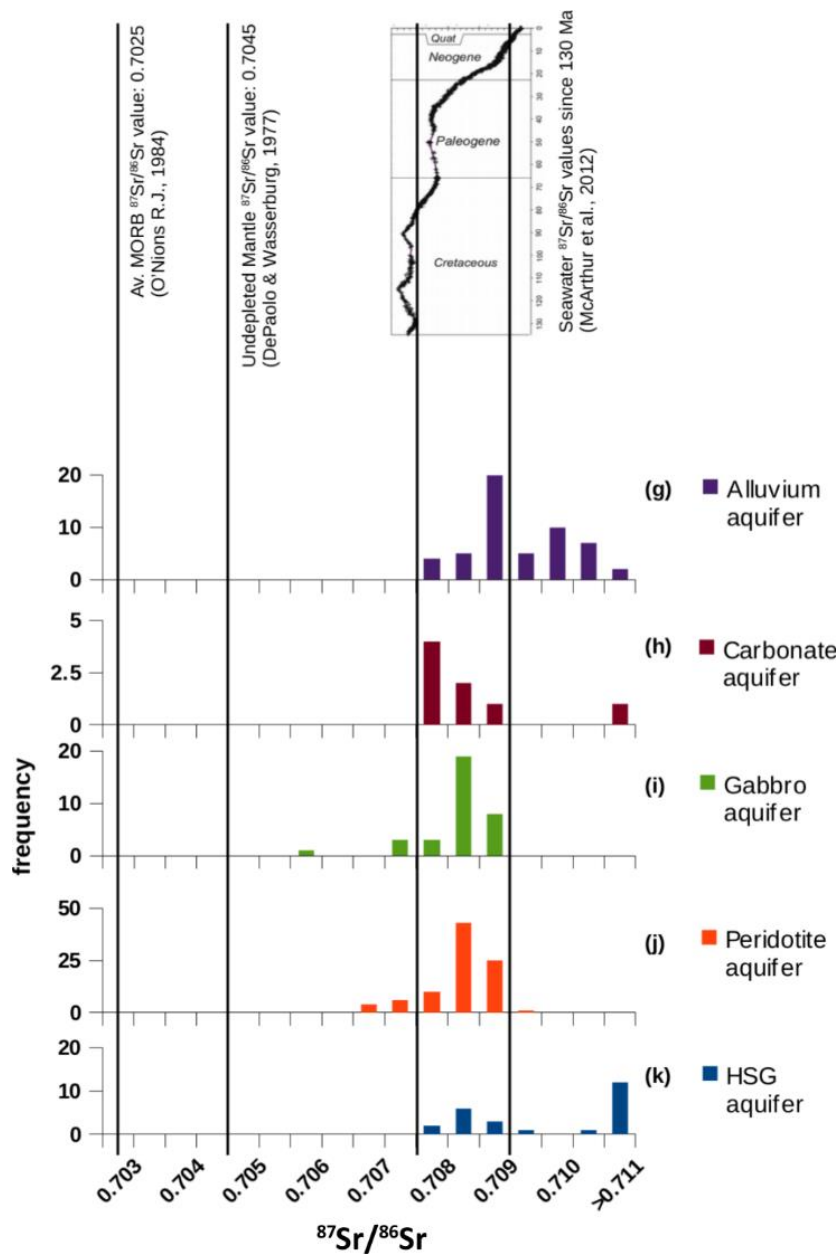
Figure 4.3: Compilation of Sr-isotope values ($^{87}Sr/^{86}Sr$) of water samples from the Oman-UAE ophiolite from the literature and this study. The frequency represents the number of samples within each interval of $^{87}Sr/^{86}Sr$ value. The water samples originate from aquifers hosted in (g) alluvium, formed by modern deposits on the northern coast or inland, southward of the ophiolite (ref 1; 2), (h) carbonate rocks deposited during the Tertiary, 65-2 Ma ago) (ref 1; 2), (i) gabbro (gabbroic and igneous rocks that form the crustal section of the ophiolite and that have a Cretaceous age, ca 120-90 Ma) (ref 1; 2). (j) Peridotite-hosted aquifers consist of low porosity altered harzburgite and dunite of Cretaceous age (ca 120-90 Ma) (ref 1; 2; 3). (k) The Hajar Super Group (HSG) comprises carbonate rocks formed 270-90 Ma ago that outcrop, among other areas, in the more elevated parts of the ophiolite: Jabal Al Akhdar (ref 2).

(1)Weyhenmeyer, 2000; (2)Semhi et al., 2017; (3)this study.
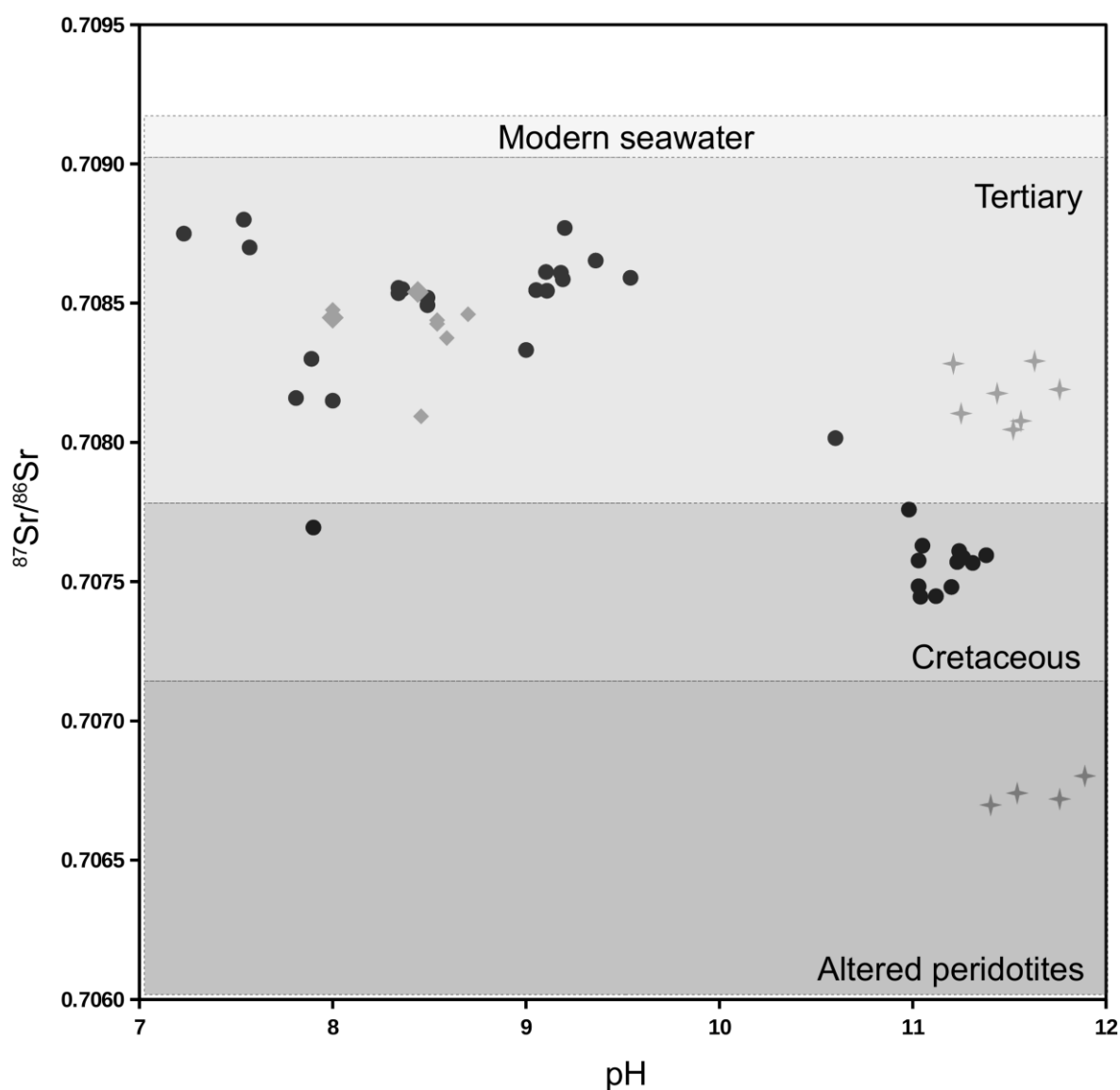
Figure 4.4: Ground waters $^{87}Sr/^{86}Sr$ values are plotted against their pH. The grey boxes encompass the $^{87}Sr/^{86}Sr$ values for Modern, Tertiary & Cretaceous seawater (McArthur et al., 2003). Altered peridotites values are a mix between seawater and mantle values (Gerbert-Gaillard, 2002).

4.3.2   Water chemistry

The progression of water/rock reactions in peridotite aquifers is best observed by the pH increase due to serpentinisation (Eq. 1). The dissolved ion concentrations are listed in Table 4.1 and plotted against pH to illustrate the chemical evolution of groundwater as it interacts with the aquifer rocks along its flow path (Figures 4.5a-h). The dissolved ion concentrations evolve with pH following different trends but all display a change in behaviour at pH 10; that defines the difference between Type I and II waters (Fig. 4.5).

Table 4.2: Setting and chemical data of water samples. *C. Weyhenmeyer (2000), "Don dePaolo (Pers. Comm.).

Sample ID	Well ID	Type of water	lithology/ Sampling context	Area	UTM coord. Easting	Northing	pH	DIC mmol/kg	Na mmol/kg	Mg mmol/kg	Ca mmol/kg	SiO$_2$ µmol/kg	Cl mmol/kg	SO$_4$ µmol/kg	Sr µmol/kg	^{87}Sr/^{86}Sr Norm.
*16F	na	Falaj water	Peridotite	Samaii (W)	585946	2557084	8.4	3.72	0.8	2.1	0.3	291.7	1.3	385.2	3.8	0.708540
OM16_05	na	Falaj water	Harzburgite	Qafifah	645780	2533441	8.0	2.58	0.9	1.2	0.3	167.1	1.0	290.6	1.5	0.708448
*OM09_W09T	na	Wadi water	Harzburgite	Qafifah	645927	2533408	8.6	-	1.4	1.4	0.3	247.5	1.8	321.9	1.9	0.708375
*576WAD	na	Wadi water	Peridotite	Samaii (N)	611490	2571644	8.7	3.7	1.4	2.0	0.7	391.7	1.5	458.1	4.3	0.708460
OM10_01D	na	Wadi water	Harzburgite	Misbit	625962	2576230	8.5	3.1	3.0	1.7	0.8	386.3	2.8	751.9	5.7	0.708094
OM14_02C	na	Wadi water	Harzburgite	Wadi Dima	671502	2536298	8.5	-	1.7	3.2	0.5	-	-	-	2.4	0.708426
OM14_03D	na	Wadi water	Harzburgite	Wadi Dima	671502	2536298	8.5	-	1.7	3.2	0.5	-	-	-	2.5	0.708439
OM16_RoW1	na	Wadi water (flash flood)	Gabbro-Peridotite	Batin (N)	670971	2531699	8.0	-	0.1	0.1	0.7	55.9	-	-	1.9	0.708476
*OM09_W10V	na	Spring water	Gabbro – moho transition	Misbit	625676	2576006	11.4	0.3	6.3	<0.1	2.0	47.7	6.5	63.8	3.9	0.706698
OM10_04S	na	Spring water	Peridotite – moho transition	Qafifah	645780	2533441	11.8	0.2	6.6	<0.1	1.8	3.4	5.1	5.7	1.5	0.706720
OM09_W06O	na	Spring water	Peridotite	Wadi Dima	663152	2542372	11.5	0.2	7.9	<0.1	1.8	6.1	6.7	12.9	2.9	0.706741
*OM09_W05L	na	Spring water	Peridotite – moho transition	Qafifah	645780	2533441	11.9	0.4	6.2	<0.1	1.7	1.1	4.7	6.6	1.4	0.706802
OM09_W02A	na	Spring water	Peridotite foothill	Falaj	608145	2525713	11.5	0.2	9.5	<0.1	1.9	1.4	7.4	5.0	1.1	0.708046
OM10_02L	na	Spring water	Peridotite foothill	Falaj	608145	2525713	11.6	0.2	9.6	<0.1	1.8	1.9	8.2	8.9	1.1	0.708077
OM12_01G	na	Spring water	Peridotite foothill	Falaj	608145	2525713	11.3	0.1	9.3	<0.1	2.0	1.2	8.0	7.3	1.0	0.708104
*OM09_W04G	na	Spring water	Peridotite foothill	Hamadiyin	585584	2522988	11.4	0.1	10.9	<0.1	1.3	2.5	8.2	30.4	2.6	0.708176
OM09_W04F	na	Spring water	Peridotite foothill	Hamadiyin	585584	2522988	11.8	0.2	11.1	<0.1	1.4	1.8	8.3	35.2	3.0	0.708190
OM12_02L	na	Spring water	Peridotite foothill	Falaj	608145	2525713	11.2	0.1	7.9	<0.1	1.9	0.6	6.8	15.1	1.6	0.708283
OM10_03R	na	Spring water	Peridotite foothill	Falaj	608145	2525713	11.6	0.2	8.6	<0.1	0.8	-	6.9	17.2	1.5	0.708292
*105W	SJA-4A	Well water	Peridotite alluvium	Samaii (N)	601962	2582964	7.5	3.26	0.6	1.0	0.9	391.7	0.3	156.2	4.3	0.708800
OM10_11AX	SJA-4B	Well water	Weathered Peridotite	Samaii (N)	601942	2582989	7.2	3.98	1.1	1.2	1.2	389.7	1.1	370.0	7.2	0.708750
OM10_11AY	SJA-4A	Well water	Peridotite alluvium	Samaii (N)	601962	2582964	7.6	3.50	0.7	1.2	1.1	428.6	0.7	255.1	5.9	0.708700
*173W	SNA-6B	Well water	Alluvium	Misbit	625156	2578031	8.0	3.18	1.7	1.8	0.5	303.3	1.8	426.8	3.1	0.708150
*179W	SMA-4B	Well water	Alluvium	Samaii (N)	613821	2587978	7.9	3.62	3.7	2.0	0.5	531.7	3.1	593.4	4.2	0.708300
OM10_15BC	SNA-3B	Well water	Alluvium	Samaii (N)	616917	2585510	7.9	2.32	4.1	1.3	1.1	356.0	4.5	802.0	5.8	0.707695
OM15-05	NSHQ-3B	Well water	Harzburgite	Qafifah	645068	2536069	8.4	2.50	0.6	1.7	0.3	217.4	0.9	279.8	2.0	0.708550
OM16_06A	WAB-104	Well water	Harzburgite	Qafifah	643099	2541124	8.5	3.19	0.7	1.9	0.1	147.5	0.8	495.1	2.2	0.708493
OM16_06B	WAB-104	Well water	Harzburgite	Qafifah	643099	2541124	8.5	3.48	0.6	1.9	0.1	180.6	0.7	458.9	2.4	0.708520
OM16_07A	WAB-105	Well water	Harzburgite	Qafifah	644678	2536524	8.3	3.11	0.6	1.6	0.3	252.1	0.8	287.8	1.9	0.708536
OM16_07B	WAB-105	Well water	Harzburgite	Qafifah	644678	2536524	8.3	3.05	0.6	1.6	0.2	252.3	0.8	285.4	1.9	0.708555
OM16_10	WAB-12	Well water	Harzburgite	Wadi Wahlat	692081	2519249	7.8	3.25	0.9	1.4	0.4	340.6	1.1	331.9	6.8	0.708159
*102W	SJA-3B	Well water	Harzburgite	Samaii (N)	602847	2582068	9.2	0.66	1.3	2.5	0.02	8.3	2.0	947.4	4.6	0.708770
OM10_12AZ	SJA-3B	Well water	Harzburgite	Samaii (N)	602847	2582068	9.4	1.42	1.4	2.2	0.05	12.6	2.1	889.2	5.7	0.708653
OM12_06T	WDA-17	Well water	Harzburgite	Bahlah	522099	2550048	9.1	2.48	0.9	2.4	0.05	0.2	1.1	725.2	2.6	0.708612
OM12_08Y	WDA-5	Well water	Harzburgite	Bahlah	526133	2539283	9.1	1.82	1.4	2.3	0.05	3.0	2.1	727.8	3.2	0.708547
OM12_08Z	WDA-5	Well water	Harzburgite	Bahlah	526133	2539283	9.1	1.75	1.4	2.3	0.05	2.8	2.0	715.7	3.4	0.708545
OM16_02	WDA-17	Well water	Harzburgite	Bahlah	522099	2550048	9.2	2.70	0.8	2.0	0.05	2.2	1.0	767.3	2.1	0.708609
OM16_11	WAB-119B	Well water	Harzburgite	Wadi Wahlat	700040	2521270	9.0	1.39	1.0	1.2	0.12	33.7	2.3	292.8	1.4	0.708332
OM16_12A	WAB-55	Well water	Harzburgite	Ibra (SW)	634782	2506103	9.2	2.50	4.1	2.7	0.08	2.6	7.3	897.0	3.0	0.708586
OM16_12B	WAB-55	Well water	Harzburgite	Ibra (SW)	634782	2506103	9.5	2.73	4.0	2.9	0.08	2.5	7.3	814.3	2.9	0.708591
OM15-06	WAB-56	Well water	Harzburgite	Ibra (SW)	634812	2501628	10.6	0.22	3.1	bdl	0.4	178.4	3.1	16.1	2.3	0.708016
OM16_13	WAB-56	Well water	Harzburgite	Ibra (SW)	634812	2501628	11.0	0.24	3.6	<0.1	0.5	100.4	3.5	5.9	2.5	0.707759
OM12_03N	NSHQ-14	Well water	Harzburgite	Batin (N)	675495	2529716	11.0	0.09	11.6	<0.1	4.1	1.0	15.8	9.8	20.0	0.707576
OM12_03O	NSHQ-14	Well water	Harzburgite	Batin (N)	675495	2529716	11.1	0.08	10.3	<0.1	3.8	2.0	14.3	34.5	17.1	0.707629
OM14_01A	NSHQ-14	Well water	Harzburgite	Batin (N)	675495	2529716	11.4	-	12.1	<0.1	3.7	13.1	16.2	78.3	18.9	0.707595
OM14_01B	NSHQ-14	Well water	Harzburgite	Batin (N)	675495	2529716	11.2	-	12.3	<0.1	4.4	77.9	16.8	38.2	21.1	0.707571
OM15-04A	NSHQ-14	Well water	Harzburgite	Batin (N)	675495	2529716	11.3	0.19	11.2	<0.1	3.4	5.0	16.1	145.9	18.0	0.707587
OM15-04B	NSHQ-14	Well water	Harzburgite	Batin (N)	675495	2529716	11.3	0.22	11.8	<0.1	4.1	136.9	16.9	10.2	19.4	0.707567
OM16_04	NSHQ-14	Well water	Harzburgite	Batin (N)	675495	2529716	11.2	0.22	9.4	<0.1	3.8	3.8	15.8	90.9	16.2	0.707610
OM14_05F	WAB-71	Well water	Harzburgite-Dunite	Batin (N)	670321	2533984	11.0	-	6.2	<0.1	4.1	19.2	12.2	42.5	9.2	0.707484
OM15-01	WAB-71	Well water	Harzburgite-Dunite	Batin (N)	670321	2533984	11.0	0.21	5.6	<0.1	3.8	16.5	12.2	34.3	8.7	0.707446
OM15-10	WAB-71	Well water	Harzburgite-Dunite	Batin (N)	670321	2533984	11.2	0.20	5.5	bdl	3.7	16.9	12.3	36.5	7.6	0.707481
OM16_03	WAB-71	Well water	Harzburgite-Dunite	Batin (N)	670321	2533984	11.1	0.23	5.2	<0.1	3.8	10.0	12.9	49.5	7.5	0.707448

Na, Cl, and Sr concentrations are below 10 mmol/kg in Type I waters and show a sharp increase in their range of concentrations in Type II waters. Mg and SO4 concentrations increase with pH in Type I water and plummet in Type II water. Dissolved inorganic carbon (DIC) and Ca concentrations decrease with pH in Type I water. In Type II water, DIC has a very low concentration (>0.2 mmol/kg), but Ca concentration increases again with pH. Finally, SiO_2 concentration decreases with pH in both types, from 531 to 0.2 µmol/kg in Type I water and from 178 to 1 µmol/kg in Type II.
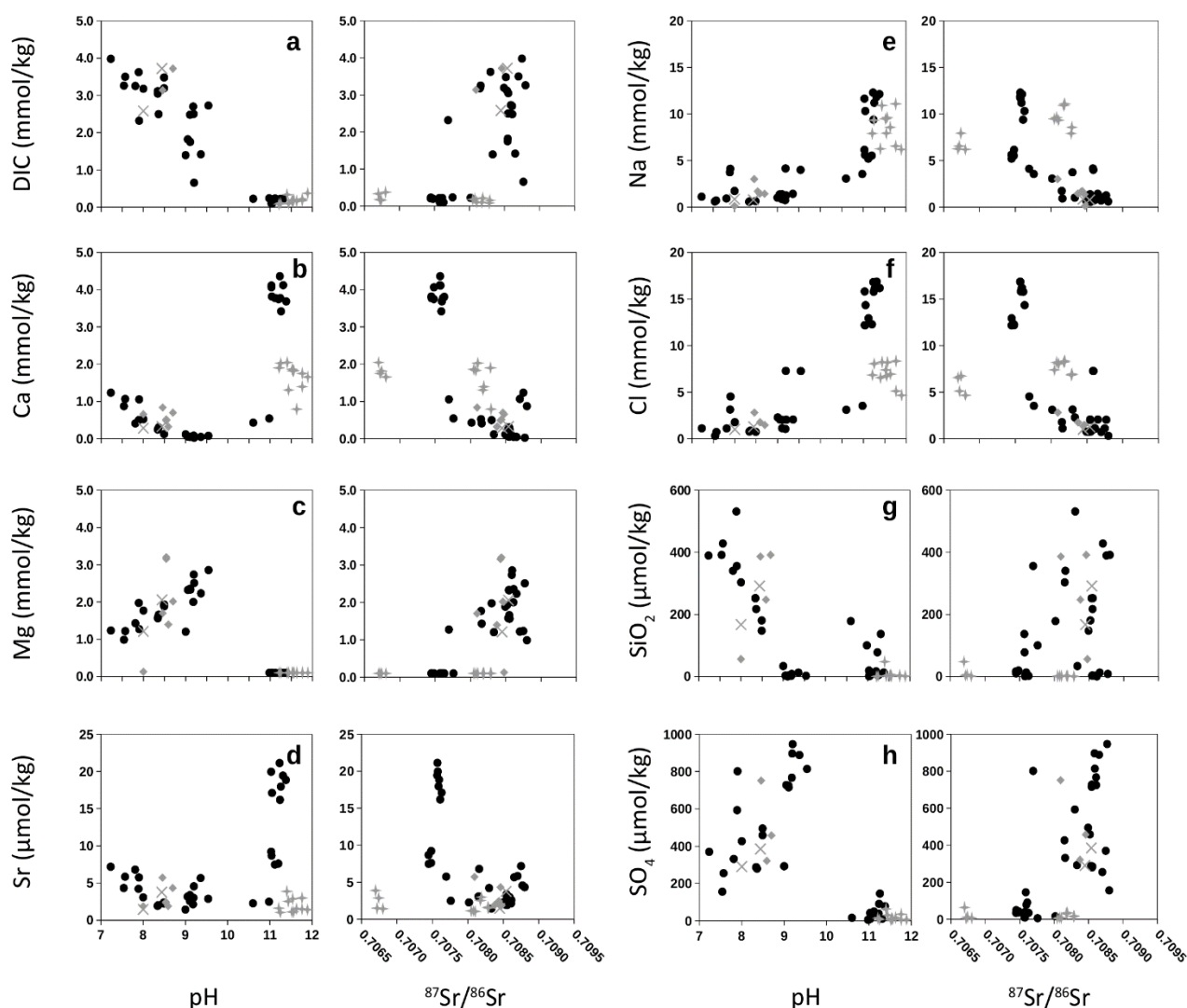
Figure 4.5: Major ion concentrations of water samples are plotted against pH (left graphs) and against the water $^{87}Sr/^{86}Sr$ ratio (right graphs). The change from type I to type II waters at pH 10 is linked to a change in most ion concentrations. These changes do not appear to be linked with the $^{87}Sr/^{86}Sr$ ratio.

4.4   Discussion

4.4.1   Sr sources

During serpentinisation Sr from peridotites is released into the fluid along with OH^- ions (Eq.1), moving the $^{87}Sr/^{86}Sr$ composition of water toward peridotite values and increasing the pH as the reaction progresses. However, peridotites have low Sr concentrations (Gerbert-Gaillard, 2002; Hanghøj *et al.*, 2010) and have a wide range of $^{87}Sr/^{86}Sr$ compositions (Fig. 4.2), thus the Sr released from secondary minerals contained within the peridotite can also interact with the fluids and mask the peridotite $^{87}Sr/^{86}Sr$ signal. These secondary minerals form under different conditions of alteration that determine their $^{87}Sr/^{86}Sr$ ratio. For example, the pervasive alteration that peridotites underwent during the Cretaceous (Lanphere, Coleman and Hopson, 1981; Bickle and Teagle, 1992) resulted in secondary minerals, such as serpentine and carbonates, with Cretaceous seawater-like $^{87}Sr/^{86}Sr$ ratios (~0.70750; McArthur et al. 2001). During the Tertiary transgression, peridotite alteration continued, enabling new secondary minerals to form with Tertiary seawater-like $^{87}Sr/^{86}Sr$ ratios (Coleman, 1981). However, because this alteration was not homogeneous (due to depth, low porosity or low permeability), some alteration minerals within the peridotite sequence retained a Cretaceous-like $^{87}Sr/^{86}Sr$ value.

The Type I water samples collected in this study have $^{87}Sr/^{86}Sr$ ratios in the same range as that of carbonates, serpentine veins and some serpentinised peridotites, and consistent with Tertiary seawater $^{87}Sr/^{86}Sr$ values (~0.70800 to ~0.70900; McArthur et al. 2001) (Fig. 4.2 and 4.3). Well waters with a pH >10, as well as serpentinised harzburgite and leachate samples have $^{87}Sr/^{86}Sr$ ratios closer to those of late Cretaceous seawater (0.70730 to 0.70770; McArthur et al. 2001). Hyperalkaline springs $^{87}Sr/^{86}Sr$ ratios form two clusters; one ~0.70817±0.0001, in the range of the Tertiary seawater values, and the other ~0.70674±0.00004, similar to that of the average value of all measured peridotite samples, ~0.70675 ±0.0016. This suggests that there are three main sources of the Sr with different $^{87}Sr/^{86}Sr$ present in groundwater: (1) carbonates and secondary alteration minerals formed during the Tertiary transgression that covered the O-UAE ophiolite (Coleman 1981); (2) secondary minerals formed by marine alteration of the rocks during the Cretaceous (Lanphere 1981); (3) the original peridotite minerals that have not yet undergone extensive alteration. We assume there is no significant Sr input from rainwater in the system as the rainfall events are scarce in this area.

4.4.2   Evolution of the water chemistry in the peridotite aquifer

Water infiltrates the peridotite aquifer and reacts with surrounding rocks to produce two types of groundwater, Type I and Type II waters (Eq. 1, 2 & 3) (Barnes & O'Neil 1969; Neal & Stanger 1985). Type I waters are formed in the shallow, unconfined aquifer, in a short amount of time, whereas Type II waters are the result of extensive water/rock interactions in a deeper, confined aquifer over a long period of time (Dewandel et al. 2005; Paukert et al. 2012).

Preliminary results of water-rock reaction experiments done in our laboratory have suggested that rainwater reacts very quickly (<1h) with the rocks (Appendix A). This first interaction would bring the water pH between 9 and 10, and >10 in the presence of brucite. Hence, the chemical composition of the water entering the aquifer could be significantly different from rainwater. In the same way, wadi waters could be the result of this fast equilibration between water and rock in direct contact with the atmosphere prior to more evolved water/rock reactions. Thus, the chemical evolution of water as a function of serpentinisation progression and carbonate precipitation is better observed in water samples collected in wells along the subsurface flow path, and we will assume a water starting pH of 7.4 (lowest pH measured in the samples).

4.4.2.1   Type I groundwater evolution

Between pH 7 and pH 10, the groundwater Mg concentration increases with pH (0.99 to 2.86mmol/kg) while Ca and DIC concentrations decrease ([Ca]=1.23 to 0.02 mmol/kg; [DIC] 3.98 to 0.66 mmol/kg) (Fig. 4.5a, b & c). This is consistent with an evolution driven by a combination of serpentinisation and carbonate precipitation (Eq. 1 & 3). The Sr concentration in Type I groundwater (Fig. 4.5d) does not concur with the evolution of $^{87}Sr/^{86}Sr$ ratios and does not fit in a simple mixing system, thus this behaviour also supports a combination of mineral dissolution and precipitation. However, the decreases in DIC (-3.32 mmol/kg) and Ca (-1.21 mmol/kg) are not stoichiometric with respect to the formation of calcite, and suggest the precipitation of Mg-bearing carbonates, such as dolomite. However, the precipitation of dolomite [$CaMg(CO_3)_2$] would only account for 2.42 mmol/kg of the DIC decrease and would require a further 0.9 mmol/kg of DIC to be bond with Mg as magnetite. But the release of Mg via serpentinisation dominates the evolution of its concentration in Type I waters, and mask any uptake of Mg in carbonates in Type I groundwater.

The increase of Mg concentration associated with the decrease of $^{87}Sr/^{86}Sr$ ratios from 0.70880 to 0.70770 (Fig. 4.4 and 4.5b) between pH 7 and 9, supports a serpentinisation process (Eq. 1). But the $^{87}Sr/^{86}Sr$ ratios rise up to 0.70877 in groundwater with pH between 9 and 10, this requires a source of more radiogenic Sr. Calcium-bearing carbonate veins ($^{87}Sr/^{86}Sr$ = 0.70856±0.00017 (n=13)) are a

potential candidate (Fig. 4.2), although their dissolution is unlikely at pH 8-9 and would generate an increase in DIC concentration that is not observed (Fig. 4.5a). A dolomitisation process (the replacement of Ca by Mg in carbonates) can also be considered. The Mg/Ca ratio in groundwater is under 10 between pH 7 and 9, but increases above 40 and up to 100 between pH 9 and 10, this could destabilise the Ca-carbonates and simultaneously re-precipitate them as Mg-rich carbonates (Machel, 2004; Kaczmarek and Sibley, 2011, 2014; Gregg *et al.*, 2015; Gabellone and Whitaker, 2016). The saturation indexes (S.I.) of dolomite and calcite in ground waters between pH 7 and 10, the similarity of $^{87}Sr/^{86}Sr$ ratios in pH 9 to 10 groundwater and in carbonate veins (Fig. 4.2, 4.4 & 4.6), and the direct observations of carbonate recrystallisation (Noel *et al.*, 2017), suggest this is a viable hypothesis. However, the increase in groundwater Ca concentration expected from a replacement of Ca by Mg in carbonates, does not start before pH 10. Therefore, the cause of this delay needs to be identified, or another source with a high $^{87}Sr/^{86}Sr$ could be involved but would need identification as well.
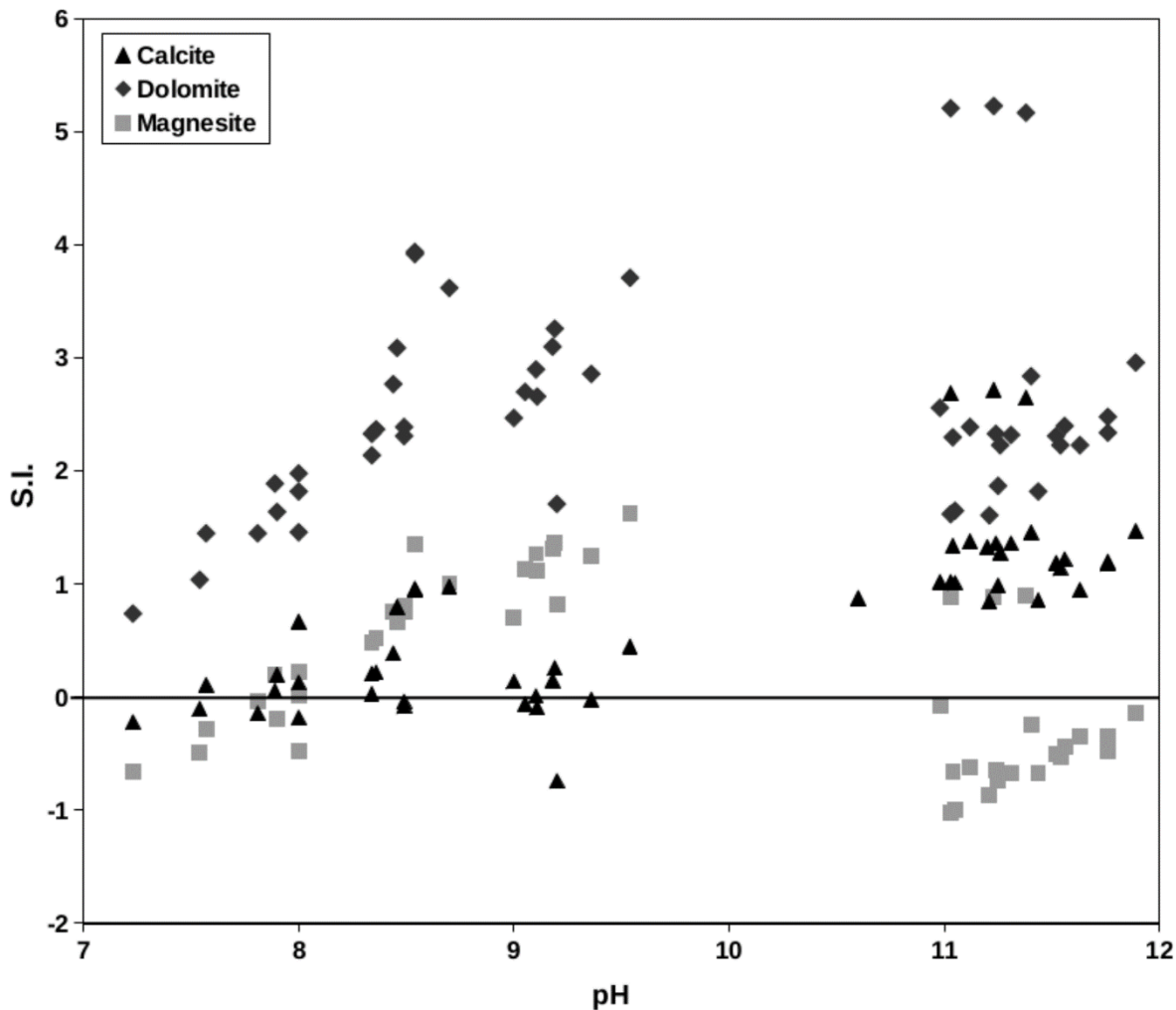
Figure 4.6: Saturation indices (S.I.) of calcite, dolomite, and magnesite in groundwater from the Oman phiolite peridotite aquifers. The saturation indices were calculated using the ions concentration of the water samples with the llnl database in PHREEQC.

4.4.2.2   Groundwater evolution from Type I to Type II

Groundwater from wells with pH 9 to 10 and pH >11 form two well-clustered groups with little change observed in their chemistry between sampling campaigns. Groundwater from the well WAB-56 was sampled during two consecutive campaigns (2015 and 2016), and is the only one sampled with a pH between 10 and 11. The two samples have $^{87}Sr/^{86}Sr$ ratios between those of the two groups (Fig. 4.4), their DIC, Mg and SO4 concentrations are close to those of Type II groundwater, whereas their Na, Cl, Ca and Sr concentrations are more similar to Type I groundwater (Table 4.2, Fig. 4.5). Furthermore, the well water appears to have evolved toward the chemistry of a Type II water within a one year time span, its pH and Na, Cl Ca and Sr concentrations have slightly increased while the $^{87}Sr/^{86}Sr$ ratio decreased (Fig. 4.4 and 4.5). This well water could be at the transition state between Type I and Type II water. As well WAB-56 is unique and was only sampled twice, we will compare the group of well waters, Type I with pH >9 and Type II with pH >11, to investigate the changes between the two types of water.

4.4.2.3   Calcium origin in Type II groundwater

The DIC concentration decreases from 2.73 mmol/kg to 0.08 mmol/kg (Fig. 4.5a), and the Mg concentration drops from 2.85 mmol/kg to <0.1 mmol/kg (Table 4.2; Fig. 4.5c) in Type II waters, in contrast the Ca concentration rises from 0.02 mmol/kg to 4.36 mmol/kg (Table 4.2; Fig. 4.5b). This supports the formation of Mg-carbonates potentially via dolomitisation. Three scenarios can explain the origin of the Ca in these fluids, all of which depend on the sink of Mg: (1) Mg (ΔMg = -2.85 mmol/kg) is solely sequestered in carbonates via dolomitisation. In this case, mass balance calculations (ΔCa – ΔMg) show an excess of 1.49 mmol/kg of Ca that has to originate from peridotite and associated non-carbonate secondary minerals. (2) Mg in solution is consumed by dolomitisation and magnesite precipitation (ΔDIC=-2.65mmol/kg); assuming no calcite precipitation. Consequently, up to 4.14 mmol/kg of Ca must originate from peridotite and associated non-carbonate secondary minerals. (3) All Mg is taken up by dolomitisation, magnesite precipitation and brucite formation, implying that all Ca in Type II groundwater may originate from peridotite and associated non-carbonate secondary minerals. A Ca source from peridotite only would require extensive water/rock reactions, but harzburgite and associated non-carbonate secondary minerals contain enough Ca to account for the concentrations found in Type II groundwaters. Harzburgites from the Wadi Tayin massif contain only traces of clinopyroxenes, but CaO still amounts for ~1 wt% of the bulk rock, mainly in orthopyroxenes (Neal and Stanger, 1985; Hanghøj *et al.*, 2010). In addition, the leachates of peridotite samples (see chapter 3) show that the secondary minerals, such as serpentine, associated with peridotite alteration analysed in this study

often contain few hundreds to few thousands ppm of Ca (Table 4.2). Depending on the fraction of Mg taken up by each sink, the origin of Ca may vary, but in all cases there no any DIC/CO_2 is released.

4.4.2.4   pH and $^{87}Sr/^{86}Sr$ evolution

The increase in pH, coupled with the decrease in $^{87}Sr/^{86}Sr$ ratios between Type I (pH >9) and Type II groundwater suggest that serpentinisation is involved in this evolution (Eq. 1; Fig. 4.4). But as the $^{87}Sr/^{86}Sr$ ratios of each group are clustered (Type I (pH >9): average = 0.70858; sd = 0.00012; Type II: average = 0.70754; sd = 0.00007), instead of progressing toward the peridotite $^{87}Sr/^{86}Sr$ signal, another explanation is considered. Type I groundwater have $^{87}Sr/^{86}Sr$ ratios in the range of Tertiary seawater, whereas Type II groundwater have $^{87}Sr/^{86}Sr$ ratios in the range of Cretaceous seawater (Fig. 4.3), this could be the result of each type of water reacting with rock that were altered at different periods. Groundwater could interact with Tertiary secondary minerals in the shallow aquifer, and with Cretaceous secondary minerals when it reaches deeper parts of the aquifer. In this setting, the high pH of Type II groundwater could either be due to extensive alteration (i.e. serpentinisation) or the dissolution of hydroxyl-rich minerals (e.g. brucite) more likely to be present in the less altered peridotites.

4.4.2.5   Surface discharge

Upon surfacing, Type II groundwater form hyperakaline springs and react with atmospheric CO_2, or HCO_3-rich surface waters. This triggers the precipitation of Ca-carbonates that forms travertine terraces. This precipitation brings the Ca concentration down from 4.36 mmol/kg to 0.79 mmol/kg and Sr concentrations from 21.10-3 to 1.10-3 mmol/kg (Fig. 4.5b & d). The spring waters $^{87}Sr/^{86}Sr$ ratios are split in two groups (Fig. 4.4). The first group comprises three hyperalkaline springs: Qafifah, Dima and Misbit (Fig. 4.1). Their $^{87}Sr/^{86}Sr$ ratios (~0.70674 ±0.00004) follow the expected evolution with harzburgite (~0.70675 ±0.0016) dissolution during serpentinisation. The second group is comprised of hyperalkaline springs from the southern part of the Samail and Wadi Tayin massifs (Fig. 4.1), their $^{87}Sr/^{86}Sr$ ratios (~0.70817 ±0.00010) (Fig. 4.4) are best explained by the interaction of the water with Tertiary altered rocks.

4.4.3   Evolution of other major ions in water

The Na and Cl concentrations steadily increase in ground waters between pH 7 and pH <11 and sharply increase in Type II (Fig. 4.5e & f; Table 4.2). Na/Cl ≠ 1 in most of the samples, they are enriched in Cl in groundwater with pH 8 to >11 (except SMA-4B and WAB-56) and wadi waters. Groundwater with pH 9 to >11 are the most clearly enriched in Cl, whereas alkaline springs are enriched in Na. This imbalance rules out marine salt as the main source for these elements, and

suggests secondary minerals formed during oceanic alteration as a source for these two ions, such as serpentine (Cl content = 90 to 14800 ppm (Kimball, Spear and Dick, 1985; Hébert, Adamson and Komor, 1990; Mével and Stamoudi, 1996).

The increase of Na and Cl concentrations in Type II groundwater requires either a change in water/rock reaction, with Na-rich and Cl-rich mineral phases, or a much longer residence time of these fluids, thus implying the need of extensive water/rock reactions to reach a pH >11. The Na concentrations are significantly different between the two Type II wells (NSHQ-14, WAB-71; Table 4.1) and between each hyperalkaline springs. The Cl concentrations are more homogeneous in Type II groundwater but decrease in alkaline springs. This points toward a lithology-dependent source for Na and a potential uptake of Cl from the water upon discharging on the surface. However, both processes need to be further investigated.

SO_4 and SiO_2 show similar behaviour as Mg and Ca, respectively. SO_4 concentrations increase with the pH in Type I groundwater before dropping to low concentrations when pH >10 (Fig. 4.5g), while SiO_2 decreases with the pH in Type I groundwater, then rises slightly in some Type II groundwater samples (Fig. 4.5h). The behaviour of SO_4 and SiO_2 agrees with our hypothese that there are two sets of processes along the flow path that are responsible for the evolution of the water chemistry: one in Type I groundwater (pH <10), one in Type II groundwater (pH >10).

4.5   Conclusion

(1) Three sources of Sr have been identified in the peridotite aquifers with an $^{87}Sr/^{86}Sr$ linked to the alteration of the peridotites: low degree of alteration, Cretaceous, and Tertiary alteration. The $^{87}Sr/^{86}Sr$ signal of alteration seems to replace the mantle $^{87}Sr/^{86}Sr$ signal in peridotite and varies throughout the ophiolite, depending on the rock permeability and accessibility of the different parts of the aquifer to water at the time.

(2) The chemical evolution of groundwater in the Oman-UAE peridotite aquifers is determined by the water/rock reactions such as serpentinisation and carbonate dissolution/precipitation, but also by the presence of secondary minerals formed during the previous alteration episodes. A clear change in the water chemistry is observed at pH 10, where it switches from a Type I to a Type II water composition.

(3) We hypothesis that a significant part of the calcium present in Type II water is provided by a dolomitisation process, the conversion of Ca-carbonates to Mg-carbonates via dissolution/re-precipitation. This process could also play an important role in the water chemical transition

between Type I and II as the main sink of Mg, and would insure that the Ca present in hyperalkaline springs is not linked to any DIC/CO_2 release.

(4) Some aspects remain unknown, such as water residence time, timing of water formation, the fraction of Mg taken up in each sink, and the fraction of Ca coming from each source, that still have to be characterised.

Chapter 5 Groundwater δ^{88}Sr and $\delta^{44/40}$Ca fractionation along flow paths in Oman peridotite aquifers: the role of serpentinisation and carbonation

Abstract

Low-temperature peridotite alteration creates steep chemical gradients that allow ecosystems to thrive away from the sunlight, and produces hyperalkaline fluids rich in Ca^{2+} that are capable of sequestering large amount of CO_2 into carbonates. The origin of the calcium ions (Ca^{2+}) in these fluids determines the impact of carbonate precipitation on the carbon cycle, as there is no impact if the source rock is a carbonate but a net uptake of CO_2 if the calcium source is a silicate. In the Oman-United Arab Emirates ophiolite, the sources of Ca^{2+} in hyperalkaline springs and the water/rock reactions responsible for the formation of these fluids are still unconstrained. In this study, the δ^{88}Sr and $\delta^{44/40}$Ca isotope systems were used to track the geochemical processes taking place along the water flowpath in peridotite aquifers. Together with other chemical parameters, including ^{87}Sr/^{86}Sr, pH, [DIC], [Ca], [Mg] and [Sr], they enable the main reactions responsible for the development of $Mg-HCO_3^-$ rich, pH < 10 (Type I), and $Ca-OH^-$ rich, pH >10 (Type II) waters to be determined. Our results demonstrate that dolomitisation (the replacement of Ca^{2+} by Mg^{2+} in carbonate) is likely to be the main process controlling the Ca and Sr chemistry of the groundwater, via dissolution/re-precipitation in Type I water and cation exchange in Type II water. Serpentinisation (the transformation of olivine and pyroxenes into serpentine and brucite) is also revealed to play a significant, albeit unquantified, role in Sr chemistry, via the mobilisation of the serpentinised matrix of peridotites in Type I water and its sorption onto brucite in Type II water. The combined use of the δ^{88}Sr and $\delta^{44/40}$Ca isotope systems in this manner is consequently able to discern the water/rock reactions that control fluid chemistry evolution through the aquifer, and thus demonstrates the potential of these geochemical tools for assessing the impacts of serpentinisation and carbonation reactions in natural systems.

5.1 Introduction

Peridotites are the main rock type found in the Earth's mantle, they are most stable under high temperature, high pressure, and reducing environments, and become unstable under low temperature, low pressure, and oxidising conditions found at the Earth's surface. Peridotite alteration creates a chemical gradient between the rocks and the environment that drives the alteration of the primary peridotite minerals (Johannes 1969; Martin and Fyfe 1970; Evans 1977; Frost 1985; Malvoisin et al. 2012). Three main exothermic reactions take place during peridotite alteration: serpentinisation, oxidation, and carbonation (Eqs. 1, 2, & 3). Serpentinisation and oxidation reactions happen between peridotites and water, while carbonation reactions occur between the products of these alteration processes and a CO_2/HCO_3^- rich environment. Together these water/rock reactions can induce rock fracturing (Jamtveit, Putnis and Malthe-Sørenssen, 2009; Kelemen and Hirth, 2012), provide a carbon sink (Kelemen and Matter, 2008; Matter and Kelemen, 2009; Kelemen et al., 2011; Paukert et al., 2012), and support extremophile microbial communities (Macleod et al., 1994; Miller et al., 2016; Shibuya, Russell and Takai, 2016; Rempfert et al., 2017)

$4Mg_2SiO_4$(Mg-olivine) + $(CaMg;Mg_2)Si_2O_6$ (pyroxenes) + $7H_2O$ = $3Mg_3Si_2O_5(OH)_4$ (serpentine) + $(Ca^{2+};Mg^{2+})_{(aq)}$ + $2OH^-_{(aq)}$ (1)

$3Fe^{2+}_2SiO_4$ (Fe-olivine) + $2H_2O$ = $2Fe^{2+}Fe^{3+}_2O_4$ (magnetite) + $3SiO_2$ (quartz) + $2H_2$ (2)

$(Ca^{2+};Mg^{2+})_{(aq)}$ + $2OH^-_{(aq)}$ + $CO_{2\ (aq)}$ = $(Ca;Mg)CO_3$ + H_2O (3)
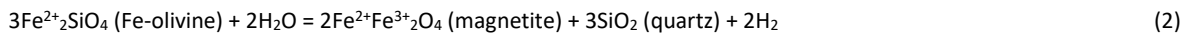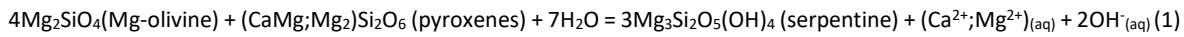
In ophiolite aquifers, the water/rock interactions that take place during peridotite alteration result in the production of Mg-HCO_3^- rich, pH<10 (Type I) fluids in the shallow aquifer, and Ca-OH^- rich, pH>10 (Type II) fluids in the deeper aquifer that ultimately form hyperalkaline springs (Barnes and O'Neil, 1971; Neal and Stanger, 1985; Bruni et al., 2002; Cipolli et al., 2004; Dewandel et al., 2005). The high pH (>11) and high Ca^{2+} content of these exiting fluids result in the precipitation of massive carbonate deposits as veins and travertine terraces upon contact with environmental CO_2 (Eq. 1 & 3) (O'Neil and Barnes, 1971; Clark, Fontes and Fritz, 1992; Kelley et al., 2001; Ludwig et al., 2006; Mervine et al., 2014).

Although the impact of these alteration reactions on the chemical evolution of the groundwater is well established, difficulties in collecting representative fluid samples mean that the conditions under which the reactions occur are not well known. Furthermore, the timescales of reaction necessary for groundwater to evolve, the sources of Ca present in the hyperalkaline springs, and the zone of reaction within the aquifer remain to be characterised. In this study, the role of serpentinisation and carbonation reactions in the chemical evolution of groundwater in the peridotite aquifers of the Oman-UAE ophiolite was investigated using the $\delta^{44/40}Ca$ and $\delta^{88}Sr$ isotopic

system. The systems were chosen owing to their sensitivity to the dissolution and precipitation of carbonates (Marriott *et al.*, 2004; Fietzke and Eisenhauer, 2006), which is of particular interest regarding the origin of Ca^{2+} ions in Type II water. Combined use of the $^{87}Sr/^{86}Sr$ and $\delta^{88}Sr$ isotope systems to explore water/rock reactions during weathering offers the ability to track both elemental input and output processes (Stevenson *et al.*, 2016). The fluid $^{87}Sr/^{86}Sr$ variations depend solely on the Sr sources and their mixing (i.e. the Sr sinks do not affect this ratio). The $\delta^{88}Sr$ values depends on both the sources and other processes occurring during transport of the Sr (Halicz et al., 2008; Stevenson et al., 2016). Including $\delta^{44/40}Ca$ helps to differentiate between the rock end-members involved in the water/rock interaction, as Sr and Ca have similar chemical properties but react differently during some geochemical processes such as carbonate precipitation, and the quantity and isotopic ratios of Sr and Ca vary from one to the other, and between processes.

5.1.1   The $\delta^{44/40}Ca$ system

The Ca isotope system has frequently been used to investigate the role of carbonate precipitation in the evolution of seawater chemistry and the carbon cycle (e.g. DePaolo 2004; Fantle & Tipper 2014; and references within). Calcium isotope values are reported as $\delta^{44/4x}Ca=((^{44}Ca/^{4x}Ca)_{SAMPLE}/(^{44}Ca/^{4x}Ca)_{STANDARD})-1) \times 1000$, typically using the isotopic ratios $^{44/40}Ca$ (Hippler *et al.*, 2003). The $\delta^{44/40}Ca$ ratios can be reported to three different standards: Bulk Silicate Earth (BSE) (DePaolo, 2004), seawater (Hippler *et al.*, 2003), and NIST SRM 915 (Fantle and Tipper, 2014). In this study, the $\delta^{44/40}Ca$ are reported relative to the BSE standard, and the $\delta^{44/40}Ca$ from literature have been converted to the same reference scale. Data suggest that $\delta^{44/40}Ca$ ratios vary by ~4‰ through the global Ca biogeochemical cycle (without taking into account the effect of radiogenic ^{40}Ca; Fantle & Tipper 2014). In the Earth's crust, silicates have $\delta^{44/40}Ca$ ranging from -0.23 to 0.12‰ (Skulan, DePaolo and Owens, 1997); peridotites $\delta^{44/40}Ca$ vary between 0.11‰ and 0.54‰ (Amini *et al.*, 2009); marine carbonates have an average $\delta^{44/40}Ca$ of -0.3±0.02‰ (with a total range of 3‰; Fantle & Tipper 2014); and the biosphere $\delta^{44/40}Ca$ ranges from -2.9 to +0.6‰ (Fantle & Tipper 2014).

Carbonate precipitation preferentially incorporates lighter Ca isotopes, with the extent of isotopic fractionation varying from 0.0‰ to -1.5‰, this is due to the Ca^{2+} ions forming stronger bonds with aqua-complexes than with carbonate ions (DePaolo, 2004; Lemarchand, Wasserburg and Papanastassiou, 2004; Marriott *et al.*, 2004; Fantle and DePaolo, 2007; Ohno *et al.*, 2008; Böhm *et al.*, 2012). The fractionation factor between carbonate and solution is determined by two main processes: (1) The availability of Ca^{2+} to precipitate with carbonate ions, which is dependant on the saturation state, pH, and temperature of the solution that control diffusion from the bulk solution to the precipitating crystal surface (Lemarchand, Wasserburg and Papanastassiou, 2004; Gussone

et al., 2005; Tang *et al.*, 2008; DePaolo, 2011); and (2) the capacity of the crystal surface to re-equilibrate with the solution before being buried in the mineral lattice, which is dependant on the rate of precipitation and the temperature (Fantle and DePaolo, 2007; Tang *et al.*, 2008; DePaolo, 2011). Given enough time, equilibrium is always reached between the carbonate and the fluid phase (i.e. $\Delta_{calcite-fluid}$ = 0‰), such as in deep sediments during diagenesis (Fantle & DePaolo 2007), and also in carbonate-hosted aquifers (Jacobson and Holmden, 2008). The fractionation factor of Ca between carbonates and fluids also depends on the type of carbonate: aragonite has been shown to have a constant offset of -0.6‰ compared to calcite at the same precipitation conditions (Gussone *et al.*, 2005; Amini *et al.*, 2008), whereas dolomite displays a maximum $\Delta_{dolomite-fluid}$ of ≤0.4‰ with $\delta^{44/40}$Ca values between -0.74‰ and 0.76‰. The average $\delta^{44/40}$Ca$_{dol}$ composition of 0.44‰ is clearly resolvable from the average marine limestones values of -0.30‰ (Fantle and Tipper, 2014; Blattler, Miller and Higgins, 2015). However, Fantle & Higgins (2014) found that dolomite formed during diagenesis had an average $\delta^{44/40}$Ca within error of the one from surrounding limestones.

In hydrothermal systems, the $\delta^{44/40}$Ca composition of the exiting fluids is close to that of silicate rocks (av. $\delta^{44/40}$Ca = -0.04 ±0.19‰; Schmitt et al., 2003), suggesting that no fractionation takes place (Zhu and Macdougall, 1998; Schmitt, Chabaux and Stille, 2003). However, anhydrites found at the Logatchev hydrothermal field have a $\delta^{44/40}$Ca composition of -0.18‰, which requires the fluid from which they precipitated to have had a $\delta^{44/40}$Ca composition between -0.25‰ and -0.53‰ (Amini et al. 2008). This challenges the assumption that no Ca isotope fractionation happens in hydrothermal fields, and would require the contribution of the rocks hosting the hydrothermal cell and demonstrates that further work is required to understand $\delta^{44/40}$Ca evolution during fluid/rock interactions.

5.1.2   The δ^{88}Sr system

The stable strontium isotope system is a relatively new geochemical tool that can be used to track and characterise rock alteration processes (Chao *et al.*, 2015; Andrews *et al.*, 2016). Unlike radiogenic ^{87}Sr/^{86}Sr values, which are normalised to a fixed ^{86}Sr/^{88}Sr ratio of 0.1194 and hence are insensitive to mass-dependant fractionation, the ^{88}Sr/^{86}Sr composition is reported as δ^{88}Sr=((^{88}Sr/^{86}Sr)$_{SAMPLE}$/(^{88}Sr/^{86}Sr)$_{NBS987}$)−1) × 1000 which is sensitive to mass-dependant fractionation occurring during geological processes. δ^{88}Sr values measured so far in natural and reference materials cover a total range of ~2.4‰ (e.g. Neymark et al. 2014; and references within). The δ^{88}Sr values reported in the literature for terrestrial rocks vary by ~0.60‰ with values between +0.1‰ and +0.3‰ for terrestrial carbonates (Halicz *et al.*, 2008; Ohno *et al.*, 2008), +0.05‰ and +0.35‰ for biogenic marine carbonates (Fietzke and Eisenhauer, 2006; Halicz *et al.*, 2008;

Rüggeberg *et al.*, 2008; Stevenson *et al.*, 2014), and an overall average carbonate value of 0.28±0.13‰ (Halicz et al. 2008). Terrestrial silicate rocks have $\delta^{88}Sr$ values between +0.2 and +0.3‰ (Moynier *et al.*, 2010; Charlier *et al.*, 2012; Ma *et al.*, 2013), with an average silicate earth $\delta^{88}Sr$ value of 0.27±0.05‰ (Moynier et al. 2010).

Hydrothermal end-member fluids have $\delta^{88}Sr$ values of ~0.24‰, which are similar to the value of the oceanic crust, although a few samples have higher $\delta^{88}Sr$ values that may be linked to the precipitation of alteration phases such as anhydrite (Pearce et al. 2015). Modern seawater has a $\delta^{88}Sr$ composition of 0.39 ±0.01‰ (Fietzke and Eisenhauer, 2006; Ohno and Hirata, 2007; Halicz *et al.*, 2008; Pearce *et al.*, 2015). Relative to the riverine (0.32±0.005‰) and hydrothermal inputs, the higher $\delta^{88}Sr$ composition of seawater can be explained by the preferential incorporation of lighter Sr isotopes into the carbonates during precipitation (Fietzke & Eisenhauer 2006; Ohno et al. 2008; Böhm et al. 2012). Aside from carbonate precipitation, other processes can uptake Sr from water and result in isotopic fractionation that include; clay formation (Halicz *et al.*, 2008; Wei *et al.*, 2013; Pearce *et al.*, 2015); plant uptake (Souza *et al.*, 2010; Andrews *et al.*, 2016); and the preferential adsorption of lighter isotopes onto particles ($\Delta^{88}Sr_{part-aq}$ = ~0.07‰; Chao et al. 2015; Shalev et al. 2017; Liu et al. 2017).

5.2   Materials and methods

Water samples were collected from boreholes, wadi/falaj, and hyperalkaline springs in areas surrounded by peridotites in the northern part of the Samail massif, the Wadi Tayin massif, and the Bahla massif of the Oman-UAE ophiolite over the course of 6 field seasons between 2009 and 2016 (see chapter 4; Fig. 4.1). Water was sampled with new syringes, filtered using 0.8/0.2µm sterile Acrodisc filters and collected into new 125mL polyethylene bottles for cation and isotopes analyses and 40mL $HgCl_2$-treated glass flasks for DIC analyses (Paukert *et al.*, 2012). Electrical conductivity (EC), pH, temperature and redox potential (Eh) were measured in the field using a WTW multi 3400i meter (see Chapter 4).

Rock samples were collected across the wadi Tayin massif in the Oman-UAE ophiolite, which represent a range of ultramafic rocks found in the mantle section. They display a range in the degree and type of alteration, from lightly serpentinised (OM15_R5) with a matrix composed of primary minerals (olivine and pyroxene) and an alteration confined to fine serpentine veins, to highly altered (OM15_R1) with very few remaining primary minerals and a dense network of serpentine and carbonate veins (Table 5.1; see chapter 3). The different mineral fractions present in these altered peridotite samples were separated by handpicking prior to leaching. The principal minerals targeted

were carbonate, serpentine, and brucite (Chapter 6). No other secondary minerals were present in enough abundance to play a meaningful role in the water/rock interactions. The choice for reagents and experimental conditions to leach each mineral phases was based on previous published experiments (Poulton & Canfield 2005; Teir et al. 2007; Wittig et al. 2009; Wang & Maroto-Valer 2011; Huang et al. 2012; see Chapter 3).

Cation concentrations were measured on an Inductively Coupled Plasma-Mass Spectrometer quadrupole Thermo X-Series 2, while anion concentrations were measured on a Dionex Ion Chromatograph 25 with IonPac AS9-HC IC columns (see chapter 4; Menzies, 2012; Marieni, 2016). Sr-isotopes ratios (both $\delta^{88}Sr$ and $^{87}Sr/^{86}Sr$) were measured on a Thermal Ionisation Mass Spectrometer (TIMS) Triton at the University of Southampton. Radiogenic ($^{87}Sr/^{86}Sr$) ratios were directly measured in an unspiked aliquot and normalised to a fixed $^{86}Sr/^{88}Sr$ ratio of 0.1194 (Nier, 1938). The stable Sr ($\delta^{88}Sr$) ratios were determined by combining unspiked and ^{84}Sr-^{87}Sr spiked aliquot data and by deconvolving them using the exponential fractionation law and Newton-Raphson iteration technique in ^{87}Sr denominator space (Pearce et al. 2015). The $\delta^{44/40}Ca$ isotopic ratios were measured on a TIMS at the department of Earth Sciences at the University of Cambridge, and in the department of Earth and Planetary Science at the University of California, Berkeley. The samples were combined with a ^{42}Ca-^{48}Ca double spike and calcium was separated using a Dionex ICS-5000$^+$ Ion Chromatograph (IC) prior to measurements (Bradbury and Turchyn, 2018). Unfortunately, the high Mg content of some samples prevented the complete separation of Ca from the mother solution using an IC system, thus the $\delta^{44/40}Ca$ composition couldn't be determined for all samples (Bradbury and Turchyn, 2018). The NIST987 standard has a $\delta^{88}Sr$ long-term 2σ of 0.01‰ and an $^{87}Sr/^{86}Sr$ long-term value of 0.710256 (2σ = 0.000013) on our instrument, the $^{87}Sr/^{86}Sr$ ratios were normalised to a NIST987 value of 0.710248 to allow the comparison between different studies (McArthur et al. 2012). The $\delta^{44/40}Ca$ average external 2σ standard deviation over 9 months on the standard NIST915B was 0.10‰ (mean = -0.28, n = 82; Bradbury and Turchyn, 2018). The $\delta^{44/40}Ca$ is reported relative to Bulk Silicate Earth (0.0212116; Russell, Papanastassiou and Tombrello, 1978), with the common standards NIST915A having a $\delta^{44/40}Ca$ of -0.99‰ (n =8, 2σ = 0.09) and seawater having a $\delta^{44/40}Ca$ of 0.96‰ (n =8, 2σ = 0.1) (Bradbury and Turchyn, 2018). We reported our samples' $\delta^{44/40}Ca$ values with the external standard deviation (2σ) of the $\delta^{44/40}Ca$ standard (2σ = 0.06‰; n=4) measured during our analyses at Cambridge rather than the internal error of each sample which was smaller (<0.04‰) but more variable.

5.3 Results

5.3.1 Fluids

The Type I fluids (pH 7 to <10) were found to have δ^{88}Sr values ranging from 0.22‰ to 0.50‰ and $\delta^{44/40}$Ca values ranging from -0.03‰ to 1.39‰ with a clear separation of the averages between samples collected in boreholes with pH < 9 (δ^{88}Sr = 0.29±0.04‰ and $\delta^{44/40}$Ca = 0.12±0.15‰), and those with pH > 9 (δ^{88}Sr = 0.45±0.02‰ and $\delta^{44/40}$Ca = 1.01±0.54‰). Wadi sample values fall between these two groups in both isotopic systems (Table 5.1). Both δ^{88}Sr and $\delta^{44/40}$Ca in the Type I water increase with pH (Fig. 5.1a and 5.1c) and display a similar behaviour with respect to the ^{87}Sr/^{86}Sr ratio (Fig. 5.1b and 5.1d). Two tendencies can be observed, δ^{88}Sr and $\delta^{44/40}$Ca values are rising with a rather constant ^{87}Sr/^{86}Sr value of ~0.70860 or are converging toward δ^{88}Sr = 0.30‰ and $\delta^{44/40}$Ca = 0.00‰ with a decreasing ^{87}Sr/^{86}Sr ratio (Fig. 5.1b and 5.1d).
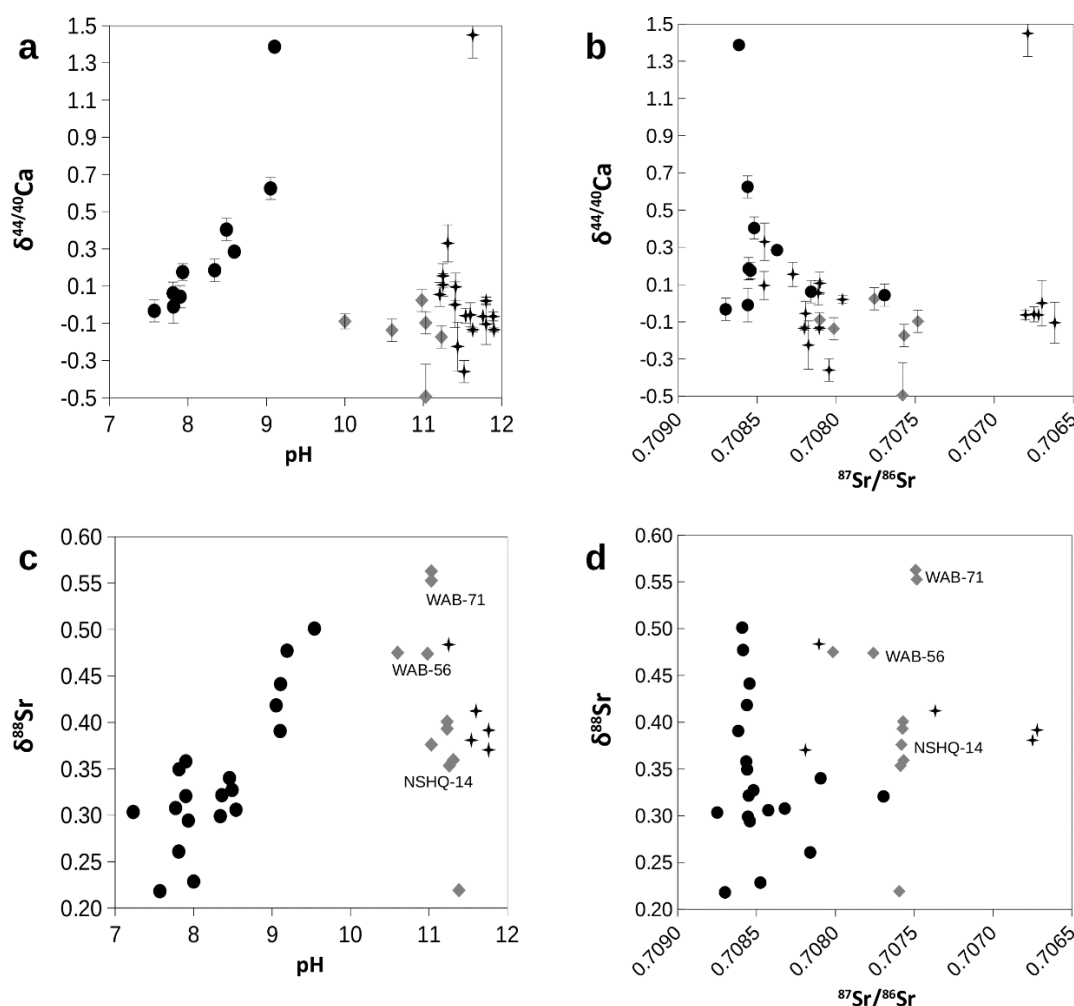
Figure 5.1: The δ^{44}Ca and δ^{88}Sr of Type I (black circles) and II (grey diamonds) water are plotted against pH and ^{87}Sr/^{86}Sr. The springs water samples (black crosses) are plotted separately from Type II well water samples to illustrate the differences and similarities between the two, such as their ^{87}Sr/^{86}Sr range. δ^{88}Sr error bars (2s.e ±0.01) are smaller than the symbols.

71

Unlike Type I waters, the δ^{88}Sr and $\delta^{44/40}$Ca system behave differently in Type II fluids: Type II waters (pH ≥10) have δ^{88}Sr values between 0.22‰ and 0.56‰, similar to Type I water, but lower $\delta^{44/40}$Ca values between -0.50‰ and 0.33‰ (with one outliner at 1.45‰ (OM09_W07R)) (Table 5.1). There is no clear relationship with pH in either of the isotope systems (Fig. 5.1b and 5.1d). Borehole samples WAB-71 and NSHQ-14 are grouped at ^{87}Sr/^{86}Sr ~ 0.70750, but have significantly different δ^{88}Sr and $\delta^{44/40}$Ca values: WAB-71 (δ^{88}Sr ~0.56; $\delta^{44/40}$Ca = -0.10‰), and NSHQ-14 (δ^{88}Sr ~0.38‰, one outliner at 0.22‰; $\delta^{44/40}$Ca = -0.17‰ to -0.50‰). Borehole WAB-56 seems to be in a transition state between Type I and II waters, with a chemistry progressing towards Type II water between the 2015 and 2016 sampling campaign (see Chapter 4). The isotopic values also vary significantly between both samples; $\delta^{44/40}$Ca = -0.14‰ and 0.02‰, and ^{87}Sr/^{86}Sr = 0.70802 and 0.70776, but not for δ^{88}Sr (0.48‰ and 0.47‰) (Table 5.1).

Table 5.1: Chemical and isotopic data of fluid samples from the Oman-United Arab Emirates ophiolite. *Samples analysed at the University of California Berkeley

Sample ID	Type	Location	UTM coord. Easting	UTM coord. Northing	$\delta^{44/40}$Ca BSE	2s.e. ‰	δ^{88}Sr NIST987	2s.e. ‰	^{87}Sr/^{86}Sr norm.	2s.e. 10^{-6}	pH	DIC mmol/L	Mg mmol/L	Ca mmol/L	Sr µmol/L
Type I water samples															
OM09_W09T*	Wadi water	Qafifah	645927	2533408	0.29	0.01	na	na	0.708375	na	8.59	0.00	1.40	0.32	1.90
OM10_01D	Wadi water	Misbit	625962	2576230	na	na	0.34	0.01	0.708094	3.9	8.46	3.14	1.70	0.84	5.73
OM10_08AP	Wadi water	Audrey II	na	na	na	na	0.36	0.01	0.708566	3.9	7.90	4.66	2.9	0.57	4.84
OM14_02C	Wadi water	Batin	671502	2536298	na	na	0.31	0.01	0.708426	4.3	8.54	na	3.16	0.49	2.36
OM16_RoW1	Wadi flash flood	Batin	670971	2531699	na	na	0.23	0.01	0.708476	3.8	na	na	0.13	0.66	1.87
OM09_11AX	Well water	SJA-4B	601942	2582989	na	na	0.30	0.01	0.708750	3.4	7.23	3.98	1.23	1.23	7.19
OM10_11AY	Well water	SJA-4A	601962	2582964	-0.03	0.06	0.22	0.01	0.708700	4.0	7.57	3.50	1.22	1.07	5.85
OM10_13BA	Well water	SLU-1B	612902	2582098	na	na	0.31	0.01	0.708321	3.5	7.77	3.14	2.49	0.70	7.63
OM10_15BC	Well water	SNA-3B	616917	2585510	0.04	0.06	0.32	0.01	0.707695	3.9	7.90	2.32	1.27	1.06	5.76
OM12_05Q*	Well water	WDA-16	528575	2539772	0.18	0.05	0.29	0.01	0.708543	3.8	7.93	0.58	1.47	0.43	4.11
OM12_05R*	Well water	WDA-16	528575	2539772	-0.01	0.09	0.35	0.01	0.708560	3.8	7.81	0.58	1.45	0.44	4.14
OM12_06T*	Well water	WDA-17	522099	2550048	1.39	0.01	0.39	0.01	0.708616	3.7	9.10	0.49	2.35	0.05	2.60
OM12_08Y*	Well water	WDA-5	526133	2539283	0.63	0.06	0.42	0.01	0.708561	3.6	9.05	0.36	2.32	0.05	3.18
OM12_08Z	Well water	WDA-5	526133	2539283	na	na	0.44	0.01	0.708545	3.7	9.11	0.34	2.33	0.05	3.38
OM15-05	Well water	NSHQ-3B	645068	2536069	na	na	0.32	0.01	0.708550	3.8	8.36	2.50	1.66	0.30	2.04
OM16_06B	Well water	WAB-104	643099	2541124	0.40	0.06	0.33	0.01	0.708520	3.9	8.49	3.48	1.93	0.12	2.40
OM16_07B	Well water	WAB-105	644678	2536524	0.18	0.06	0.30	0.01	0.708555	3.7	8.34	3.05	1.56	0.25	1.93
OM16_10	Well water	WAB-12	692081	2519249	0.06	0.06	0.26	0.01	0.708159	3.7	7.81	3.25	1.43	0.41	6.81
OM16_12A	Well water	WAB-55	634782	2506102.94	na	na	0.48	0.01	0.708586	4.0	9.19	2.50	2.74	0.08	3.02
OM16_12B	Well water	WAB-55	634782	2506102.94	na	na	0.50	0.01	0.708591	3.8	9.54	2.73	2.86	0.08	2.89
Type II water samples															
OM12_03M*	Well water	NSHQ-14	675495	2529716	-0.09	0.04	na	na	0.708105	3.6	10.00	0.08	0.04	1.23	7.47
OM12_03N*	Well water	NSHQ-14	675495	2529716	-0.50	0.18	0.38	0.01	0.707581	3.7	11.03	0.09	4E-3	4.11	19.96
OM14_01A	Well water	NSHQ-14	675495	2529716	na	na	0.22	0.01	0.707595	3.9	11.38	na	0.01	3.69	18.87
OM14_01B	Well water	NSHQ-14	675495	2529716	-0.17	0.06	0.40	0.01	0.707571	3.6	11.23	na	0.06	4.36	21.14
OM14_01B	Well water	NSHQ-14	675495	2529716	na	na	0.39	0.01	0.707574	3.9	11.23	na	0.06	4.36	21.14
OM14_05F	Well water	WAB-71	670321	2533984	-0.10	0.06	0.55	0.01	0.707484	3.9	11.03	0.21	0.08	4.07	9.22
OM14_05F	Well water	WAB-71	670321	2533984	na	na	0.56	0.01	0.707490	4.2	11.03	0.21	0.08	4.07	9.22
OM15_04A	Well water	NSHQ-14	675495	2529716	na	na	0.35	0.01	0.707587	3.7	11.26	0.19	6E-4	3.42	17.98
OM15_04B	Well water	NSHQ-14	675495	2529716	na	na	0.36	0.01	0.707567	4.1	11.31	0.22	0.27	4.12	19.45
OM15-06	Well water	WAB-56	634812	2501628	-0.14	0.06	0.48	0.01	0.708016	4.1	10.60	0.22	0.00	0.43	2.28
OM16_13	Well water	WAB-56	634812	2501628	0.02	0.06	0.47	0.01	0.707759	3.8	10.98	0.24	9E-4	0.54	2.50
OM09_W02A*	Spring Source	Falaij	608145	2525713	-0.36	0.06	na	na	0.708046	na	11.52	0.18	4E-4	1.87	1.14
OM09_W04F*	Spring Source	Hamadiyin	585584	2522988	na	na	0.37	0.01	0.708190	4.1	11.76	0.22	7E-4	1.40	2.99
OM09_W04G*	Spring Source	Hamadiyin	585584	2522988	-0.23	0.13	na	na	0.708176	na	11.44	0.02	7E-4	1.31	2.56
OM09_W05L*	Spring Source	Qafifah	645780	2533441	-0.06	0.02	na	na	0.706802	na	11.89	0.37	1E-3	1.66	1.42
OM09_W06O*	Spring Source	Dima	663152	2542372	-0.06	0.04	0.38	0.01	0.706749	3.7	11.54	0.16	4E-4	1.82	2.88
OM09_W14I*	Spring Source	unknown	na	na	-0.14	0.01	na	na	0.708108	na	11.63	na	4E-4	2.23	1.70
OM09_W15K*	Spring Source	unknown	na	na	0.02	0.02	na	na	0.707961	na	11.80	na	1E-2	2.52	3.73
OM09_W16M*	Spring Source	unknown	na	na	-0.11	0.11	na	na	0.706617	na	11.80	na	3E-3	1.75	3.17
OM10_04S	Spring Source	Qafifah	645780	2533441	-0.06	na	0.39	0.01	0.706720	3.9	11.76	0.18	6E-4	1.75	1.49
OM10_09AT	Spring Source	unknown	na	na	na	na	0.41	0.01	0.707366	4.4	11.60	na	na	1.78	2.08
OM12_01G	Spring Source	Falaij	608145	2525713	0.11	0.06	0.48	0.01	0.708104	5.2	11.25	0.02	5E-4	2.03	1.05
OM12_01G*	Spring Source	Falaij	608145	2525713	0.16	0.07	na	na	0.708275	na	11.25	0.02	5E-4	2.03	1.05
OM12_02L*	Spring Source	Falaij	608145	2525713	0.06	0.07	na	na	0.708114	na	11.21	0.02	1E-3	1.90	1.61
OM12_07X*	Spring Source	Al Bana	na	na	-0.06	0.07	na	na	0.708194	na	11.60	na	5E-4	1.60	1.37
OM09_W04I*	Spring downstream	Falaij	608145	2525713	-0.14	0.01	na	na	0.708202	na	11.90	0.20	5E-4	1.07	2.95
OM09_W07R*	Spring downstream	Qafifah	645780	2533441	1.45	0.12	na	na	0.706788	na	11.63	0.45	8E-3	0.17	0.22
OM09_W10V*	Spring downstream	Misbit	625676	2576006	0.00	0.12	na	na	0.706698	na	11.40	0.33	7E-3	2.05	3.88
OM12_09AA*	Spring downstream	Falaij	608145	2525713	0.33	0.10	na	na	0.708454	na	11.31	0.03	9E-4	0.82	2.66
OM12_09AC*	Spring downstream	Falaij	608145	2525713	0.10	0.08	na	na	0.708457	na	11.41	0.03	7E-4	1.42	3.65

5.3.2 Rocks

The calcite and dolomite samples from altered peridotites yield an average δ^{88}Sr composition of 0.30‰ (n=3), while serpentine and serpentinised peridotite have an average δ^{88}Sr value of 0.24‰ (n=3) (Table 5.2). These results are consistent with published average carbonate (δ^{88}Sr = 0.28±0.13‰; Halicz et al. 2008) and average silicate composition (δ^{88}Sr = 0.27±0.05‰; Moynier et al. 2010). Two very low δ^{88}Sr values were measured in a highly altered peridotite (0.06±0.01‰) and the leachate of the olivine-rich fraction of a pyroxenite dyke (0.07±0.01‰). The leachate of the pyroxene fraction of the pyroxenite yielded an intermediate δ^{88}Sr value of 0.15±0.01‰. The $\delta^{44/40}$Ca appears dependant on the type of carbonate, with dolomite showing a value of -0.23±0.06‰ (n=1) and calcite -0.06±0.06‰ (n=2), both of which are higher than the carbonate average ($\delta^{44/40}$Ca = -0.3‰; Fantle & Tipper 2014). The pyroxene leachate has a $\delta^{44/40}$Ca of -0.09±0.06‰, close to the Bulk Silicate Earth value (Skulan, DePaolo and Owens, 1997).

Table 5.2: Chemical and isotopic data of rock samples from the Oman-UAE ophiolite.

Sample ID	Type	Treatment	$\delta^{44/40}$Ca BSE	2s.e. ‰	δ^{88}Sr	2s.e. ‰	^{87}Sr/^{86}Sr norm.	2s.e. 10^{-6}	Mg mmol/kg	Ca mmol/kg	Sr µmol/kg
OM15_R1c	Carbonate vein (Dolomite)	Full digestion	-0.23	0.06	0.31	0.01	0.708587	3.8	3723	4154	5105
OM15_R1w	Heavily serpentinised peridotite	Full digestion	na	na	0.06	0.01	0.708460	4.2	7448	267	302
OM15_R2c	Carbonate vein (Calcite)	Full digestion	-0.04	0.06	0.30	0.01	0.708376	4.1	2129	5393	6292
OM15_R2s	Serpentine vein (carbonate fraction)	Leaching	-0.08	0.06	0.30	0.01	0.708355	9.1	1501	771	750
OM15_R2s-2	Serpentine vein (decarbonated)	Full digestion	na	na	0.23	0.01	0.708291	4.1	7660	164	103
OM15_R2w	Serpentinised peridotite	Full digestion	na	na	0.23	0.01	0.707856	7.1	8279	15	57
OM15_R3b	Pyroxenite dyke (olivine-rich fraction)	Leaching	na	na	0.07	0.01	0.707633	3.8	4837	18	28
OM15_R3f	Pyroxenite dyke (pyroxene-rich fraction)	Leaching	-0.09	0.06	0.15	0.01	0.706935	3.8	331	77	11
OM15_R5	Lightly serpentinised peridotite	Leaching	na	na	0.24	0.01	0.706190	4.0	6276	96	6

5.4 Discussion

5.4.1 Sr and Ca sources

The main sources of Sr and Ca in the peridotite aquifer are calcite and dolomite, and secondary silicate minerals (e.g. serpentine) as shown by the δ^{88}Sr and $\delta^{44/40}$Ca data (Table 5.2). These minerals were mostly formed by reaction between the peridotite and seawater on the seafloor during the Cretaceous, or on the continental shelf after obduction during the Tertiary transgression events, (Chapter 4). Calcite and dolomite have a δ^{88}Sr of 0.30±0.01‰ (n=3) and $\delta^{44/40}$Ca of -0.06±0.06‰ (n=2), and serpentine has a δ^{88}Sr of 0.24±0.01‰ (n=3) (Table 2), close to the average δ^{88}Sr value of mid-oceanic ridge basalt (Neymark et al. 2014; Pearce et al. 2015). Unfortunately, $\delta^{44/40}$Ca of serpentine could not be determined due to the very high Mg/Ca ratio. However, previous studies have reported a $\delta^{44/40}$Ca in fresh peridotites between 0.11‰ and 0.25‰ (Amini *et al.*, 2009). As secondary silicate minerals have been shown to preferentially incorporate the lighter isotopes (Halicz *et al.*, 2008), it can be assumed that the $\delta^{44/40}$Ca composition of serpentine and other

secondary silicate minerals would be lower than that of peridotite. The pyroxene leachate $\delta^{44/40}$Ca composition of -0.09±0.06‰ is consequently considered to represent the $\delta^{44/40}$Ca of secondary silicate minerals in the aquifer. Calcite and dolomite (δ^{88}Sr = 0.30‰; $\delta^{44/40}$Ca = -0.06‰) and secondary silicate minerals (δ^{88}Sr = 0.24‰; $\delta^{44/40}$Ca = -0.09‰) are most likely the main sources of Sr and Ca in the peridotite aquifers of the Oman-UAE ophiolite, with ^{87}Sr/^{86}Sr compositions that are representative of their period of formation (Table 5.2).

5.4.2 Type I water isotopic evolution

Serpentinisation and carbonate precipitation are the main processes that determine the chemical and isotopic composition of Type I water in this aquifer (Kelemen & Matter 2008; Kelemen et al. 2011; Chapter 4). The combined decrease in Ca and DIC concentrations between pH 7 and 10 supports calcium carbonate precipitation as one of the main processes taking place during the evolution of Type I water (Fig. 5.2), while the increase of Mg concentration combined with the low ^{87}Sr/^{86}Sr ratio (0.70769) indicates the dissolution of mafic minerals associated with serpentinisation (Table 5.1; Chapter 4). The narrow range of ^{87}Sr/^{86}Sr (0.70856; 2σ = 3.10^{-5}; n = 10) of most of Type I water samples (Fig. 5.1b and 5.1d) suggests that carbonate precipitation dominantly occurs in the shallow part of the aquifer, where rocks have been altered during the Tertiary transgression and now exhibit an ^{87}Sr/^{86}Sr signal similar to that of Tertiary seawater (0.7080 to 0.7085; Chapter 4). The deeper aquifer rocks were also altered during the Cretaceous but their lower permeability prevented seawater infiltration during the Tertiary transgressions (see Chapter 4). A few samples with lower ^{87}Sr/^{86}Sr ratios seem to be on a trend converging towards δ^{88}Sr and $\delta^{44/40}$Ca carbonate values, and Cretaceous seawater ^{87}Sr/^{86}Sr ratios (0.7072 to 0.7079) (Fig. 5.1b and 5.1d; McArthur et al., 2012), suggesting that mineral dissolution, including carbonate dissolution, could be dominant in these deeper parts of the peridotite aquifer.
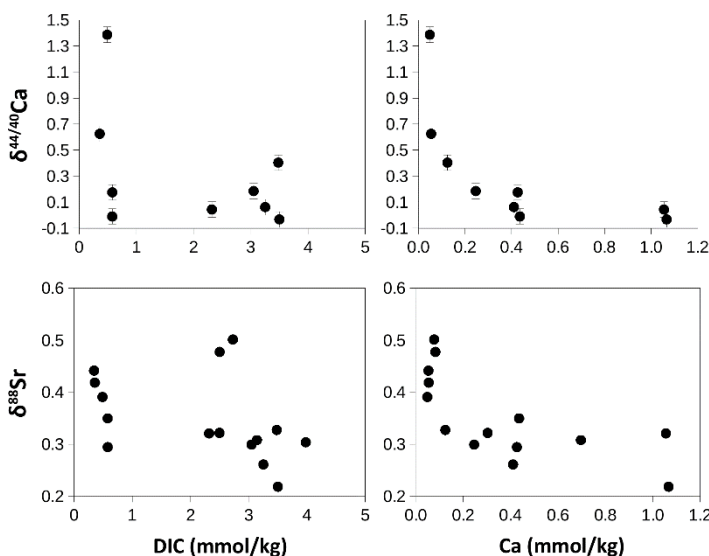

Figure 5.2: Type I water stable isotopes ratios are plotted against DIC concentration (left) and Ca concentration (right).

The $\delta^{88}Sr$ and $\delta^{44/40}Ca$ exhibit similar behaviours in Type I water, with both increasing between pH 7 and 10, starting from serpentine-like values at pH 7 ($\delta^{88}Sr$ = 0.24‰; $\delta^{44/40}Ca$ = -0.09‰) to calcite-like values at pH 8 ($\delta^{88}Sr$ = 0.30‰; $\delta^{44/40}Ca$ = -0.06‰), and up to 0.50‰ and 1.39‰ at pH>9, respectively (Fig. 5.1a and 5.1c). The transition from serpentine to calcite values is best observed with $\delta^{88}Sr$ (0.22‰ to 0.30‰; Fig. 5.1c) as the $\delta^{44/40}Ca$ of serpentine and calcite are similar within error bars (-0.09±0.06‰ and -0.06±0.06‰). In Type I water, the $\delta^{44/40}Ca$ values plotted against the remaining fraction of Ca (f_{Ca}) follow a Rayleigh isotopic fractionation curve, owing to the complete consumption of Ca^{2+} from the fluid (Chapter 4; Fig. 5.3a).
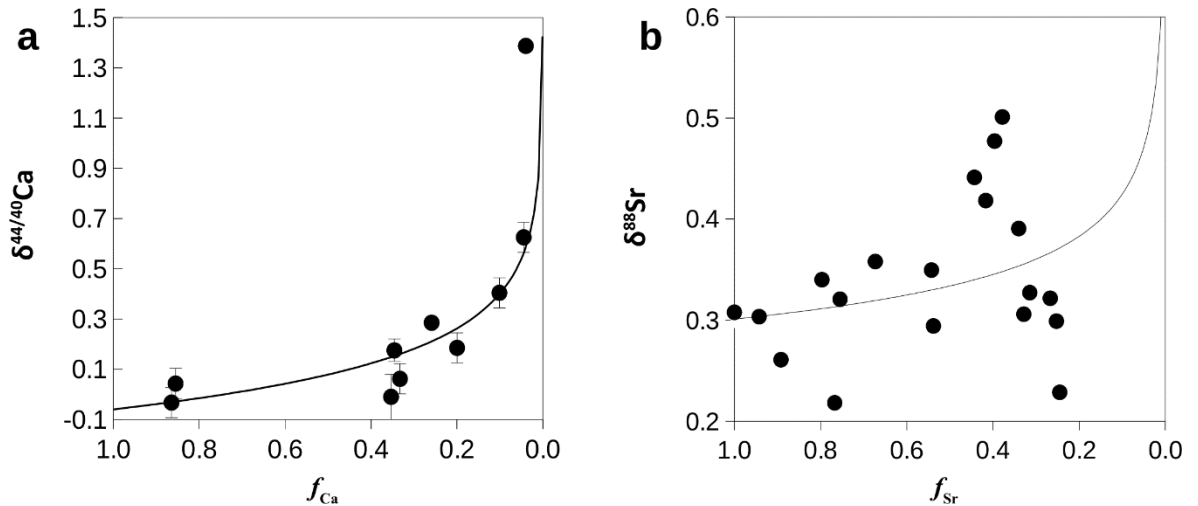
Figure 5.3: (a) Type I water $\delta^{44/40}Ca$ are plotted against f_{Ca}, f_{Ca} is calculated as $[Ca]_{sample}/[Ca]_{initial}$. With $[Ca]_{initial}$ being the highest Ca concentration measured in a Type I water sample, at pH 7. The theoretical Rayleigh fractionation curve was calculated with $\delta^{44/40}Ca_i$ = -0.06‰ and $\alpha_{water-carb}$ = 0.99980. The good fit of the values on the curve supports a carbonate precipitation from a solution with a finite amount of calcium ($[Ca]_{out} >> [Ca]_{in}$ as the main process driving the evolution of Ca isotopes and concentration in Type I water. (b) Type I water $\delta^{88}Sr$ are plotted against f_{Sr} (calculated the same way as f_{Ca}). The theoretical Rayleigh fractionation curve was calculated with $\delta^{88}Sr_i$ = 0.30‰ and $\alpha_{water-carb}$ = 0.99995. The $\delta^{88}Sr$ error bars (2s.e ±0.01) are smaller than the symbols. The Sr values are scattered away from the curve, hinting that carbonate precipitation is not the main process driving the Sr chemistry in Type I water. Other secondary mineral precipitation ($[Sr]_{out}$), and mineral dissolution ($[Sr]_{in}$) are playing important roles.

Calcite and dolomite are the two main secondary Ca-bearing minerals found in the peridotite aquifer. To differentiate between calcite or dolomite formation, $\delta^{44/40}Ca$ was plotted against their saturation indices (S.I.) (Fig. 5.4a and 5.4c). Saturation indices of calcite indicate saturation for most of the Type I samples, but the S.I. values do not show any correlation with $\delta^{44/40}Ca$. In contrasts, the S.I. of dolomite is positively correlated with $\delta^{44/40}Ca$ and shows supersaturation with respect to dolomite. This suggests that dolomite is potentially the main carbonate being formed, and that the

Ca present in Type I water is entirely consumed via carbonate precipitation without any significant input of Ca from mineral dissolution. The δ^{88}Sr values plotted against f_{Sr} are scattered and do not display a behaviour consistent with a Rayleigh fractionation, suggesting that mineral precipitation is not the only process involved, and that mineral dissolution plays a significant role in the Sr chemistry (Fig. 5.3b). The δ^{88}Sr of some Type I water samples plot on a mass-dependant fractionation trend with $\delta^{44/40}$Ca (Fig. 5.5), and is positively correlated with the S.I. of dolomite in Type I water (Fig. 5.4d). This suggests that the $\delta^{44/40}$Ca values of Type I waters are determined by dolomite precipitation, whereas the δ^{88}Sr values are the result of additional processes such as dissolution of secondary silicate minerals. Nevertheless, mineral dissolution could also impact the Ca chemistry but the isotopic fractionation due to carbonate precipitation is much stronger for $\delta^{44/40}$Ca than for δ^{88}Sr ($\Delta^{44/40}$Ca$_{carb-Type\ I}$ = -1.62‰ to -0.03‰; Δ^{88}Sr$_{carb-Type\ I}$ = −0.20‰ to 0.00‰) and would mask any mineral dissolution effect on the $\delta^{44/40}$Ca values.
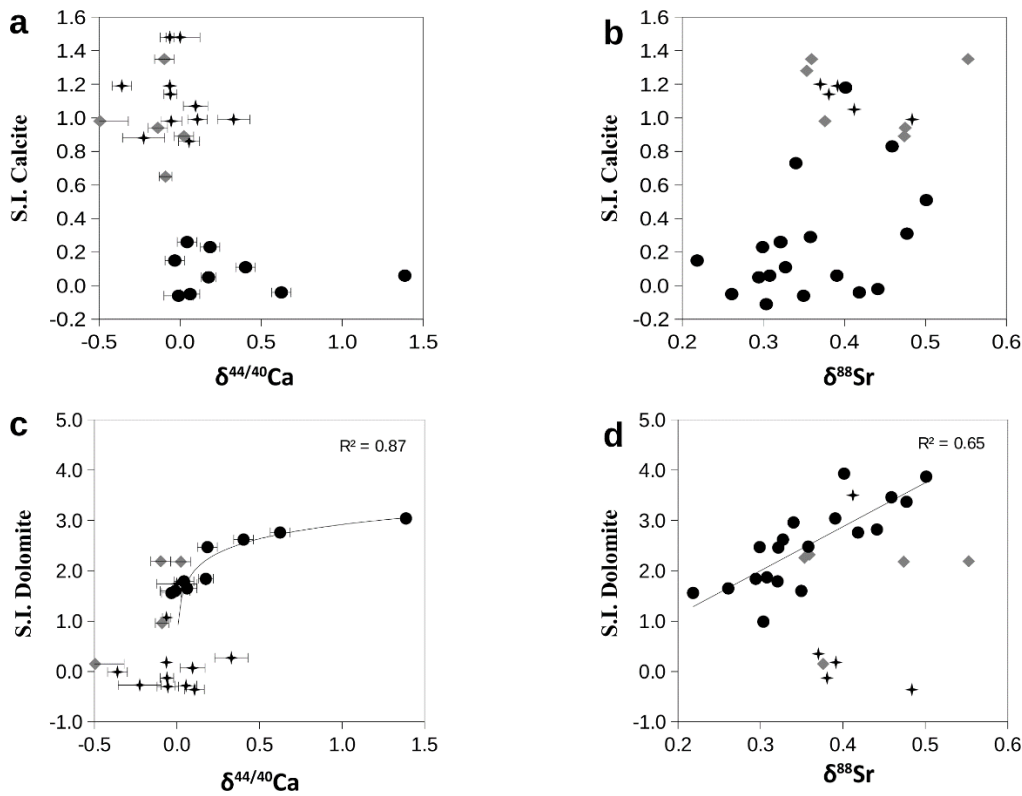
Figure 5.4: The saturation indices (S.I.) of calcite and dolomite are plotted against the $\delta^{44/40}$Ca and δ^{88}Sr of groundwater: Type I water (black circles), Type II well water (grey diamonds), and hyperalkaline springs (black crosses), δ^{88}Sr error bars (2s.e ±0.01) are smaller than the symbols. The S.I. of calcite in groundwater show no clear correlation with the $\delta^{44/40}$Ca or δ^{88}Sr (a and b). However, the dolomite S.I. has a clear positive correlation with the $\delta^{44/40}$Ca of Type I water and with the δ^{88}Sr of Type I and some Type II water samples (c and d). Due to the Rayleigh effect (Fig. 5.3a), the correlation between $\delta^{44/40}$Ca and dolomite S.I. follows a logarithmic curve, whereas δ^{88}Sr follows a linear trend. The saturation indices were calculated using the ion concentrations of the water samples with the llnl database in PHREEQC.

5.4.3 Type II water isotopic evolution

5.4.3.1 Dolomitisation

The transition from Type I to Type II water is accompanied by the release of Ca and Sr in groundwater, but there is not an associated increase in the DIC. Consequently the dissolution of Ca-bearing carbonates is unlikely to be responsible for the shift (Table 5.1). It has been previously proposed that a part of the Ca present in Type II waters was released into solution through dolomitisation (Chapter 4). Dolomitisation of calcium carbonate minerals would allow the release of Ca from calcite without dissolving it and thus releasing bicarbonate ions into solution (Chapter 4). The drop in Mg concentration between Type I and II waters (Table 5.1), and the negative $\delta^{44/40}Ca$ values of Type II waters from boreholes (-0.09‰ > $\delta^{44/40}Ca$ > -0.50‰) support this hypothesis (Fig. 5.1a). In order to identify the type of carbonate reacting, an isotope mixing equation (Eq. 4) was used to determine the $\delta^{44/40}Ca$ value of these dolomitised Ca-carbonates. For this calculation, we assume that Type II water $\delta^{44/40}Ca$ values result from a simple mixing of Type I water and the reacting carbonate. In this setting, Type I water with pH >9 ($\delta^{44/40}Ca = 1.01$‰; n = 2) would need a calcium input from the reacting carbonates with an average $\delta^{44/40}Ca$ value of -0.24‰ (-0.12‰ to -0.52‰) to reach Type II water values ($\delta^{44/40}Ca = -0.21$‰; n = 4).

$$\delta^{44/40}Ca_{Type\ II} = f \times \delta^{44/40}Ca_{Type\ I} + (1-f) \times \delta^{44/40}Ca_{carb} \tag{4}$$

With f being the fraction of Ca ions in Type II water coming from Type I water. An obvious candidate would be dolomite ($\delta^{44/40}Ca = -0.23$‰). The calcium present in dolomite would continue to be replaced by Mg to form magnesite. Even though magnesite is found in the Oman-UAE ophiolite, this process had never been reported in previous studies, and is only supported by this one dolomite $\delta^{44/40}Ca$ value. Another potential source of Ca could be an analogue of the aragonite found in the hydrothermally altered peridotites at the Logatchev field, which have a $\delta^{44/40}Ca = -0.90$ to -0.56‰ (Bach *et al.*, 2004, 2006; Amini *et al.*, 2008). However, no Ca-carbonates with similarly low $\delta^{44/40}Ca$ values were found in the peridotites of the Oman-UAE ophiolite. The $\delta^{44/40}Ca$ values of Type II waters stay in the range of carbonate values, but their $\delta^{88}Sr$ reach much higher values, up to 0.56‰ (Fig. 5.1a and 5.1c), suggesting that additional processes are involved.

5.4.3.2 Alternative sources of isotopically light Sr

The $\delta^{88}Sr$ of Type II water have the same range of values as in Type I water and vary significantly from one borehole location to another (Fig. 5.1c; Table 5.1). $\delta^{88}Sr$ in samples from borehole NSHQ-14 ($\delta^{88}Sr = 0.22$‰ to 0.40‰) is lighter compared to Type I water at pH >9 ($\delta^{88}Sr = 0.39$‰ to 0.50‰), suggesting mineral dissolution is dominant; mineral precipitation would result in heavier isotope values. Assuming that Type II waters $\delta^{88}Sr$ values result from a mix between Type I waters with pH

>9 and dissolved rocks from the aquifer, isotopic mixing calculations point to a Sr source with an overall $\delta^{88}Sr$ value of 0.33‰ (0.17‰ to 0.40‰). This value is similar to the average $\delta^{88}Sr$ of carbonates (0.30‰) in the peridotites. Thus, carbonates could be a potential source of Sr in NSQH-14 groundwater, which suggests that Sr could be provided through the same dolomitisation process as Ca. However, mass-balance calculations based on the input of Ca from carbonates in NSHQ-14 water (3.65 mmol/L) and the Sr/Ca ratio of carbonates (1.12 µmol/mol) reveal that dissolution of carbonates would only account for ca. 27% of the Sr input (15 µmol/L) in the Type II water from NSHQ-14. Thus, either the Sr is preferentially removed from calcite during dolomitisation or another isotopically light source of Sr is needed to explain the measured $\delta^{88}Sr$. The Sr concentration in borehole WAB-56, lower than in Type I water, and the $\delta^{88}Sr$ in borehole WAB-71, higher than in Type I water, are also incompatible with simple dolomitisation as a single process.
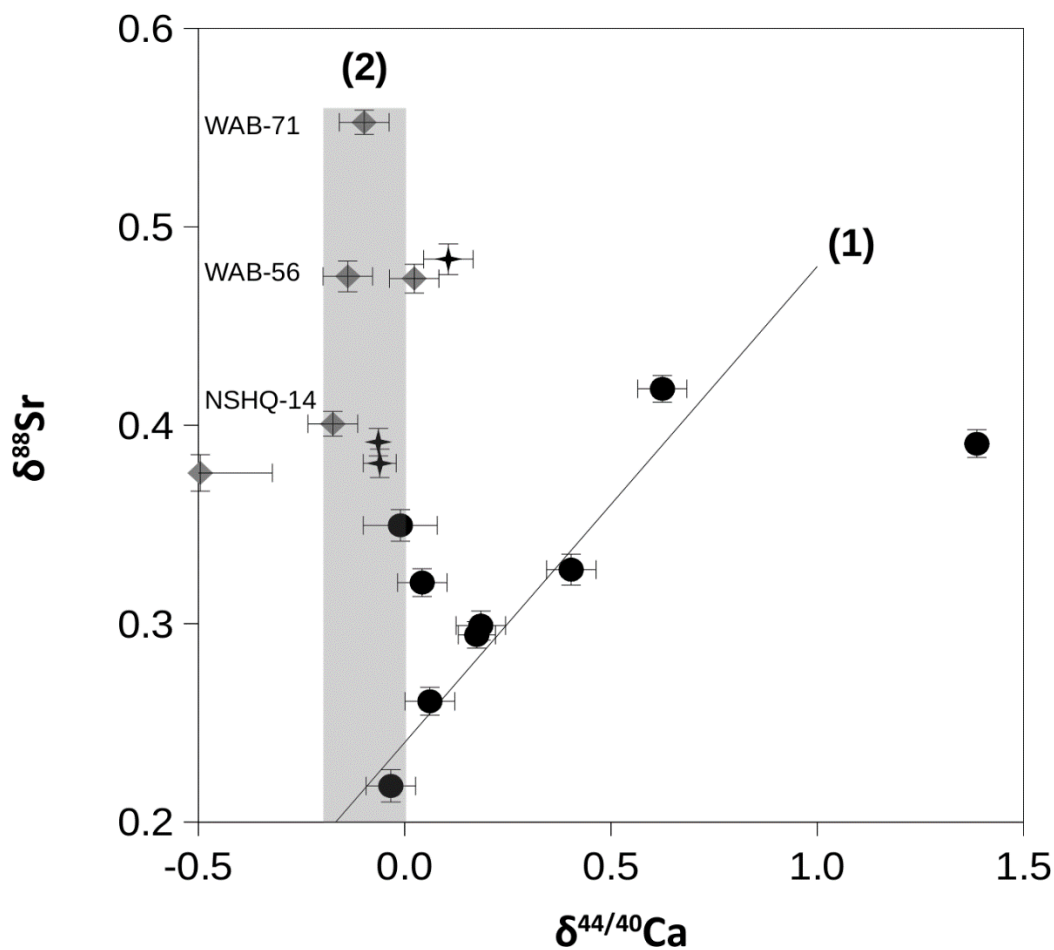
Figure 5.5: The $\delta^{44/40}Ca$ and $\delta^{88}Sr$ of groundwater are following two trends: (1) $\delta^{44/40}Ca$ and $\delta^{88}Sr$ values plot close to the mass-dependant fractionation trend (slope = 0.24) calculated by Böhm et al. (2012) for a kinetic fractionation of the isotopes in a diffusive boundary layer, also similar to the value of 0.25 proposed by Ohno et al. (2008), during carbonate precipitation. (2) Samples show little variations in $\delta^{44/40}Ca$, and stay in the range of calcite and dolomite values, whereas $\delta^{88}Sr$ increase steadily. The two outliners ($\delta^{44/40}Ca$ = -0.5 and $\delta^{44/40}Ca$ = 1.39) may explained by the dissolution of hydrothermal aragonite (Amini et al., 2008) and by complete precipitation of the calcium present in water, respectively.

Borehole WAB-71 is in the middle of one of the largest dunite body in the Oman-UAE ophiolite. As Ca and Sr behave similarly, and the USGS dunite reference material DTS-1 has a $\delta^{44/40}Ca_{DTS-1}$ composition of 0.54‰ (the highest in ultramafic rocks; Amini et al., 2009), one could expect a high $\delta^{88}Sr$ value in dunite as well, which could explain the high $\delta^{88}Sr$ in WAB-71 water by simple rock dissolution. But the WAB-71 $\delta^{44/40}Ca$ composition (-0.10±0.06‰) does not reflect dunite dissolution (Figure 5.1a), thus the higher $\delta^{88}Sr$ value in WAB-71 could be explained by the precipitation of secondary minerals during dunite alteration, such as brucite and chrysotile-serpentine. The saturation indices of both minerals show a positive correlation with the $\delta^{88}Sr$ in Type I and II waters (Fig. 5.6). Chrysotile was reported to contain Sr in the tens of μmol/kg (Kodolányi and Pettke, 2011). Furthermore, brucite showed a high sorption capacity relative to Sr at high pH (Bochkarev and Pushkareva, 2009).
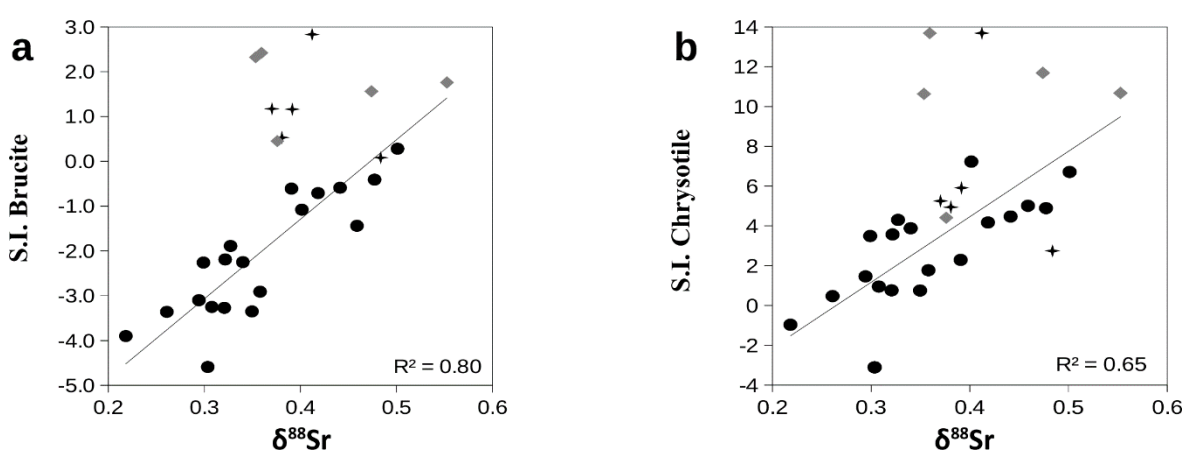
Figure 5.6: The saturation indices (S.I.) of brucite and chrysotile plotted against the $\delta^{88}Sr$ of groundwater: Type I water (black circles), Type II well water (grey diamonds), and hyperalkaline springs (black crosses), $\delta^{88}Sr$ error bars (2s.e ±0.01) are smaller than the symbols. The S.I. of (a) brucite and (b) chrysotile in groundwater show a clear correlation with $\delta^{88}Sr$ in Type I and some Type II water samples. The saturation indices were calculated using the ions concentration of the water samples with the llnl database in PHREEQC.

The hypothesis that Sr is sorbed by brucite is supported by the extensive presence of brucite in the dunites of WAB-71 associated with a low Sr concentration in the well water ([Sr]$_{WAB-71}$ = 8.3 ±0.8 μmol/kg), whereas no brucite was found in the rocks around borehole NSHQ-14 which present a higher Sr concentration ([Sr]$_{NSHQ-14}$ = 18.7 ±1.7 μmol/kg). The sorption of Sr onto brucite could potentially fractionate Sr isotopes by preferentially sorbing the lighter isotopes (Chao *et al.*, 2015; Liu *et al.*, 2017; Shalev *et al.*, 2017). Mineral precipitation is likely to be significant in the Type II water boreholes. However, the dissolution of minerals such as brucite could also play an important role by releasing isotopically light Sr in the groundwater while raising its pH. Unfortunately isotopic and chemical data on the rocks and associated secondary minerals are lacking to confirm this hypothesis.

5.4.3.3   Hyperalkaline springs

Hyperalkaline spring $\delta^{44/40}$Ca (-0.36‰ to 1.45‰) fractionation may be driven by carbonate precipitation along the surface flowpath through a Rayleigh fractionation process (Fig. 5.7). Their δ^{88}Sr (0.37‰ to 0.48‰) have the same range as the Type II water from boreholes (Fig. 5.1c), suggesting that the same processes of mineral precipitation, dissolution, and sorption determine the Sr chemistry in the hyperalkaline springs. The ^{87}Sr/^{86}Sr (0.70662 to 0.70846) suggests that fluids forming hyperalkaline springs interacted with less and more altered peridotite before surfacing (see Chapter 4).
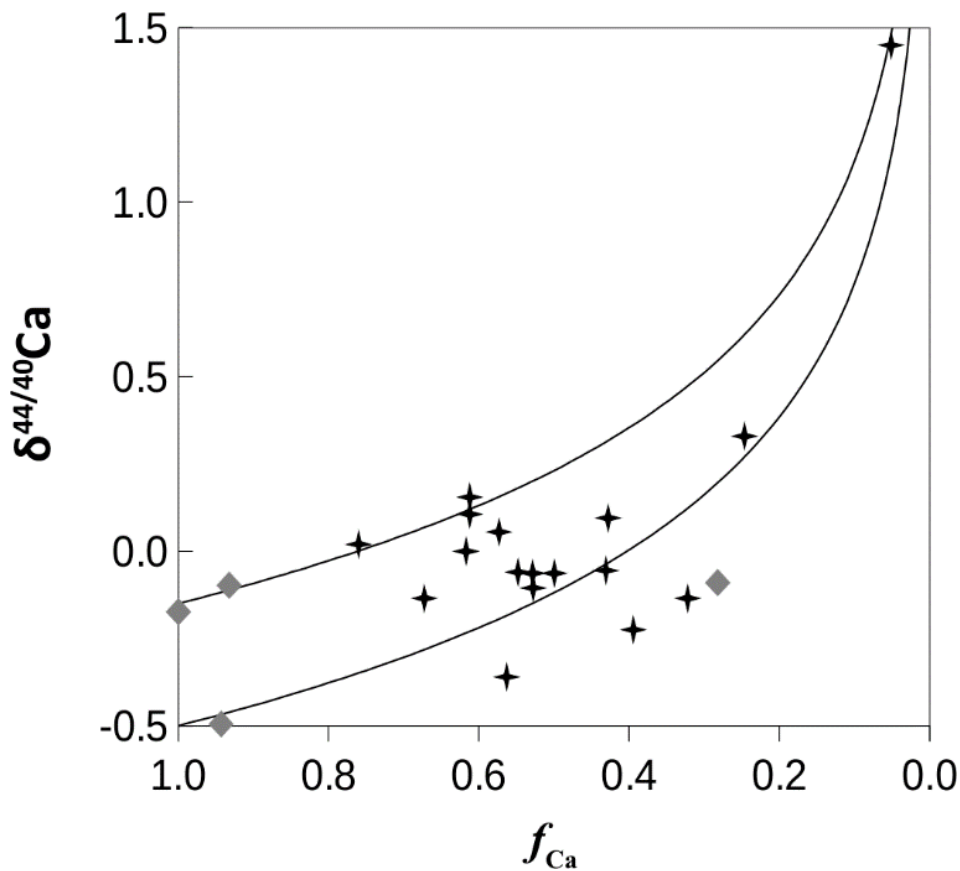
Figure 5.7: Type II water $\delta^{44/40}$Ca are plotted against f_{Ca}, from boreholes NSHQ-14 and WAB-71 (grey diamonds) and hyperalkaline springs (black crosses). f_{Ca} is calculated as [Ca]$_{sample}$/[Ca]$_{initial}$. With springs [Ca]$_{initial}$ being the average Ca concentration in Type II water from boreholes, and borehole [Ca]$_{initial}$ being the highest Ca concentration measured in a sample. The two theoretical Rayleigh fractionation curves were calculated with a $\delta^{44/40}$Ca$_i$ of -0.15‰ or -0.5‰ and $\alpha_{water\text{-}carb}$ = 0.99945 for both. The values mostly fit between the two curves. This supports that the evolution of $\delta^{44/40}$Ca and Ca concentration in hyperalkaline springs is driven by the precipitation of carbonates, but may start from different initial Type II water.

5.4.3.4   Summary

These data demonstrate that the Ca and Sr chemistry are driven by different processes in both Type I and II waters. The combined use of $\delta^{44/40}$Ca and δ^{88}Sr enables two regimes to be identified, each taking place on one of the trends observed in Figure 5.5: (1) Type I water is formed in a regime dominated by dolomitisation via a dissolution/re-precipitation process, which takes place in the shallow aquifer and results in the increase of both $\delta^{44/40}$Ca and δ^{88}Sr following a mass-dependent fractionation; (2) Type II and some Type I water samples evolve in a cation exchange regime in the deeper aquifer, where Ca is extracted from Ca-bearing carbonates via a Mg-Ca exchange, which results in the fluid having a $\delta^{44/40}$Ca composition close to carbonate values. The increase in fluid δ^{88}Sr in this regime may be the result of Sr sorption on brucite, or non-carbonate mineral precipitation, such as chrysotile. These minerals could become the sources of isotopically light Sr for groundwater during subsequent weathering, such as in NSHQ-14, or as in Type I water with δ^{88}Sr <0.30‰.

5.5   Conclusions

Peridotite alteration in the Oman-UAE ophiolite produces two types of fluids, Mg-HCO$_3^-$ rich, pH <10 water (Type I) and Ca-OH$^-$ rich, pH >10 water (Type II). Carbonate precipitation in the peridotite aquifer and hyperalkaline springs could be an important atmospheric CO_2 sink, and play a major role in the global carbon cycle, if the Ca present in Type II water does not result from carbonate dissolution. The combined use of three isotopic systems, $\delta^{44/40}$Ca, δ^{88}Sr, ^{87}Sr/^{86}Sr, and elemental concentrations has enabled us to further constrain the water/rock reactions happening in the peridotite aquifer, and unveil different types of geochemical processes responsible for the formation of both type of water.

(1) Type I water $\delta^{44/40}$Ca increase reveals that carbonate precipitation is dominant in the shallow aquifer, and mineral saturation indices suggest that dolomite is the main carbonate that precipitates.

(2) The decrease of $\delta^{44/40}$Ca between Type I and II waters, combined with the absence of a DIC increase, as well as the decrease in Mg concentration, indicates a remobilisation of Ca by cation exchange with Mg from an isotopically light source. Potential candidates for this source could be an analogue of hydrothermal aragonite or dolomite, possibly providing an explanation for the formation of magnesite in the field.

(3) The δ^{88}Sr data are compatible with dolomite formation in both Type I and II waters, but require the contribution of other minerals with isotopically light Sr, as a source or sink. The serpentinised

matrix of peridotite would be the ideal candidate, but data from borehole WAB-71 also suggests brucite as a plausible source of isotopically light Sr. In Type II water, the preferential release of Sr during the exchange of Ca with Mg ("dry dolomitisation") could be an alternative to the dissolution of other minerals, such as serpentine or brucite.

(4) Although the $\delta^{44/40}$Ca data suggest carbonates as the main source for Ca in Type II water, the process involved in the Ca remobilisation prevents any DIC release from the carbonates by binding CO_3^{2-} ions with Mg^{2+}. This means that carbonate precipitation in hyperalkaline springs is a net uptake of carbon from the atmosphere.

The combined use of the three isotopic systems has enabled new processes to be discerned. However, more data is needed in order to constrain the different geochemical processes at play during peridotite alteration. Secondary minerals, such as brucite and serpentine, are of prime interest as they may play a significant role in determining the water chemistry. Dolomite needs to be further investigated to establish the existence, or not, of two processes of formation: (1) dissolution/re-precipitation in Type I water and (2) cation exchange in Type II water ("dry dolomitisation"). The key role of dolomitisation in Ca remobilisation, and hence in the potential of peridotite alteration as a CO_2 trap, makes it determinant in regards to the use of peridotite in a strategy of climate change mitigation.

Chapter 6   Conclusions

6.1   Results summary

Peridotite alteration in the Oman-UAE ophiolite produces two types of fluids, Mg-HCO_3^- rich, pH <10 water (Type I) in the shallow subsurface, and Ca-OH^- rich, pH >10 water (Type II) deeper in the aquifer. When Type II water surfaces the calcium reacts with environmental CO_2 and precipitate massive carbonate terraces, potentially providing a powerful mean to mitigate climate change.

The primary objective of this thesis was to constrain the water-rock reactions responsible for the chemical evolution of groundwater, from Type I to Type II, along its flow path in the peridotite aquifers of the Oman-UAE ophiolite. The reactions of interest were (1) serpentinisation, responsible for the increase of pH in Type I and II waters, and the increase of dissolved Mg and Ca in Type I and Type II waters, respectively. (2) Ca-carbonate precipitation, responsible for Ca concentration decrease in Type I waters, and (3) Mg-carbonate and serpentine precipitation, responsible for the low Mg concentration in Type II waters.

The approach applied during this study was based on the conceptual hydrogeological model of peridotite aquifers in the Oman-UAE ophiolite proposed by Dewandel et al. (2005) and the use of the $^{87}Sr/^{86}Sr$ ratio to track serpentinisation reactions in these aquifers. Based on this model, it was initially predicted that the progressive water-rock reactions would result in increasing pH, and groundwater $^{87}Sr/^{86}Sr$ approaching the mantle peridotite primary $^{87}Sr/^{86}Sr$ ratio found at spreading ridges (0.7023 – 0.7033), while the increase of Sr concentration in groundwater is limited through carbonate precipitation. Instead, the results reveal that additional processes are responsible for the observed evolution of Type I and II waters. In order to determine these processes, $^{87}Sr/^{86}Sr$ analysis have been combined with novel isotopic tools such as $\delta^{44/40}Ca$ and $\delta^{88}Sr$. Focus was given to the investigation of the rocks that react with the different water types, in particular the secondary minerals that were formed during previous alteration episodes. Using $\delta^{44/40}Ca$ and $\delta^{88}Sr$ allowed the identification of the major water-rock reactions taking place in the peridotite aquifer, whereas the $^{87}Sr/^{86}Sr$ ratio allowed to define the origins of the $^{87}Sr/^{86}Sr$ signals found in the groundwater and thus the sources of the Sr.

The major findings of this study are: (1) Dissolution of secondary minerals, such as serpentine and brucite, play an important role in the water chemistry evolution in the peridotite aquifer. (2) Dolomitisation of pre-existing Ca-carbonate and dolomite precipitation are determinant in the water chemistry. (3) The Ca^{2+} remobilisation associated with dolomitisation is the main source of

Ca^{2+} in Type II water. This would prevent any CO_2 release from the carbonates by binding the CO_3^{2-} ions with Mg^{2+}, and ensure that the precipitation of carbonates in hyperalkaline springs has a net impact on the global carbon cycle.

6.2 Sr chemistry and $^{87}Sr/^{86}Sr$ signals in the peridotite aquifers

One of the questions asked during this study was about the absence of water samples with a mantle peridotite primary $^{87}Sr/^{86}Sr$ signal. The ophiolite mantle section has gone through a number of alteration episodes throughout its geological history: (1) hydrothermal alteration at or near the spreading ridge in the Tethyan ocean; (2) alteration during obduction of the oceanic lithosphere and its emplacement onto the Arabian plate; (3) alteration during the Tertiary sea transgressions when the submerged ophiolite further reacted with seawater; and (4) low-temperature weathering during the Late Tertiary until to date. The peridotites in the Oman-UAE ophiolite are generally 30-70% serpentinised (Kelemen et al., 2011). However, the portion of serpentine and other alteration minerals formed during the different alteration periods is not known. With regard to the $^{87}Sr/^{86}Sr$ ratio, four main signals were observed in the mantle section of the Oman-UAE ophiolite: (1) primary mantle ($^{87}Sr/^{86}Sr$ = 0.7023-0.7033), (2) Cretaceous seawater ($^{87}Sr/^{86}Sr$ = 0.7072-0.7079, 95 to 65 Ma ago), (3) Tertiary seawater ($^{87}Sr/^{86}Sr$ = 0.7080 to 0.7085, 24 to 18 Ma ago), and (4) modern seawater ($^{87}Sr/^{86}Sr$ = ~0.7092). The Tertiary seawater $^{87}Sr/^{86}Sr$ signal is the most common ratio yielded by the analysed rocks, and is displayed by calcite, dolomite, and the serpentinised rock matrix of peridotites (Chapter 6), suggesting extensive water/rock reactions. However, the extent of replacement varies throughout the peridotite, and Cretaceous seawater and primary mantle signals are present in the least altered rocks. This can be due to the presence of refractory minerals in the peridotite such as pyroxenes, but also due to lower rock permeabilities and geologic features that limited the access of water to different parts of the ophiolite.

In peridotite-hosted aquifers, Type I waters mostly have Tertiary seawater-like $^{87}Sr/^{86}Sr$ ratios (0.7080 to 0.7085), whereas Type II waters have $^{87}Sr/^{86}Sr$ ratios covering a range from a mantle-seawater mixture ($^{87}Sr/^{86}Sr$ = 0.7065) to a Tertiary seawater signal ($^{87}Sr/^{86}Sr$ = 0.7085) (Chapter 4). This suggests that the secondary minerals play an important role in the water-rock interactions and in the water chemistry evolution in the peridotite aquifers. Hence, the Sr chemistry is not solely depending on peridotite dissolution and carbonate precipitation, it is also influenced by secondary minerals formed during previous alteration episodes, which are recycled by dissolution and precipitation reactions. Thus, applying a simple mixing model between water and mantle peridotite to investigate the progression of water-rock reactions in the peridotite aquifers of the Oman-UAE ophiolite is inappropriate.

6.3   Water-rock reactions

The chemical evolution of groundwater in the peridotite aquifers of the Oman-UAE ophiolite is determined by water-rock reactions such as serpentinisation and carbonate precipitation, but pre-existing secondary minerals, such as Ca-Mg-carbonate, serpentine, and brucite formed during earlier alteration episodes, can also interact with ground waters and influence their chemistry.

The chemical evolution of Type I water is clearly displayed through the changes in pH, $[Mg^{2+}]$, $[Ca^{2+}]$, and [DIC]. Previous studies have linked the water pH and Mg^{2+} concentration rise to serpentinisation:

$$4\underline{Mg_2SiO_4} \text{ (Mg-olivine)} + 6H_2O = 2Mg_3Si_2O_5(OH)_4 \text{ (serpentine)} + 2\underline{Mg^{2+}}_{(aq)} + 4\underline{OH^-}_{(aq)} \tag{1}$$
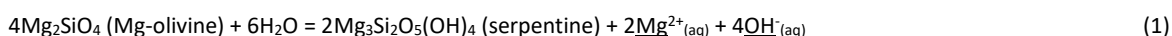
And the Ca^{2+} and DIC concentration decrease to the precipitation of calcite:

$$Ca^{2+}_{(aq)} + HCO_3^-_{(aq)} + OH^-_{(aq)} = \underline{CaCO_3}_{(solid)} + H_2O \tag{2}$$

The dominant role of these two reactions is challenged by the new $\delta^{44/40}Ca$ and $\delta^{88}Sr$ data, suggesting that additional processes are involved in the chemical evolution of Type I waters (Chapter 5). These involve: (1) Dolomite $[(Ca;Mg)CO_3]$ precipitation during the evolution of Type I waters. This is supported by the good correlations of $\delta^{44/40}Ca$ and $\delta^{88}Sr$ values with the saturation indices of dolomite yet no relationship with that of calcite in Type I water samples, and by the higher DIC decrease (-3.32 mmol/kg) than that of Ca (-1.21 mmol/kg) implying that part of the DIC bonds with Mg^{2+}. The total consumption of Ca by carbonate precipitation is demonstrated by the Rayleigh-type evolution of the groundwater $\delta^{44/40}Ca$. (2) Dissolution of pre-existing secondary minerals as suggested by the evolution of $\delta^{88}Sr$ in Type I waters that requires the contribution of minerals containing isotopically lighter Sr ($\delta^{88}Sr < 0.30$‰) than in carbonate minerals ($\delta^{88}Sr = 0.30$‰). These pre-existing minerals could be the serpentinised matrix of peridotite ($\delta^{88}Sr = 0.24$‰) or potentially brucite. Both the serpentinised matrix and brucite contain Mg^{2+} and OH^- groups and thus their dissolution contributes to the observed increase of pH and Mg^{2+} concentration in the Type I waters.

The main reactions involved in the formation of Type II waters induce an increase in pH and $[Ca^{2+}]$, and a sharp decrease of $[Mg^{2+}]$ and [DIC]. These changes have been previously linked to the involvement of Ca-poor pyroxenes in the serpentinisation reaction:

$$4Mg_2SiO_4 \text{ (Mg-olivine)} + (Ca;Mg)_2Si_2O_6 \text{ (orthopyroxenes)} + 7H_2O = 3Mg_3Si_2O_5(OH)_4 \text{ (serpentine)} + \underline{Ca}^{2+}_{(aq)} + 2\underline{OH^-}_{(aq)} \tag{3}$$
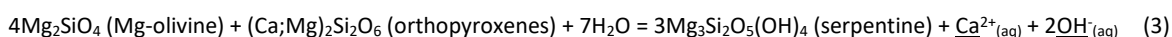
and the precipitation of magnesite and brucite:

$$Mg^{2+}_{(aq)} + HCO_3^-_{(aq)} + OH^-_{(aq)} = \underline{MgCO_3}_{(solid)} + H_2O \tag{4}$$

$$Mg^{2+} + 2OH^- = \underline{Mg(OH)_2}_{(solid)} \tag{5}$$

The dominance of these reactions over the chemical changes between Type I and Type II waters is also challenged by the new $\delta^{44/40}Ca$ and $\delta^{88}Sr$ data. A "dry dolomitisation" process, meaning the simple cation exchange of Ca^{2+} for Mg^{2+} in pre-existing carbonates, could play an important role in the increase of $[Ca^{2+}]$ and decrease of $[Mg^{2+}]$ in Type II waters without affecting the [DIC] (Chapter 5). This hypothesis is supported by the decrease of $\delta^{44/40}Ca$ between Type I and II water pointing towards the remobilisation of Ca from carbonates as peridotites have a higher $\delta^{44/40}Ca$ (0.11‰ to 0.54‰). The DIC concentration remains unchanged, which disqualifies carbonate dissolution, and the observations of re-crystallisation of Ca-carbonate to Mg-rich carbonates support a dissolution/re-precipitation process (Noel et al., 2017). However, if this process is the main source of Ca^{2+} in Type II waters, mass-balance calculations show that ~34% of Ca^{2+} still has to come from the peridotites (e.g. pyroxene, serpentine) or from another unknown source. This percentage would further increase if Mg^{2+} is also precipitated as magnesite and/or brucite.

6.4 CO₂ sequestration

The source of the calcium present in Type II water is of prime interest to assess the impact of peridotite alteration on the global carbon cycle and its potential as an approach to mitigate against global warming and climate change. It was previously thought that if the Ca originates from carbonates, then the precipitation of travertine terraces in hyperalkaline springs wouldn't have any impact on the atmospheric CO_2 concentration:

$$CaCO_3 + H_2O \leftrightarrow Ca^{2+}_{(aq)} + CO_{2(gas)} + 2OH^-_{(aq)} \tag{6}$$

In contrast, if Ca comes from peridotite the precipitation of travertine terraces would result in a net uptake of CO_2 from the atmosphere. However, the dolomitisation process proposed would prevent any CO_2 release from the carbonates during remobilisation of Ca^{2+} by binding the CO_3^{2-} ions with Mg^{2+} sourced from the dissolution of silicate minerals. Therefore, the precipitation of carbonates in hyperalkaline springs does play a significant role as a sink in the global carbon cycle, and peridotite alteration in the Oman-UAE ophiolite could be an asset in a climate change mitigation strategy.

6.5 Other ophiolite massifs

The chemical data of water samples from previous studies in ophiolite massifs: the Cedars ophiolite, the Voltri group ophiolite, the Troodos ophiolite, and the Oman-UAE ophiolite, were compared with our water data (Fig. 6.1). The two types of water, I and II, are found in most of ophiolite massifs, however, the different water types are not reported the same way in every study, for example up to five different types of water were catalogued in Cyprus (Neal and Shand, 2002), which makes it difficult to compare the data. Some of the studies do not identify the mixing of Type I and Type II

waters which makes a pH-based differentiation between the two water types irrelevant; pH is not a marker of the progression of water-rock reaction anymore (Monnin *et al.*, 2014; see chapter 4). Most of the water samples were collected on the surface, in open wells, or water stations (Bruni *et al.*, 2002; Neal and Shand, 2002; Chavagnac *et al.*, 2013), which makes water mixing with surface contaminants and airborne dust more likely. The geological environment is not always reported in enough details, such as water collected from an "ophiolite" aquifer instead of a "peridotite" or "gabbro" aquifer, limiting the constrains on the water-rock reactions (Semhi *et al.*, 2017). Another challenge to modelling is the difference of climates influencing the water-rock interactions in the different ophiolite massifs: the Troodos ophiolite has 500 mm to 1000 mm of annual rainfall compared to the 250mm in the Oman-UAE ophiolite (Neal and Shand, 2002; Dewandel *et al.*, 2005). The Voltri group ophiolite has a Mediterranean climate which results in a dense vegetation coverage and more runoff water that readily dilutes alkaline springs, making their sampling difficult. Finally, each ophiolite massif has a different history of emplacement which can result in disparity between their lithology. The Voltri group ophiolite main peridotite-type is lherzolite and its main serpentine-type is antigorite instead of harzburgite and lizardite/chrysotile as in Oman (Cipolli *et al.*, 2004; Chavagnac *et al.*, 2013).

Despite these environmental differences, the evolution of the calcium concentration vs pH in waters is very similar across the peridotite-hosted aquifers from the different ophiolite massifs (Fig. 6.1b). And the DIC present the same higher concentration in Type I water and very low concentration in Type II water in most of them (Fig. 6.1a). Na and Cl concentration in water are both obviously increasing with the pH in the Oman, Voltri group and Troodos ophiolite aquifers (Fig. 6.1d and 6.1e). This would suggest that the evolution of water chemistry is similar in the different peridotite-hosted aquifers and that our model could be used to investigate water-rock reactions in peridotite-hosted aquifers in general. However, the evolution of Mg concentration with pH does not seem to follow the same pattern, and neither does Sr concentration (Fig 6.1c and 6.1f). A more thorough investigation is needed to characterise the Mg behaviour in peridotite-hosted aquifers, as well as the link between Mg concentration in water and the presence of brucite in the altered peridotites. This will help improve the modelling of water-rock reaction along the flow path in peridotite-hosted aquifers.
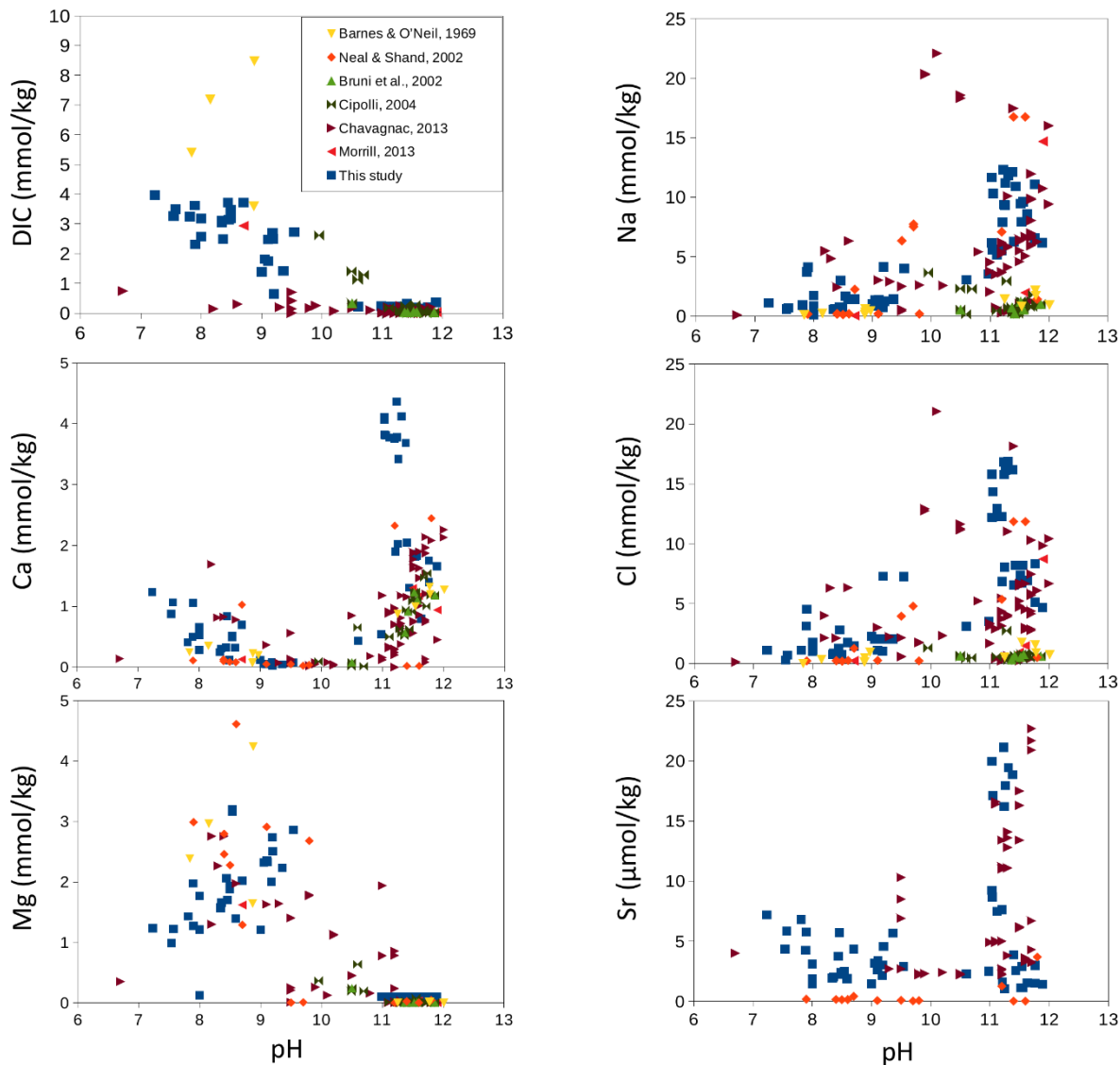
Figure 6.1: Major ion concentrations of water samples are plotted against pH. The behaviour of majors concentration against pH is similar across the studies with the exception of Mg. There are not enough studies reporting the Sr concentration to make a meaningful comparison of its behaviour between the different peridotite-hosted aquifers.

6.6   Future work

Some aspects of the groundwater evolution in peridotite-hosted aquifers of the Oman-UAE ophiolite remain unknown, such as water residence time, timescale of water formation, fraction of Mg consumed by each process, and fraction of Ca provided by each source to the Type II waters, all of which remain poorly constrained.

However, this work has enabled the uncovering of new water-rock processes involved in the chemical evolution of different water types and better constraints those already known. The use of the three isotopic systems, $\delta^{44/40}Ca$, $\delta^{88}Sr$, $^{87}Sr/^{86}Sr$, combined with ion concentration in solution has enabled the identification of the dominant geochemical processes responsible for the

formation of both type of waters. In particular, the combination of $\delta^{44/40}$Ca and δ^{88}Sr highlighted the potential role of brucite.

The leaching of targeted mineral phases within altered peridotite via a set of chemical attacks is a promising method to investigate the alteration history of the ophiolite and needs to be improved in order to develop a protocol that allows the impacts of different primary and secondary minerals to be quantified. Following improvements are suggested: using an ^{87}Sr/^{86}Sr analytical procedure requiring lower quantity of Sr to reduce the quantity of rock needed, devising ways of eliminating reagents such as NH_4Cl and acetate buffer to reduce the volume of the dry residue obtained from the leaching solution.

Future work needs to focus on gathering more data in order to confirm the role of pre-existing secondary minerals, such as Ca-carbonates, brucite and serpentine, in governing the observed water chemistry. Dolomite needs to be investigated to establish the existence, or not, of two processes of formation, via dissolution/re-precipitation in Type I water and via cations exchange in Type II water. Furthermore, the behaviour of Ca isotopes and stable Sr isotopes during water-rock reactions needs further investigation, in particular during serpentine formation and adsorption on brucite, in order to further develop the combined use of $\delta^{44/40}$Ca and δ^{88}Sr as a new geochemical tool.

Appendix A   Water-peridotite equilibration

An experiment was run to determine the water pH and chemical composition when it first enters in contact with the peridotites from the mantle section of the Oman-UAE ophiolite.

Material and Method

The five rock samples used in this experiment were collected across the wadi Tayin massif in the Oman-UAE ophiolite, and are described in chapter 6. Four MilliQ water-based solutions were prepared: one pure, three adjusted by addition of KOH to a pH of 9, 10 and 11. Eight falcon tubes with 1 g of finely ground powder were prepared per rock sample. Each falcon tube was then filled with 20 mL of stock solution, two tubes per stock solutions for each rock samples to allow for different reaction time. The powders were left to react for 1 hour (1h) or 1 day (1d) in a water bath set at 30°C. The pH was measured with a pHmeter Accumet Basic AB 15, in the stock solution, in the falcon tube at the start and at the end of the reaction, and after separation of the supernatant from the powder. Supernatant and powder were separated by centrifuging the falcon tubes for 5 min at 3000 rpm, and transferring the supernatant in another falcon tube. A selection of 9 of the supernatants retrieved were analysed for cation concentrations.

Results

Every combination of rock sample and stock solution has a final pH between 9 and 10, with two exceptions: reactions with the pH 11 stock solution and reactions with the OM15_R4 sample that have a final pH >10 (Table A.1). Difference in the final pH between the 1h and 1d reactions, varies from -0.60 to +0.47 pH unit with the least variations (-0.1 to 0.0) for the reactions with the pH 9 solution. The final pH of the solutions, depending on the initial stock solution used on a rock sample, shows similar range after 1d or 1h of reaction (s.d.$_{1h}$ = 0.31 to 0.42; s.d.$_{1d}$ = 0.28 to 0.42), with exception for OM15_R4 (s.d.$_{1d}$=0.1) (Table A.1). The final pH values after 1d seems correlated to the stock solution used: ranked high to low pH 11, MQ, pH 9 and pH 10 when reacted with OM15_R1, R2, R3, R4. But when reacted with OM15_R5 the order become pH 11, pH 10, pH 9 and MQ, somehow more intuitive (Table A.1).

The rock reacting with the stock solution also influences the solution final pH (s.d.$_{1d}$ = 0.43 to 0.48) across the 5 rock samples used, with the exception of the reactions with the pH 11 solution that show a narrower range (s.d.$_{1d}$ = 0.28) (Table A.1). The pH values measured for the 1h reaction with pH 10 stock solution are surprisingly close (s.d.$_{1h}$ = 0.13), and is the only one that yield a final pH

<10 when reacted with OM15_R4, an error of manipulation during the pH measurement might have happened.

Cations screening analyses were run on 9 final solutions that were thought to be representative of the range of solution-rock reactions, 1h and 1d with pH 11 and 1h with pH 9 on OM15_R1, R4 and R5. The Mg concentration of final solutions appears positively correlated with the pH across the rock samples, whereas the Ca concentration is also positively correlated but within each rock, idem for the Sr (Table A.2). Fe and Ni concentrations are positively correlated, OM15_R4 and R5 have clustered values (Fe ~22 ppb and Ni ~1.5 ppb), but OM15_R4 reacted with pH 11 stock solution for 1h that yields higher values (Fe = 309 ppb and Ni = 43 ppb). OM15_R1 yields higher concentrations for 1h reactions (Fe = ~44 ppb and Ni = ~4.6 ppb), but when reacted for 1d with pH 11 stock solution their concentration increase drastically (Fe = 262 ppb and Ni = 23 ppb) (Table A.1). The other screened elements show little or no variations in their concentrations.

Discussion

When the water enters in contact with rocks for the first time, either as rainfall or as high pH water, its chemistry changes by equilibrating with the minerals present. Beside the release of elements, the water pH is also impacted. We determined that if the water already has a pH >10 or if the new rock contains brucite, the water will have a pH >10 after reacting with a new rock for 1h and will keep it for at least 24h. In other cases, the water have a pH between 9 and 10. This challenges the current model proposed by Dewandel et al. (2005) and developed by Paukert et al. (2012) in which the Type II water (pH >10) are formed after extensive water-rock reactions away from the atmosphere. It also challenges the hypothesis that the pH is solely determined by serpentinisation and carbonate precipitation, the rock mineralogy appears to play a role in determining the pH starting value, which is far from the assumed value pH 7 (Chapter 4). If the water has a pH >9 when entering the shallow aquifer then it must be brought down, probably by CO_2 uptake from the atmosphere, considering that waters in the shallow aquifer (Type I) have pH >7 and <10 (Chapter 4). This experiment demonstrates that the pH of water in peridotite aquifer is not only determined by serpentinisation and carbonate precipitation, but also by the mineral composition of the rocks, and that a pH >10 can be achieved in a very short period of time. This, anyway, doesn't invalid that the pH evolution is linked to the water-rock reactions.

Conclusion

When water enters in contact with an altered peridotite its pH changes to a values between 9 and 10, unless the rock has a brucite component or the water has already a pH >10, in which cases the water pH will be >10. This challenges the current model in which the groundwater pH progresses from pH 7 to 11 via serpentinisation (Dewandel et al., 2005; Kelemen et al., 2011; Paukert et al., 2012). The groundwater starting pH value could depend on the type of rock interacting with the water and be much higher than pH 7, at least for the first 24h of water-rock reaction. However, serpentinisation and carbonate precipitation are playing a role in the evolution of pH, in particular to reach a pH >11 (serpentinisation) in type II water and to lower the pH value (carbonate precipitation) in Type I water, which have an average pH of 8.5.

Table A.1: Solution pH after 1 hour (1h) and 1 day (1d) reaction with rock samples from the mantle section of the Oman-UAE ophiolite.

Stock solution	Sample	pH after 1h	pH after 1d
pH11 (pH = 11.10)	witness	10.93	10.64
	R1	10.06	9.68
	R2	10.31	10.02
	R3	10.53	10.32
	R4	10.57	10.39
	R5	10.41	10.10
pH10 (pH =10.05)	witness	8.87	7.65
	R1	9.52	8.92
	R2	9.63	9.36
	R3	9.82	9.36
	R4	9.75	10.22
	R5	9.53	9.60
pH9 (pH =8.95)	witness	6.09	6.13
	R1	9.22	9.13
	R2	9.66	9.59
	R3	9.60	9.53
	R4	10.37	10.33
	R5	9.53	9.55
MQ (pH = 4.83)	witness	5.82	5.07
	R1	9.58	9.22
	R2	9.83	9.77
	R3	9.76	9.60
	R4	10.41	10.36
	R5	9.67	9.42

Table A.2: Cation concentration of selected solutions after reaction with rock samples from the mantle section of the Oman-UAE ophiolite.

Sample	Stock solution	Time	pH	23Na ppb	24Mg ppb	27Al ppb	44Ca ppb	52Cr ppb	56Fe ppb	60Ni ppb	65Cu ppb	88Sr ppb
OM15_R1	pH 11	1d	9.7	1588	2527	60	3450	6.7	262	22.7	39	35.1
OM15_R1	pH 11	1h	10.1	1175	6122	19	6805	4.3	44	5.5	39	74.9
OM15_R1	pH 9	1h	9.2	888	1335	17	1380	2.4	44	3.7	41	13.5
OM15_R4	pH 11	1d	10.4	1469	4928	12	2709	1.6	20	1.5	39	4.6
OM15_R4	pH 11	1h	10.6	871	11943	12	3874	2.7	309	42.9	39	1.7
OM15_R4	pH 9	1h	10.4	684	3966	12	713	1.6	22	1.4	38	0.9
OM15_R5	pH 11	1d	10.1	1013	3439	11	2283	3.5	24	1.3	39	3.5
OM15_R5	pH 11	1h	10.4	979	9591	12	3913	2.8	22	1.5	39	3.6
OM15_R5	pH 9	1h	9.5	3133	2951	13	1167	2.0	21	1.7	41	0.7

Bibliography

Åberg, G., Jacks, G. & Joseph Hamilton, P., 1989. Weathering rates and $^{87}Sr/^{86}Sr$ ratios: An isotopic approach. *Journal of Hydrology*, 109(1–2), pp.65–78.

Allen, D.E. & Seyfried, W.E., 2004. Serpentinization and heat generation: Constraints from Lost City and Rainbow hydrothermal systems. *Geochimica et Cosmochimica Acta*, 68(6), pp.1347–1354.

Alt, J.C. et al., 2013. The role of serpentinites in cycling of carbon and sulfur: Seafloor serpentinization and subduction metamorphism. *Lithos*, 178, pp.40–54.

Amini, M. et al., 2008. Calcium isotope ($\delta^{44/40}Ca$) fractionation along hydrothermal pathways, Logatchev field (Mid-Atlantic Ridge, 14°45'N). *Geochimica et Cosmochimica Acta*, 72(16), pp.4107–4122.

Amini, M. et al., 2009. Calcium isotopes ($\delta^{44/40}Ca$) in MPI-DING reference glasses, USGS rock powders and various rocks: Evidence for Ca isotope fractionation in terrestrial silicates. *Geostandards and Geoanalytical Research*, 33(2), pp.231–247.

Andreani, M. et al., 2009. Experimental study of carbon sequestration reactions controlled by the percolation of CO_2-rich brine through peridotites. *Environmental Science and Technology*, 43(4), pp.1226–1231.

Andrews, M.G. et al., 2016. Radiogenic and stable Sr isotope ratios ($^{87}Sr/^{86}Sr$, $\delta^{88/86}Sr$) as tracers of riverine cation sources and biogeochemical cycling in the Milford Sound region of Fiordland, New Zealand. *Geochimica et Cosmochimica Acta*, 173, pp.284–303.

Bach, W. et al., 2004. Seawater-peridotite interactions: First insights from ODP Leg 209, MAR 15°N. *Geochemistry, Geophysics, Geosystems*, 5(9).

Bach, W. et al., 2006. Unraveling the sequence of serpentinization reactions: Petrography, mineral chemistry, and petrophysics of serpentinites from MAR 15°N (ODP Leg 209, Site 1274). *Geophysical Research Letters*, 33(13), pp.4–7.

Bailey, E.H. & Coleman, R.G., 1975. Mineral deposits in the Samail ophiolite of northern Oman. *Geol. Soc. Amer. Abstr. Program*, 7(3), p.293.

Bailey, S.W. et al., 1996. Calcium inputs and transport in a base-poor forest ecosystem as interpreted by Sr isotopes. *Water Resources Research*, 32(3), pp.707–719.

Bain, D.C. & Bacon, J.R., 1994. Strontium isotopes as indicators of mineral weathering in catchments. *Catena*, 22(3), pp.201–214.

Barnes, I. & O'Neil, J.R., 1969. The relationship between fluids in some fresh Alpine-type ultramafics and possible modern serpentinization, western United States. *Geological Society Of America Bulletin*, 80(October), pp.1947–1960.

Bibliography

Barnes, I., O'Neil, J.R. & Trescases, J.J., 1978. Present day serpentinization in New Caledonia, Oman and Yugoslavia. *Geochimica et Cosmochimica Acta*, 42(1), pp.144–145.

Barriga, F.J.A.. et al., 1998. Discovery of the Saldanha Hydrothermal Field on the FAMOUS Segment of the MAE (36°30'N). *Eos*, 67.

Benoit, M., Polvé, M. & Ceuleneer, G., 1996. Trace element and isotopic characterization of mafic cumulates in a fossil mantle diapir (Oman ophiolite). *Chemical Geology*, 134(1–3), pp.199–214.

Benson, R.F., 1982. Method for leaching magnesium from magnesium hydroxide-containing composition. , p.9.

Berner, R.A., Lasaga, A.C. & Garrels, R.M., 1983. The carbonate-silicate geochemical cycle and its effect on atmospheric carbon dioxide over the past 100 million years. *American Journal of Science*, 283(7), pp.641–683.

Bickle, M.J. & Teagle, D.A.H., 1992. Strontium alteration in the Troodos ophiolite: implications for fluid fluxes and geochemical transport in mid-ocean ridge hydrothermal systems. *Earth and Planetary Science Letters*, 113(1–2), pp.219–237.

Blattler, C.L. et al., 2015. Mg and Ca isotope signatures of authigenic dolomite in siliceous deep-sea sediments. *Earth and Planetary Science Letters*, 419, pp.32–42.

Bochkarev, G.R.. & Pushkareva, G.I., 2009. Strontium removal from aqueous media by natural and modified sorbents. *Journal of Mining Science*, 45(3), pp.290–294.

Bogdanov, Y. et al., 1995. A study of the hydrothermal field at 14 45′ N on the Mid-Atlantic Ridge using the "MIR" submersibles. *BRIDGE newsl*, 9, pp.9–13.

Bogdanov, Y.A. et al., 1997. A New Type of Modern Mineral-forming System: Black Smokers of the Hydrothermal Field at 14 45'N Latitude, Mid-Atlantic Ridge. *GEOLOGY OF ORE DEPOSITS C/C OF GEOLOGIIA RUDNYKH MESTOROZHDENII*, 39, pp.58–78.

Böhm, F. et al., 2012. Strontium isotope fractionation of planktic foraminifera and inorganic calcite. *Geochimica et Cosmochimica Acta*, 93, pp.300–314.

Bosch, D. et al., 2004. Deep and high-temperature hydrothermal circulation in the Oman ophiolite - Petrological and isotopic evidence. *Journal of Petrology*, 45(6), pp.1181–1208.

Boudier, F., Ceuleneer, G. & Nicolas, A., 1988. Shear zones, thrusts and related magmatism in the Oman ophiolite: Initiation of thrusting on an oceanic ridge. *Tectonophysics*, 151(1–4), pp.275–296.

Boudier, F. & Coleman, R.G., 1981. Cross section through the peridotite in the Samail Ophiolite, southeastern Oman Mountains. *Journal of Geophysical Research: Solid Earth*, 86(B4), pp.2573–2592.

Bradbury, H.J. & Turchyn, A. V., 2018. Calcium isotope fractionation in sedimentary pore fluids from ODP Leg 175: Resolving carbonate recrystallization. *Geochimica et Cosmochimica Acta*.

Brasier, M.D. et al., 2002. Questioning the evidence for Earth's oldest fossils. *Nature*, 416(6876), pp.76–81.

Brazelton, W.J. et al., 2010. Archaea and bacteria with surprising microdiversity show shifts in dominance over 1,000-year time scales in hydrothermal chimneys. *Proceedings of the National Academy of Sciences*, 107(4), pp.1612–1617.

Brocks, J.J. et al., 2003. A reconstruction of Archean biological diversity based on molecular fossils from the 2.78 to 2.45 billion-year-old Mount Bruce Supergroup, Hamersley Basin, Western Australia. *Geochimica et Cosmochimica Acta*, 67(22), pp.4321–4335.

Brocks, J.J. et al., 1999. Archean molecular fossils and the early rise of eukaryotes. *Science (New York, N.Y.)*, 285(5430), pp.1033–1036.

Brookfield, M.E., 1977. The emplacement of giant ophiolite nappes I. Mesozoic-cenozoic examples. *Tectonophysics*, 37(4), pp.247–303.

Bruni, J. et al., 2002. Irreversible water-rock mass transfer accompanying the generation of the neutral, Mg-HCO3 and high-pH, Ca-OH spring waters of the Genova province, Italy. *Applied Geochemistry*, 17(4), pp.455–474.

Bryan, C.G. et al., 2011. The efficiency of indigenous and designed consortia in bioleaching stirred tank reactors. *Minerals Engineering*, 24(11), pp.1149–1156.

Capo, R.C., Stewart, B.W. & Chadwick, O.A., 1998. Strontium isotopes as tracers of ecosystem processes : theory and methods. , 82, pp.197–225.

Cenki-Tok, B. et al., 2009. The impact of water-rock interaction and vegetation on calcium isotope fractionation in soil- and stream waters of a small, forested catchment (the Strengbach case). *Geochimica et Cosmochimica Acta*, 73(8), pp.2215–2228.

Chao, H.C. et al., 2015. Evidence for stable Sr isotope fractionation by silicate weathering in a small sedimentary watershed in southwestern Taiwan. *Geochimica et Cosmochimica Acta*, 165, pp.324–341.

Charlier, B.L.A. et al., 2012. High temperature strontium stable isotope behaviour in the early solar system and planetary bodies. *Earth and Planetary Science Letters*, 329–330, pp.31–40.

Charlou, J.L. et al., 2002. Geochemistry of high H2 and CH4 vent fluids issuing from ultramafic rocks at the Rainbow hydrothermal field (36°14′N,MAR). *Chemical Geology*, 191(4), pp.345–359.

Chavagnac, V. et al., 2013. Mineralogical assemblages forming at hyperalkaline warm springs hosted on ultramafic rocks: A case study of Oman and Ligurian ophiolites. *Geochemistry, Geophysics, Geosystems*, 14(7), pp.2474–2495.

Bibliography

Cipolli, F. et al., 2004. Geochemistry of high-pH waters from serpentinites of the Gruppo di Voltri (Genova, Italy) and reaction path modeling of CO_2 sequestration in serpentinite aquifers. *Applied Geochemistry*, 19(5), pp.787–802.

Clark, I.D. et al., 1992. Stable isotope disequilibria in travertine from high pH waters: Laboratory investigations and field observations from Oman. *Geochimica et Cosmochimica Acta*, 56(5), pp.2041–2050.

Clauer, N. et al., 1993. Effects of experimental leaching on RbSr and KAr isotopic systems and REE contents of diagenetic illite. *Chemical Geology*, 103(1–4), pp.1–16.

Clauer, N., 1979. Relationship between the isotopic composition of strontium in newly formed continental clay minerals and their source material. *Chemical Geology*, 27(1–2), pp.115–124.

Coleman, R.G., 1981. Tectonic Setting for Ophiolite Obduction in Oman. *Journal of Geophysical Research*, 86(B4), pp.2497–2508.

Coleman, R.G. & Hopson, C.A., 1981. Introduction to the Oman ophiolite. *Journal of Geophysical Research*, 86(B4), pp.2495–2496.

Dananjayan, R.R.T., Kandasamy, P. & Andimuthu, R., 2016. Direct mineral carbonation of coal fly ash for CO_2 sequestration. *Journal of Cleaner Production*, 112, pp.4173–4182.

Daval, D. et al., 2010. Dissolution kinetics of diopside as a function of solution saturation state: Macroscopic measurements and implications for modeling of geological storage of CO_2. *Geochimica et Cosmochimica Acta*, 74(9), pp.2615–2633.

Daval, D. et al., 2011. Influence of amorphous silica layer formation on the dissolution rate of olivine at 90°C and elevated pCO_2. *Chemical Geology*, 284(1–2), pp.193–209.

Daval, D. et al., 2013. Lizardite serpentine dissolution kinetics as a function of pH and temperature, including effects of elevated pCO_2. *Chemical Geology*, 351, pp.245–256.

Davis, A.C., 2003. *The hydrothermal contribution to the oceanic strontium budget: insights from the Oman ophiolite*. PhD Thesis. Univ. of Cambridge, UK. 192 pp

Demergasso, C. et al., 2010. Microbial succession during a heap bioleaching cycle of low grade copper sulfides: Does this knowledge mean a real input for industrial process design and control? *Hydrometallurgy*, 104(3–4), pp.382–390.

DePaolo, D.J., 2004. Calcium Isotopic Variations Produced by Biological, Kinetic, Radiogenic and Nucleosynthetic Processes. *Reviews in Mineralogy and Geochemistry*, 55(1), pp.255–288.

DePaolo, D.J., 2011. Surface kinetic model for isotopic and trace element fractionation during precipitation of calcite from aqueous solutions. *Geochimica et Cosmochimica Acta*, 75(4), pp.1039–1056.

DePaolo, D.J. & Wasserburg, G.J., 1977. The Sources of Island Arcs as Indicated by Nd and Sr Isotopic Studies. *October*, 4(10), pp.4–7.

Dewandel, B. et al., 2005. A conceptual hydrogeological model of ophiolite hard-rock aquifers in Oman based on a multiscale and a multidisciplinary approach. *Hydrogeology Journal*, 13(5–6), pp.708–726.

Dewandel, B. et al., 2003. Seismic wave velocity and anisotropy of serpentinized peridotite in the Oman ophiolite. *Tectonophysics*, 370(1–4), pp.77–94.

Dewey, J.F., 1976. Ophiolite obduction. *Tectonophysics*, 31(1–2), pp.93–120.

Dias, Á.S. et al., 2011. Geochemistry and stable isotope constraints on high-temperature activity from sediment cores of the Saldanha hydrothermal field. *Marine Geology*, 279(1–4), pp.128–140.

Dias, Á.S. et al., 2010. Tracing fluid-rock reaction and hydrothermal circulation at the Saldanha hydrothermal field. *Chemical Geology*, 273(3–4), pp.168–179.

Douville, E. et al., 2002. The rainbow vent fluids (36°14'N, MAR): the influence of ultramafic rocks and phase sep aration on trace metal content in Mid-Atlantic Ridge hydrothermal fluids. *Chemical Geology*, 184, pp.37–48.

Escartin, J. et al., 1997. Effects of serpentinization on the lithospheric strength and the style of normal faulting at slow-spreading ridges. *Earth and Planetary Science Letters*, 151, pp.181–189.

Evans, B.W., 1977. Metamorphism of Alpine Peridotite and Serpentinite. *Annual Review in Earth and Planetary Sciences*, 5(1), pp.397–447.

Fantle, M.S. & DePaolo, D.J., 2007. Ca isotopes in carbonate sediment and pore fluid from ODP Site 807A: The $Ca^{2+}_{(aq)}$-calcite equilibrium fractionation factor and calcite recrystallization rates in Pleistocene sediments. *Geochimica et Cosmochimica Acta*, 71(10), pp.2524–2546.

Fantle, M.S. & Higgins, J., 2014. The effects of diagenesis and dolomitization on Ca and Mg isotopes in marine platform carbonates: Implications for the geochemical cycles of Ca and Mg. *Geochimica et Cosmochimica Acta*, 142, pp.458–481.

Fantle, M.S. & Tipper, E.T., 2014. Calcium isotopes in the global biogeochemical Ca cycle: Implications for development of a Ca isotope proxy. *Earth-Science Reviews*, 129, pp.148–177.

Faure, G. & Hurley, P.M., 1963. The isotopic composition of strontium in oceanic and continental basalts: Application to the origin of igneous rocks. *Journal of Petrology*, 4(1), pp.31–50.

Faure, G. & Mensing, T.M., 2005. Radiogenic Isotope Geochronometers: The Rb-Sr Method. *Isotopes principles and applications, Third edition*, pp.75–112.

Fietzke, J. & Eisenhauer, A., 2006. Determination of temperature-dependent stable strontium isotope (88Sr/86Sr) fractionation via bracketing standard MC-ICP-MS. *Geochemistry, Geophysics, Geosystems*, 7(8).

Fouquet, Y. et al., 1998. FLORES diving cruise with the Nautile near the Azores - First dives on the Rainbow field: hydrothermal seawater/mantle interaction. *InterRidge News*, 7, pp.24–28.

Bibliography

Francis, T.J.G., 1981. Serpentinization faults and their role in the tectonics of slow spreading ridges. *Journal of Geophysical Research*, 86(B12), p.11616.

Frost, C.D. & Toner, R.N., 2004. Strontium Isotopic Identification of Water-Rock Interaction and Ground Water Mixing. *Ground Water*, 42(3), pp.418–432.

Frost, R.B., 1985. On the stability of sulfides, oxides, and native metals in serpentinite. *Journal of Petrology*, 26(1), pp.31–63.

Frost, R.B. & Beard, J.S., 2007. On silica activity and serpentinization. *Journal of Petrology*, 48(7), pp.1351–1368.

Fruchter, N. et al., 2016. ^{88}Sr/^{86}Sr fractionation in inorganic aragonite and in corals. *Geochimica et Cosmochimica Acta*, 178, pp.268–280.

Fruh-Green, G.L. et al., 2003. 30,000 Years of Hydrothermal Activity at the Lost City Vent Field. *Science*, 301(July), pp.495–498.

Gabellone, T. & Whitaker, F., 2016. Secular variations in seawater chemistry controlling dolomitization in shallow reflux systems: Insights from reactive transport modelling. *Sedimentology*.

Gast, P.W., Tilton, G.R. & Hedge, C., 1964. Isotopic Composition of Lead and Strontium from Ascension and Gough Islands. *Science*, 145(3637), pp.1181–1185.

Gealey, W.K., 1977. Ophiolite obduction and geologic evolution of the Oman Mountains and adjacent areas. *Bulletin of the Geological Society of America*, 88(8), pp.1183–1191.

Gerbert-Gaillard, L., 2002. *Caractérisation Géochimique des Péridotites de l'ophiolite d'Oman : Processus Magmatiques aux Limites Lithosphère/Asthénosphère.*, PhD Thesis, Univ. Montpellier II, France. 241 pp.

Gerdemann, S.J. et al., 2007. Ex situ aqueous mineral carbonation Environ. *Sci Technol*, 41(7), pp.2589–2593.

Gislason, S.R. et al., 2010. Mineral sequestration of carbon dioxide in basalt: A pre-injection overview of the CarbFix project. *International Journal of Greenhouse Gas Control*, 4(3), pp.537–545.

Glennie, K.W. et al., 1974. Geology of the Oman Mountains, parts 1 and 2. *The Royal Dutch Geological and Mining Society (KNGMG), Utrecht, The Netherlands*.

Glennie, K.W. et al., 1973. Late Cretaceous nappes in Oman Mountains and their geologic evolution. *AAPG Bulletin*, 57(1), pp.5–27.

Godard, M. et al., 1995. Effects of mineralogical reactions on trace element redistributions in mantle rocks during percolation processes: A chromatographic approach. *Earth and Planetary Science Letters*, 133(3–4), pp.449–461.

Godard, M. et al., 2000. Relationships between geochemistry and structure beneath a palaeo-spreading centre: A study of the mantle section in the Oman ophiolite. *Earth and Planetary Science Letters*, 180(1–2), pp.133–148.

Goldstein, J.I. et al., 2003. Special Topics in Electron Beam X-Ray Microanalysis. In J. I. Goldstein et al., eds. *Scanning Electron Microscopy and X-ray Microanalysis: Third Edition*. Boston, MA: Springer US, pp. 453–536.

Gregg, J.M. et al., 2015. Mineralogy, nucleation and growth of dolomite in the laboratory and sedimentary environment: A review. *Sedimentology*, pp.1749–1769.

Gregory, R.T. & Taylor, H.P.J., 1981. An Oxygen Isotope Profile in a Section of Cretaceous Oceanic Crust, Samail Ophiolite, Oman: Evidence for δ18O Buffering of the Oceans by Deep (>5km) Seawater-Hydrothermal Circulation at Mid-Ocean Ridges. *Journal of Geophysical Research*, 86(B4), pp.2737–2755.

Gussone, N. et al., 2005. Calcium isotope fractionation in calcite and aragonite. *Geochimica et Cosmochimica Acta*, 69(18), pp.4485–4494.

Hacker, B.R., 2008. H2O subduction beyond arcs. *Geochemistry, Geophysics, Geosystems*, 9(3).

Halicz, L. et al., 1999. High-precision measurement of calcium isotopes in carbonates and related materials by multiple collector inductively coupled plasma mass spectrometry (MC-ICP-MS). *Journal of Analytical Atomic Spectrometry*, 14, pp.1835–1838.

Halicz, L. et al., 2008. Strontium stable isotopes fractionate in the soil environments? *Earth and Planetary Science Letters*, 272(1–2), pp.406–411.

Hänchen, M. et al., 2006. Dissolution kinetics of fosteritic olivine at 90-150°C including effects of the presence of CO_2. *Geochimica et Cosmochimica Acta*, 70(17), pp.4403–4416.

Hanghøj, K. et al., 2010. Composition and genesis of depleted mantle peridotites from the Wadi Tayin massif, Oman ophiolite; Major and trace element geochemistry, and Os isotope and PGE systematics. *Journal of Petrology*, 51(1–2), pp.201–227.

Haqq-Misra, J.D. et al., 2008. A revised, hazy methane greenhouse for the Archean Earth. *Astrobiology*, 8(6), pp.1127–1137.

Harrison, A.L. et al., 2013. Accelerated carbonation of brucite in mine tailings for carbon sequestration. *Environmental Science and Technology*, 47(1), pp.126–134.

Hart, S.R., 1988. Heterogeneous mantle domains: signatures, genesis and mixing chronologies. *Earth and Planetary Science Letters*, 90(3), pp.273–296.

Hart, S.R., Erlank, A.J. & Kable, E.J.D., 1974. Sea floor basalt alteration: Some chemical and Sr isotopic effects. *Contributions to Mineralogy and Petrology*, 44(3), pp.219–230.

Bibliography

Hébert, R. et al., 1990. Metamorphic petrology of ODP Leg 109, Hole 670A serpentinized peridotites: serpentinization processes at a slow spreading ridge environment. In *Detrick, R., Honnorez, J., Bryan, WB, Juteau, T., et al., Proc. ODP, Sci. Results*. pp. 103–115.

Hilairet, N. & Reynard, B., 2009. Stability and dynamics of serpentinite layer in subduction zone. *Tectonophysics*, 465(1–4), pp.24–29.

Hippler, D. et al., 2003. Calcium isotopic composition of various reference materials and seawater. *Geostandards Newsletter*, 27(1), pp.13–19.

Hirauchi, K.I. et al., 2010. Inhibition of subduction thrust earthquakes by low-temperature plastic flow in serpentine. *Earth and Planetary Science Letters*, 295(3–4), pp.349–357.

Holland, H.D., 2006. The Oxygenation of the aAtmosphere and Oceans. *Philosophical transactions of the Royal Society of London. Series B, Biological sciences*, 361(1470), pp.903–915.

Hopson, C. a. et al., 1981. Geologic section through the Samail Ophiolite and associated rocks along a Muscat-Ibra Transect, southeastern Oman Mountains. *Journal of Geophysical Research*, 86(B4), p.2527.

Hövelmann, J. et al., 2011. Experimental study of the carbonation of partially serpentinized and weathered peridotites. *Geochimica et Cosmochimica Acta*, 75(22), pp.6760–6779.

Hövelmann, J. et al., 2012. Microstructure and porosity evolution during experimental carbonation of a natural peridotite. *Chemical Geology*, 334, pp.254–265.

Huang, J.X. et al., 2012. Seeking the primary compositions of mantle xenoliths: Isotopic and elemental consequences of sequential leaching treatments on an eclogite suite. *Chemical Geology*, 328, pp.137–148.

Hurley, P.M. et al., 1962. Radiogenic strontium-87 model of continent formation. *Journal of Geophysical Research*, 67(13), pp.5315–5334.

IPCC, 2005. IPCC Special Report on Carbon Dioxide Capture and Storage. Prepared by Working Group III of the Intergovernmental Panel on Climate Change. Metz B, Davidson O, de Coninck HC, Loos M, Meyer LA (eds) Cambridge University Press, Cambridge, United Kingdom and New York, USA

Jacobson, A.D. et al., 2015. Silicate versus carbonate weathering in Iceland: New insights from Ca isotopes. *Earth and Planetary Science Letters*, 416, pp.132–142.

Jacobson, A.D. & Holmden, C., 2008. δ^{44}Ca evolution in a carbonate aquifer and its bearing on the equilibrium isotope fractionation factor for calcite. *Earth and Planetary Science Letters*, 270(3–4), pp.349–353.

Jamtveit, B. et al., 2009. Reaction induced fracturing during replacement processes. *Contributions to Mineralogy and Petrology*, 157(1), pp.127–133.

Johannes, W., 1969. An experimental investigation of the system MgO-SiO_2-H_2O-CO_2. *American Journal of Science*, 267(9), pp.1083–1104.

Jousselin, D. & Mainprice, D., 1998. Melt topology and seismic anisotropy in mantle peridotites of the Oman ophiolite. *Earth and Planetary Science Letters*, 164(3–4), pp.553–568.

Jousselin, D. & Nicolas, A., 2000. Oceanic ridge off-axis deep structure in the Mansah region (Sumail Massif, Oman ophiolite). *Marine Geophysical Researches*, 21(3–4), pp.243–257.

Kaczmarek, S.E. & Sibley, D.F., 2014. Direct physical evidence of dolomite recrystallization. *Sedimentology*, 61(6), pp.1862–1882.

Kaczmarek, S.E. & Sibley, D.F., 2011. On the evolution of dolomite stoichiometry and cation order during high-temperature synthesis experiments: An alternative model for the geochemical evolution of natural dolomites. *Sedimentary Geology*, 240(1–2), pp.30–40.

Kandji, E.H.B. et al., 2017. Kinetic testing to evaluate the mineral carbonation and metal leaching potential of ultramafic tailings: Case study of the Dumont Nickel Project, Amos, Québec. *Applied Geochemistry*, 84, pp.262–276.

Kawahata, H. et al., 2001. Sr isotope geochemistry and hydrothermal alteration of the Oman ophiolite. *Journal of Geophysical Research*, 106(B6), p.11083.

Kelemen, P.B. et al., 2011. Rates and Mechanisms of Mineral Carbonation in Peridotite: Natural Processes and Recipes for Enhanced, in situ CO_2 Capture and Storage. *Annual Review of Earth and Planetary Sciences*, 39(1), pp.545–576.

Kelemen, P.B. et al., 2011. Supplement Information: Rates and Mechanisms of Mineral Carbonation in Peridotite: Natural Processes and Recipes for Enhanced, in situ CO_2 Capture and Storage. *Annual Review in Earth and Planetary Sciences*, 39(1), pp.S1–S48.

Kelemen, P.B. & Hirth, G., 2012. Reaction-driven cracking during retrograde metamorphism: Olivine hydration and carbonation. *Earth and Planetary Science Letters*, 345–348, pp.81–89.

Kelemen, P.B. & Matter, J., 2008. In situ carbonation of peridotite for CO_2 storage. *Proceedings of the National Academy of Sciences*, 105(45), pp.17295–17300.

Kelley, D.S. et al., 2005. A Serpentinite-Hosted Ecosystem: The Lost City Hydrothemal Field. *Science*, 307(March), pp.1428–1434.

Kelley, D.S. et al., 2001. An off-axis hydrothermal vent eld near the Mid-Atlantic Ridge at 30°N. *Nature*, 412(July), pp.145–149.

Kelley, D.S. et al., 2001. An off-axis hydrothermal vent field near the Mid-Atlantic Ridge at 30 degrees N. *Nature*, 412(6843), pp.145–9.

Kimball, K.L. et al., 1985. High temperature alteration of Abyssal ultramafics from the Islas Orcadas Fracture Zone, South Atlantic. *Contributions to Mineralogy and Petrology*, 91(4), pp.307–320.

Bibliography

King, H.E. et al., 2010. Effect of secondary phase formation on the carbonation of olivine. *Environmental science & technology*, 44(16), pp.6503–9.

Klein, F. et al., 2009. Iron partitioning and hydrogen generation during serpentinization of abyssal peridotites from 15°N on the Mid-Atlantic Ridge. *Geochimica et Cosmochimica Acta*, 73(22), pp.6868–6893.

Kodolányi, J. & Pettke, T., 2011. Loss of trace elements from serpentinites during fluid-assisted transformation of chrysotile to antigorite - An example from Guatemala. *Chemical Geology*, 284(3–4), pp.351–362.

Koschinsky, A. & Halbach, P., 1995. Sequential leaching of marine ferromanganese precipitates: Genetic implications. *Geochimica et Cosmochimica Acta*, 59(24), pp.5113–5132.

Kuhn, T. et al., 2004. The Logatchev hydrothermal field - revisited: preliminary results of the R/V Meteor Cruise Hydromar I (M60/3). *InterRidge News*, 13, pp.1–4.

Kwarteng, A.Y. et al., 2001. Analysis of a 27-year rainfall data (1977–2003) in the Sultanate of Oman. *Encyclopedia of Atmospheric Sciences*, 4(December 2007), p.1549–1555.

Lackner, K.S. et al., 1995. Carbon dioxide disposal in carbonate minerals. *Energy*, 20(11), pp.1153–1170.

Lafay, R. et al., 2014. Simultaneous precipitation of magnesite and lizardite from hydrothermal alteration of olivine under high-carbonate alkalinity. *Chemical Geology*, 368, pp.63–75.

Lanphere, M.A., 1981. K-Ar ages of metamorphic rocks at the base of the Samail Ophiolite, Oman. *Journal of Geophysical Research: Solid Earth*, 86(B4), pp.2777–2782.

Lanphere, M.A., Coleman, R.G. & Hopson, C.A., 1981. Sr isotopic tracer study of the Samail Ophiolite, Oman. *Journal of Geophysical Research: Solid Earth*, 86(B4), pp.2709–2720.

Lehn, G.O. et al., 2013. Precise analysis of Ca isotope ratios ($\delta^{44/40}$Ca) using an optimized ^{43}Ca-^{42}Ca double-spike MC-TIMS method. *International Journal of Mass Spectrometry*, 351, pp.69–75.

Lemarchand, D. et al., 2004. Rate-controlled calcium isotope fractionation in synthetic calcite. *Geochimica et Cosmochimica Acta*, 68(22), pp.4665–4678.

Lerouge, C. et al., 2010. Strontium distribution and origins in a natural clayey formation (Callovian-Oxfordian, Paris Basin, France): A new sequential extraction procedure. *Geochimica et Cosmochimica Acta*, 74(10), pp.2926–2942.

Liu, H.C. et al., 2017. Effect of calcite precipitation on stable strontium isotopic compositions: Insights from riverine and pool waters in a karst cave. *Chemical Geology*, 456, pp.85–97.

Lowell, R.P. & Rona, P.A., 2002. Seafloor hydrothermal systems driven by the serpentinization of peridotite. *Geophysical Research Letters*, 29(11), pp.0–3.

Ludwig, K.A. et al., 2006. Formation and evolution of carbonate chimneys at the Lost City Hydrothermal Field. *Geochimica et Cosmochimica Acta*, 70(14), pp.3625–3645.

Ma, J.L. et al., 2013. Precise measurement of stable ($\delta^{88/86}Sr$) and radiogenic ($^{87}Sr/^{86}Sr$) strontium isotope ratios in geological standard reference materials using MC-ICP-MS. *Chinese Science Bulletin*, 58(25), pp.3111–3118.

Machel, H.G., 2004. Concepts and models of dolomitization: a critical reappraisal. *Geological Society, London, Special Publications*, 235(1), pp.7–63.

Macleod, G. et al., 1994. Hydrothermal and oceanic pH conditions of possible relevance to the origin of life. *Origins of Life and Evolution of the Biosphere*, 24(1), pp.19–41.

Madeddu, S. et al., 2015. Extraction of $Mg(OH)_2$ from Mg silicate minerals with NaOH assisted with H_2O: implications for CO_2 capture from exhaust flue gas. *Faraday Discuss.*, 183, pp.369–387.

Malvoisin, B. et al., 2012. Serpentinization of oceanic peridotites: 2. Kinetics and processes of San Carlos olivine hydrothermal alteration. *Journal of Geophysical Research: Solid Earth*, 117(4), pp.1–13.

Malvoisin, B. et al., 2012. Serpentinization of oceanic peridotites: 1. A high-sensitivity method to monitor magnetite production in hydrothermal experiments. *Journal of Geophysical Research: Solid Earth*, 117(1), pp.1–10.

Marieni, C., 2016. *Geological Storage of Carbon Dioxide in Oceanic Crust*. PhD Thesis. Univ. of Southampton, UK. 245 pp.

Marriott, C.S. et al., 2004. Temperature dependence of δ^7Li, $\delta^{44}Ca$ and Li/Ca during growth of calcium carbonate. *Earth and Planetary Science Letters*, 222(2), pp.615–624.

Martin, B. & Fyfe, W.S., 1970. Some experimental and theoretical observations on the kinetics of hydration reactions with particular reference to serpentinization. *Chemical Geology*, 6(C), pp.185–202.

Maruyama, S. & Okamoto, K., 2007. Water transportation from the subducting slab into the mantle transition zone. *Gondwana Research*, 11(1–2), pp.148–165.

Matter, J.M. et al., 2016. Rapid carbon mineralization for permanent disposal of anthropogenic carbon dioxide emissions. *Science*, 352(6291), p.1312 LP-1314.

Matter, J.M. & Kelemen, P.B., 2009. Permanent storage of carbon dioxide in geological reservoirs by mineral carbonation. *Nature Geoscience*, 2(12), pp.837–841.

McArthur, J.M. et al., 2012. Strontium Isotope Stratigraphy. *The Geologic Time Scale*, pp.127–144.

McCollom, T.M., 2016. Abiotic methane formation during experimental serpentinization of olivine. *Proceedings of the National Academy of Sciences*, 113(49), pp.13965–13970.

Bibliography

McCollom, T.M. et al., 2010. The influence of carbon source on abiotic organic synthesis and carbon isotope fractionation under hydrothermal conditions. *Geochimica et Cosmochimica Acta*, 74(9), pp.2717–2740.

McCollom, T.M. & Bach, W., 2009. Thermodynamic constraints on hydrogen generation during serpentinization of ultramafic rocks. *Geochimica et Cosmochimica Acta*, 73(3), pp.856–875.

McCulloch, M.T. et al., 1980. A neodymium, strontium, and oxygen isotopic study of the Cretaceous Samail ophiolite and implications for the petrogenesis and seawater-hydrothermal alteration of oceanic crust. *Earth and Planetary Science Letters*, 46(2), pp.201–211.

Ménez, B. et al., 2012. Life in the hydrated suboceanic mantle. *Nature Geoscience*, 5(2), pp.133–137.

Menzies, C.D., 2012. *Fluid Flow Associated with the Alpine Fault, South Island, New Zealand.*, PhD Thesis. Univ. of Southampton, UK. 477 pp.

Menzies, C.D. et al., 2016. The fluid budget of a continental plate boundary fault: Quantification from the Alpine Fault, New Zealand. *Earth and Planetary Science Letters*, 445, pp.125–135.

Menzies, M.M. & Murthy, V.R., 1978. Strontium Isotope Geochemistry of Alpine Tectonite Lherzolites: Data Compatible with a Mantle Origin. *Earth and Planetary Science Letters*, 38, pp.346–354.

Mervine, E.M. et al., 2014. Carbonation rates of peridotite in the Samail Ophiolite, Sultanate of Oman, constrained through ^{14}C dating and stable isotopes. *Geochimica et Cosmochimica Acta*, 126, pp.371–397.

Mével, C., 2003. Serpentinization of abyssal peridotites at mid-ocean ridges. *Comptes Rendus Geoscience*, 335(10–11), pp.825–852.

Mével, C. & Stamoudi, C., 1996. Hydrothermal alteration of the upper-mantle section at Hess Deep. *Proceedings of the Ocean Drilling Program, Scientific Results*, 147, pp.293–309.

Miller, H.M. et al., 2016. Modern water/rock reactions in Oman hyperalkaline peridotite aquifers and implications for microbial habitability. *Geochimica et Cosmochimica Acta*, 179, pp.217–241.

Monnin, C. et al., 2014. Fluid chemistry of the low temperature hyperalkaline hydrothermal system of Prony Bay (New Caledonia). *Biogeosciences,* 11, pp.5687–5706

Moore, J. et al., 2013. Tracking the relationship between mountain uplift, Silicate weathering, and long-term CO_2 consumption with Ca isotopes: Southern Alps, New Zealand. *Chemical Geology*, 341, pp.110–127.

Morrill, P. L. et al., 2013. Geochemistry and geobiology of a present-day serpentinization site in California: The Cedars. *Geochimica et Cosmochimica Acta,* 109, pp.222–240

Moynier, F. et al., 2010. Sr stable isotope composition of Earth, the Moon, Mars, Vesta and meteorites. *Earth and Planetary Science Letters*, 300(3–4), pp.359–366.

Neal, C. & Shand, P., 2002. Spring and surface water quality of the Cyprus ophiolites. *Hydrology and Earth System Sciences*, 6(5), pp.797–817.

Neal, C. & Stanger, G., 1983. Hydrogen generation from mantle source rocks in Oman. *Earth and Planetary Science Letters*, 66(C), pp.315–320.

Neal, C. & Stanger, G., 1985. Past & present serpentinisation of ultramafic Rocks; an example from the Semail ophiolite nappe of northern Oman. In *The Chemistry of Weathering*. pp. 249–275.

Negrel, P. et al., 2003. Strontium isotopic characterization of the Palmottu hydrosystem (Finland): Water-rock interaction and geochemistry of groundwaters. *Geofluids*, 3(3), pp.161–175.

Neymark, L.A. et al., 2014. Precise determination of δ^{88}Sr in rocks, minerals, and waters by double-spike TIMS: a powerful tool in the study of geological, hydrological and biological processes. *J. Anal. At. Spectrom.*, 29(1), pp.65–75.

Nicolas, A. et al., 2000(1). Accretion of Oman and United Arab Emirates ophiolite - Discussion of a new structural map. *Marine Geophysical Researches*, 21(3–4), pp.147–179.

Nicolas, A. et al., 2000(2). Aswad massif (United Arab Emirates): Archetype of the Oman-UAE ophiolite belt. *Special paper - Geological Society of America*, (349), pp.499–512.

Nicolas, A. et al., 2000(3). Dike distribution in the Oman-United Arab Emirates ophiolite. *Marine Geophysical Researches*, 21(3–4), pp.269–287.

Nicolas, A. et al., 1988. Structural mapping in the Oman ophiolites: Mantle diapirism along an oceanic ridge. *Tectonophysics*, 151(1–4), pp.27–56.

Nicolas, A. & Boudier, F., 1995. Mapping oceanic ridge segments in Oman ophiolite. *Journal of Geophysical Research*, 100(B4), p.6179.

Nier, A.O., 1938. The Isotopic Constitution of Strontium, Barium, Bismuth, Thallium and Mercury. *Physical Review*, 5(August), pp.275–278.

Noel, J. et al., 2017. Evidence of polygenic CO_2 trapping in the Oman ophiolite peridotites. Abstract, *Goldschmidt conference*.

O'Neil, J.R. & Barnes, I., 1971. C^{13} and O^{18} compositions in some fresh-water carbonates associated with ultramafic rocks and serpentinites: western United States. *Geochimica et Cosmochimica Acta*, 35(7), pp.687–697.

O'Nions, R.K. & Pankhurst, R.J., 1974. Petrogenetic significance of isotope and trace element variations in volcanic rocks from the mid-Atlantic. *Journal of Petrology*, 15(3), pp.603–634.

Ockert, C. et al., 2013. Isotope fractionation during Ca exchange on clay minerals in a marine environment. *Geochimica et Cosmochimica Acta*, 112, pp.374–388.

Oelkers, E.H., 2001. An experimental study of forsterite dissolution rates as a function of temperature and aqueous Mg and Si concentrations. *Chemical Geology*, 175(3–4), pp.485–494.

Bibliography

Oelkers, E.H. & Schott, J., 2001. An experimental study of enstatite dissolution rates as function of pH, temperature, and aqueous Mg and Si concentration, and the mechanism of pyroxene/pyroxenoid dissolution. *Geochimica et Cosmochimica Acta*, 65(8), pp.1219–1231.

Ohno, T. et al., 2008. Determination of $^{88}Sr/^{86}Sr$ mass-dependent isotopic fractionation and radiogenic isotope variation of $^{87}Sr/^{86}Sr$ in the Neoproterozoic Doushantuo Formation. *Gondwana Research*, 14(1–2), pp.126–133.

Ohno, T. & Hirata, T., 2007. Simultaneous determination of mass-dependent isotopic fractionation and radiogenic isotope variation of strontium in geochemical samples by multiple collector-ICP-mass spectrometry. *Analytical sciences : the international journal of the Japan Society for Analytical Chemistry*, 23(11), pp.1275–1280.

Ohtani, E. et al., 2004. Water transport into the deep mantle and formation of a hydrous transition zone. *Physics of the Earth and Planetary Interiors*, 143(1–2), pp.255–269.

Oskierski, H.C., Dlugogorski, B.Z. & Jacobsen, G., 2013. Sequestration of atmospheric CO_2 in chrysotile mine tailings of the Woodsreef Asbestos Mine, Australia: Quantitative mineralogy, isotopic fingerprinting and carbonation rates. *Chemical Geology*, 358, pp.156–169.

Palmer, M. & Edmond, J., 1992. Controls over the strontium isotope composition of river water. *Geochimica et Cosmochimica Acta*, 56(5), pp.2099–2111.

Paukert, A.N. et al., 2012. Reaction path modelling of enhanced in situ CO_2 mineralization for carbon sequestration in the peridotite of the Samail Ophiolite, Sultanate of Oman. *Chemical Geology*, 330–331, pp.86–100.

Pavlov, A.A. et al., 2000. Greenhouse warming by CH_4 in the atmosphere of early Earth. *Journal of Geophysical Research*, 105(E5), p.11,981-11,990.

Pearce, C.R. et al., 2015. Reassessing the stable ($\delta^{88/86}Sr$) and radiogenic ($^{87}Sr/^{86}Sr$) strontium isotopic composition of marine inputs. *Geochimica et Cosmochimica Acta*, 157, pp.125–146.

Philippot, P. et al., 2009. Early traces of life investigations in drilling Archean hydrothermal and sedimentary rocks of the Pilbara Craton, Western Australia and Barberton Greenstone Belt, South Africa. *Comptes Rendus - Palevol*, 8(7), pp.649–663.

Poinar, K., 2012. The Carbon Cycle in the Mantle: Implications for timescales, geochemistry, and mantle convection. *PCC 588 Project*, pp.1–11.

Pokrovsky, O.S. & Schott, J., 2000. Kinetics and mechanism of forsterite dissolution at 25°C and pH from 1 to 12. *Geochimica et Cosmochimica Acta*, 64(19), pp.3313–3325.

Poulton, S.W. & Canfield, D.E., 2005. Development of a sequential extraction procedure for iron: Implications for iron partitioning in continentally derived particulates. *Chemical Geology*, 214(3–4), pp.209–221.

Poulton, S.W., Fralick, P.W. & Canfield, D.E., 2004. The transition to a sulphidic ocean, 1.84 billion years ago. *Nature*, 431(September), pp.173–177.

Power, I. et al., 2014. Strategizing Carbon-Neutral Mines: A Case for Pilot Projects. *Minerals*, 4, pp. 399-436.

Power, I.M. et al., 2013. Carbon Mineralization: From Natural Analogues to Engineered Systems. *Reviews in Mineralogy and Geochemistry*, 77(1), pp.305–360.

Power, I.M. et al., 2011. Microbially mediated mineral carbonation: Roles of phototrophy and heterotrophy. *Environmental Science and Technology*, 45(20), pp.9061–9068.

Power, I.M. et al., 2010. Bioleaching of ultramafic tailings by Acidithiobacillus spp. for CO_2 sequestration. *Environmental Science and Technology*, 44(1), pp.456–462.

Pradhan, N. et al., 2008. Heap bioleaching of chalcopyrite: A review. *Minerals Engineering*, 21(5), pp.355–365.

Qafoku, O. et al., 2012. Fayalite dissolution and siderite formation in water-saturated supercritical CO_2. *Chemical Geology*, 332–333, pp.124–135.

Raddatz, J. et al., 2013. Stable Sr-isotope, Sr/Ca, Mg/Ca, Li/Ca and Mg/Li ratios in the scleractinian cold-water coral Lophelia pertusa. *Chemical Geology*, 352, pp.143–152.

Rempfert, K.R. et al., 2017. Geological and Geochemical Controls on Subsurface Microbial Life in the Samail Ophiolite, Oman. *Frontiers in Microbiology*, 8(56).

Reynard, B., 2013. Serpentine in active subduction zones. *Lithos*, 178, pp.171–185.

Rioux, M. et al., 2012. Rapid crustal accretion and magma assimilation in the Oman-U.A.E. ophiolite: High precision U-Pb zircon geochronology of the gabbroic crust. *Journal of Geophysical Research: Solid Earth*, 117(7), pp.1–12.

Robinson, P., 1980. Determination of calcium, magnesium, manganese, strontium, sodium and iron in the carbonate fraction of limestones and dolomites. *Chemical Geology*, 28(C), pp.135–146.

Rosing, M.T. et al., 2010. No climate paradox under the faint early Sun. *Nature*, 464(7289), pp.744–747.

Rüggeberg, A. et al., 2008. Stable strontium isotopes ($\delta^{88/86}Sr$) in cold-water corals - A new proxy for reconstruction of intermediate ocean water temperatures. *Earth and Planetary Science Letters*, 269(3–4), pp.569–574.

Russell, W.A. et al., 1978. Ca isotope fractionation on the Earth and other solar system materials. *Geochimica et Cosmochimica Acta*, 42(8), pp.1075–1090.

Saldi, G.D. et al., 2009. Magnesite growth rates as a function of temperature and saturation state. *Geochimica et Cosmochimica Acta*, 73(19), pp.5646–5657.

Saldi, G.D. et al., 2013. The role of Fe and redox conditions in olivine carbonation rates: An experimental study of the rate limiting reactions at 90 and 150°C in open and closed systems. *Geochimica et Cosmochimica Acta*, 118, pp.157–183.

Bibliography

Sanna, A. et al., 2014. A review of mineral carbonation technologies to sequester CO_2. *Chem. Soc. Rev.*, 43(23), pp.8049–8080.

Sanna, A. et al., 2014. Silicate rock dissolution by ammonium bisulphate for pH swing mineral CO_2 sequestration. *Fuel Processing Technology*, 120, pp.128–135.

Sanna, A. et al., 2016. Alternative regeneration of chemicals employed in mineral carbonation towards technology cost reduction. *Chemical Engineering Journal*, 306, pp.1049–1057.

Santelli, C.M., 2009. Biogeochemistry: Life in the deep sea. *Nature Geoscience*, 2(12), pp.825–826.

Schmidt, K. et al., 2007. Geochemistry of hydrothermal fluids from the ultramafic-hosted Logatchev hydrothermal field, 15°N on the Mid-Atlantic Ridge: Temporal and spatial investigation. *Chemical Geology*, 242(1–2), pp.1–21.

Schmitt, A.D. et al., 2003. The calcium riverine and hydrothermal isotopic fluxes and the oceanic calcium mass balance. *Earth and Planetary Science Letters*, 213(3–4), pp.503–518.

Schmitt, A.D. & Stille, P., 2005. The source of calcium in wet atmospheric deposits: Ca-Sr isotope evidence. *Geochimica et Cosmochimica Acta*, 69(14), pp.3463–3468.

Schrenk, M.O., Brazelton, W.J. & Lang, S.Q., 2013. Serpentinization, Carbon, and Deep Life. *Reviews in Mineralogy and Geochemistry*, 75(1), pp.575–606.

Searle, M. & Cox, J., 1999. Tectonic setting, origin, and obduction of the Oman ophiolite. *Geological Society Of America Bulletin*, 111(1), pp.104–122.

Searle, M.P. & Cox, J., 2002. Subduction zone metamorphism during formation and emplacement of the Semail ophiolite in the Oman Mountains. *Geological Magazine*, 139(3), pp.241–255.

Seifritz, W., 1990. CO_2 disposal by means of silicates. *Nature*, 345(6275), pp.486.

Semhi, K. et al., 2017. Strontium isotopes as a tool for estimation of groundwater recharge and aquifer connectivity. *Groundwater for Sustainable Development*, 4(February 2016), pp.1–11.

Shalev, N. et al., 2017. Enrichment of [88]Sr in continental waters due to calcium carbonate precipitation. *Earth and Planetary Science Letters*, 459, pp.381–393.

Shibuya, T. et al., 2016. Free energy distribution and hydrothermal mineral precipitation in Hadean submarine alkaline vent systems: Importance of iron redox reactions under anoxic conditions. *Geochimica et Cosmochimica Acta*, 175, pp.1–19.

Sissmann, O. et al., 2013. The deleterious effect of secondary phases on olivine carbonation yield: Insight from time-resolved aqueous-fluid sampling and FIB-TEM characterization. *Chemical Geology*, 357, pp.186–202.

Skulan, J. et al., 1997. Biological control of calcium isotopic abundances in the global calcium cycle. *Geochimica et Cosmochimica Acta*, 61(12), pp.2505–2510.

Snæbjörnsdóttir, S. et al., 2014. CO_2 storage potential of basaltic rocks in Iceland and the oceanic Ridges. *Energy Procedia*, 63, pp.4585–4600.

Snow, J.E., Hart, S.R. & Dick, H.J.B., 1994. Nd and Sr Isotope Evidence Linking Mid-Ocean-Ridge Basalts and Abyssal Peridotites. *Nature*, 371(6492), pp.57–60.

Souza, G.F. de et al., 2010. Evidence for mass-dependent isotopic fractionation of strontium in a glaciated granitic watershed. *Geochimica et Cosmochimica Acta*, 74(9), pp.2596–2614.

Stanger, G., 1986. *The hydrogeology of the Oman mountains.* Vol.1. PhD Thesis. The Open University, UK. 369 pp.

Stephen, A.L., 2014. *Carbon sources and sinks within the Oman-UAE ophiolite: implications for natural atmospheric CO_2 sequestration rates*. PhD Thesis. Univ. of Leicester, UK. 249 pp

Stern, R.J. & Smoot, N.C., 1998. A bathymetric overview of the Mariana forearc. *Island Arc*, 7(3), pp.525–540.

Stevenson, E.I. et al., 2014. Controls on stable strontium isotope fractionation in coccolithophores with implications for the marine Sr cycle. *Geochimica et Cosmochimica Acta*, 128, pp.225–235.

Stevenson, E.I. et al., 2016. Insights into combined radiogenic and stable strontium isotopes as tracers for weathering processes in subglacial environments. *Chemical Geology*, 429, pp.33–43.

Tang, J. et al., 2008. Sr^{2+}/Ca^{2+} and $^{44}Ca/^{40}Ca$ fractionation during inorganic calcite formation: II. Ca isotopes. *Geochimica et Cosmochimica Acta*, 72(15), pp.3733–3745.

Teir, S. et al., 2007. Dissolution of natural serpentinite in mineral and organic acids. *International Journal of Mineral Processing*, 83, pp.36–46.

Tessier, A., Campbell, P.G.C. & Bisson, M., 1979. Sequential extraction procedure for the speciation of particulate trace metals. *Analytical Chemistry*, 51(7), pp.844–851.

Tilton, G.R., Hopson, C.A. & Wright, J.E., 1981. Uranium-lead isotopic ages of the Samail Ophiolite, Oman, with applications to Tethyan Ocean ridge tectonics. *Journal of Geophysical Research: Solid Earth*, 86(B4), pp.2763–2775.

Ulmer, P. & Trommsdorff, V., 1995. Serpentine Stability to Mantle Depths and Subduction-Related Magmatism. *Science*, 268(5212), pp.858–861.

Urey, H.C., 1952. On the Early Chemical History of the Earth and the Origin of Life. *Proceedings of the National Academy of Sciences of the United States of America*, 38(4), p.351.

Vollstaedt, H. et al., 2014. The Phanerozoic $\delta^{88/86}Sr$ record of seawater: New constraints on past changes in oceanic carbonate fluxes. *Geochimica et Cosmochimica Acta*, 128, pp.249–265.

VonderHaar, D.L., Mahoney, J.J. & McMurtry, G.M., 1995. An evaluation of strontium isotopic dating of ferromanganese oxides in a marine hydrogenous ferromanganese crust. *Geochimica et Cosmochimica Acta*, 59(20), pp.4267–4277.

Wang, X. & Maroto-Valer, M.M., 2011. Dissolution of serpentine using recyclable ammonium salts for CO_2 mineral carbonation. *Fuel*, 90(3), pp.1229–1237.

Wei, G. et al., 2013. Seasonal changes in the radiogenic and stable strontium isotopic composition of Xijiang River water: Implications for chemical weathering. *Chemical Geology*, 343, pp.67–75.

Welland, M.J.P. & Mitchell, A.H.G., 1977. Emplacement of the Oman ophiolite: A mechanism related to subduction and collision. *Bulletin of the Geological Society of America*, 88(8), pp.1081–1088.

Weyhenmeyer, C.E., 2000. *Origin and Evolution of Groundwater in the Alluvial Aquifer of the Eastern Batinah Coastal Plain, Sultanate of Oman: A Hydrogeochemical approach*. PhD thesis. Univ. Bern, Switz. 202 pp

Wittig, N. et al., 2009. The U, Th and Pb elemental and isotope compositions of mantle clinopyroxenes and their grain boundary contamination derived from leaching and digestion experiments. *Geochimica et Cosmochimica Acta*, 73(2), pp.469–488.

Zhu, P. & Macdougall, J.D., 1998. Calcium isotopes in the marine environment and the oceanic calcium cycle. *Geochimica et Cosmochimica Acta*, 62(10), pp.1691–1698.